UNIVERSIDADE FEDERAL DE SANTA CATARINA
PROGRAMA DE PÓS-GRADUAÇÃO EM CIÊNCIA E ENGENHARIA DE MATERIAIS

LUCAS FREITAS BERTI

RBMAO: Uma nova rota de produção para cerâmica porosa (RBMAO: A novel production route for porous ceramics)

Tese submetida ao Programa de Pós-Graduação em Ciência e Engenharia de Materiais da Universidade Federal de Santa Catarina para a obtenção do Grau de Doutor em 2012
Orientador: Prof. Dr. Dachamir Hotza
Coorientador: Prof. Dr. Carlos Renato Rambo
Supervisor: Dr. Rolf Janssen

Florianópolis

2012

Berti, Lucas Freitas
RBMAO: Uma nova rota de produção para cerâmica porosa [tese] : (RBMAO: A novel production route for porous ceramics) / Lucas Freitas Berti ; orientador, Dachamir Hotza ; co-orientador, Carlos Renato Rambo, supervisor, Rolf Janssen. - Florianópolis, SC, 2012.
137 p. ; 21cm

Tese (doutorado) - Universidade Federal de Santa Catarina, Centro Tecnológico. Programa de Pós-Graduação em Ciência e Engenharia de Materiais.

Inclui referências

1. Ciência e Engenharia de Materiais. 2. Sinterização Reativa. 3. Compósitos. 4. Fibras Longas. 5. Alumina e Mulita. I. Hotza, Dachamir. II. Rambo, Carlos Renato. III. Janssen, Rolf IV.Universidade Federal de Santa Catarina. Programa de Pós-Graduação em Ciência e Engenharia de Materiais. V. Título.

LUCAS FREITAS BERTI

TÍTULO: RBMAO: Uma nova rota de produção para cerâmicas porosas
(RBMAO: A novel production route for porous ceramics)

Esta Tese foi julgada adequada para obtenção do Título de "Doutor", e aprovada em sua forma final pelo Programa de Pós-Graduação em Ciência e Engenharia de Materiais.

Florianópolis, 11 de Junho de 2012.

_____
Prof. Dr. Antonio Pedro Novaes de Oliveira
Coordenador do Programa

Banca Examinadora:

_____ Prof. Dr. Dachamir Hotza, Orientador Universidade Federal de Santa Catarina	_____ Prof. Dr. Carlos Renato Rambo, Coorientador Universidade Federal de Santa Catarina
_____ Prof. Dr. Carlos Pérez Bergmann, Universidade Federal do Rio Grande do Sul	_____ Prof. Amir A. Oliveira Jr., Universidade Federal de Santa Catarina
_____ Prof. Dr. Celso Peres Fernandes, Universidade Federal de Santa Catarina	_____ Prof. Dr. Edson Bazzo, Universidade Federal de Santa Catarina

_____
Prof. Dr. Antonio Pedro Novaes de Oliveira,
Universidade Federal de Santa Catarina

O senhor Jesus, o Cristo, é o único que merece minha dedicação.

Não obstante, gostaria muito de lembrar nesta tese minha família, que sempre me incentivou e deu suporte para que eu estudasse – minha mãe, meu pai (*in memoriam*), meu irmão e sua esposa. Não deixo, nem de fora nem em segundo lugar, mas em sequência, sem ordem, de agradecer minha esposa e família por todo apoio e palavras de incentivo, mesmo nos momentos mais difíceis desta jornada, que foi o doutorado.

AGRADECIMENTOS

Aos meus orientadores, Dachamir Hotza, Carlos Rambo, Rolf Janßen, Edson Bazzo, meu muito obrigado pelas valiosas discussões que fizeram esse trabalho tomar a forma que ele tem.
Aos amigos e colegas de trabalho Eduardo Reimbrecht, Lorenço Neckel, Rafael Gonçalves, Daniel Garcia, Hansu Birol, Rodrigo Pacher, Luis Prado, Felipe Darabas, Guilherme Wagner, Edevaldo Reinaldo, Valtair (LMP), que ajudaram de forma direta a obter informações importantes para este trabalho, meu muito obrigado!
Aos integrantes do grupo do projeto BRAGECRIM na TUHH, Paula Guglielmi, Gabriel Nunes, João Pereira, os quais contribuíram de forma muito valiosa para a obtenção dos resultados desse trabalho, sou grato a vocês.
Aos conhecidos durante a estada em Hamburgo e Göttingen, Humberto e Camila Coelho, Rosana e Jürgen Lehmberg, Lukas e Barbara Grzybowski, entre outros, meus agradecimentos por fazer da minha estada uma experiência melhor.
To the head of the Advanced Ceramic Institute, Prof. Dr. Gerold Schneider, for allowing me to get access to institute facilities. To my colleges ceramists, Hüseyin Özcoban, Roman Kubrin, Kristina Brandt, Hans Jelitto, Andrea Engert, Katharina Wiegandt, Henry Mgbemere, Claudia Neusel, Anja Borchert, Manfred Geerken, Dieter Schmidt, Seyed Goushegir, Deepak and Ezgi, for helping me directly or indirectly with information for my thesis or with valuable conversations.
Meinen herzlichen Dank an Bastian Brinkmann, der nicht nur bei vielen Situationen in Deutschland mir geholfen hat, sondern auch mir wertvolle Hinweise in unseren Gesprächen gegeben hat.
À CAPES/DAAD/CNPq pelo apoio financeiro através da bolsa de doutorado sanduíche concedida para realização do estágio de doutorado na TU Hamburg-Harburg.
Às empresas que, de prontidão, forneceram amostras de matéria-prima que foram utilizadas neste trabalho. Elas são: Treibacher Schleifmittel Brasil e Alemanha, Alcoa S.A. e Hexion LLC (Momentive Performance Materials Holdings Inc.) and Zschimmer & Schwarz Group.

"Nós não ficamos mais sábios com a idade, nem sempre os velhos sabem o que é certo."

(Jó 32:9)

RESUMO

O presente trabalho visou desenvolver uma rota alternativa para produção de matrizes porosas de cerâmicas óxidas para aplicação em materiais compósitos. Para tanto, foram realizadas caracterizações para obter uma suspensão de partículas cerâmicas, estável e com viscosidade dentro de um valor desejável. Igualmente, foram feitas caracterizações para o tratamento térmico, ao qual as matérias-primas são submetidas, envolvendo análise térmica diferencial e termogravimetria. Análise de imagem foi aplicada à matriz cerâmica produzida. Por se tratar de um processo de sinterização reativa, foram determinados os parâmetros de cinética de oxidação. O processo desenvolvido se baseia na obtenção de uma matriz óxida através da oxidação indireta de uma fase secundária, formada a partir de um pó metálico. Dentre os resultados alcançados podem-se citar: porosidade obtida dentro dos valores esperado, i.e. ~50%; parâmetro de Weibull de 10,54, σ_0 de 14,15 MPa com σ_{max} de 16,1 MPa; Energia de ativação de oxidação do carbeto de alumínio isolado de 129,65 kJ/mol em baixa temperatura e 16,91 kJ/mol em alta temperatura.

Palavras-chave: Sinterização Reativa. Compósitos. Fibras Longas. Alumina. Mulita.

ABSTRACT

The present work focuses mainly on the development of an alternative novel route for production of oxide ceramic matrices for application in composite material. In this context, the following characterizations were carried out: viscosity determinations for obtaining stable/ homogenous slurry with desired viscosity; thermal treatment set points determinations, which involve thermogravimetric analyses and differential thermal analyses; morphology characterization of the produced oxide porous ceramic matrix. Due to the fact that the production route is related to reaction bonding then oxidation kinetics parameters were also determined. An oxide-based process was developed, wherein a final oxide phase is produced through the indirect oxidation of an intermediate phase, which is formed from metallic powder. The main results found were: porosity within the expected values, i.e. ~50%; Weibull parameter of 10.54, σ_0 of 14.15 MPa with σ_{max} of 16.1 MPa; Activation energy of oxidation of the isolated aluminum carbide of 129.65 kJ/mol at lower temperatures and of 16.91 kJ/mol at higher temperatures.

Keywords: Reaction Bonding. Composites. Long fibres. Alumina. Mullite.

LIST OF FIGURES

LIST OF TABLES

ABBREVIATIONS AND ACRONYMS

ACRONYMS	DESCRIPTION
3A	Sintered Alumina Aluminide Alloys
A	Alumina Phase (in XRD Analysis)
Al	Aluminium Phase
AlC	Aluminium Carbide Phase
BET	Brunauer, Emmet and Teller Analysis
BSE	Back Scattered Electrons Detection
CFCC	Continuous Fibre-Reinforced Ceramic Composites
C_f-SiC	Carbon Long Fibres Reinforced Silicon Carbide Composite
CMC	Ceramic Matrix Composites
DSC	Differential Scanning Calorimetry
DTA	Differential Thermal Analysis
FESEM	Field Emission Gun Scanning Electron Microscopy
FRCMC	Fibre-Reinforced Ceramic Composites
GADDS	General Area Detector Diffraction System
M	Mullite Phase
MMC	Metal Matrix Composites
OM	Optical Microscopy
PDA	Precursor-Derived Alumina
PE	Phosphate Ester Based Dispersant
PMC	Polymeric Matrix Composites
RB	Reaction Bonded Technique
RBAO	Reaction-Bonded Aluminium Oxide
RBM	Reaction Bonded Mullite

RBMAO		Reaction Bonded Mullite Aluminium Oxide
SE		Secondary Electrons Detection
SEM		Scanning Electron Microscopy
TEM		Transmission Electron Microscopy
TG		Thermogravimetry Analysis
TUHH		Technische Universität Hamburg-Harburg (In German)
UFSC		Universidade Federal de Santa Catarina (In Portuguese)
WOR200		Samples without Resin Pressed at 200 MPa
WOR50		Samples without Resin Pressed at 50 MPa
WR50		Samples with Resin Pressed At 50 MPa
XRD		X-Ray Diffractometry

GLOSSARY OF SYMBOLS

SYMBOL	DESCRIPTION
	GREEK SYMBOLS
α	Elastic Mismatch Parameter
Γ^{0}_{m}	Toughness of The Fully Dense Matrix
Γ_{f}	Fibre Toughness
Γ_{i}	Fibre-Matrix Interface Toughness
η	Intrinsic Viscosity
η_{r}	Relative Viscosity
η_{s}	Solvent Viscosity
λ	Wavelength of The Incident X-Radiation
σ_{0}	Scale Parameter or Characteristic Strength
σ_{max}	Maximum Flexural Strength for a particular group
Φ	Volume Fraction of Particles
Φ_{m}	Maximum Volume Fraction of Particles
	LATIN SYMBOLS
$\overline{\mathbf{E}}_{f}$	Fibre Plane Strain Modulus
$\overline{\mathbf{E}}_{m}$	Matrix Plane Strain Modulus
A	Specific Surface Area (in Oxidation Kinetics)
k	Oxidation Parameter
m	Weibull Parameter
P	Porosity
P_{o}	Initial Porosity
V_{crit}	Critical Fibres Volume Fraction
V_{f}	Fibres Volume Fraction
$\Delta E_{activation}$	Apparent Activation Energy Of Oxidation
ΔW	Weight Variation

TABLE OF CONTENTS

1 INTRODUCTION

Modern structural ceramic composites possess a number of unique properties that cannot be achieved by any single material. For instance, composites can bear moderate loads at high temperatures, i.e. 1200°C (CHAWLA, 1993), and at room temperature they may present damage tolerance characteristics. They have a potential for saving energy, reducing wear, and increasing the lifetime of components (JANSSEN, *et al.*, 2008). Conversely, regardless of their excellent properties, structural ceramics are not as widely used in industry as they should and could be. Among the reasons for the reluctance of industry to introduce structural ceramic as components are (JANSSEN, *et al.*, 2008):

- high price of ceramic parts,
- insufficient knowledge in "traditional" metal-oriented engineering,
- low toughness,
- need to redesign components to meet specific ceramic requirements.

There are a number of examples where components based on ceramic composites have been designed and tested successfully, but, despite their superior properties, they have not been put into production, basically due to their high price. In some cases machining costs can account for 80% of the overall manufacturing costs of a ceramic component. (KLOCKE, 1997)

Challenging approaches are provided by synthesis routes which exhibit reduced shrinkage, and capabilities for shaping by machining in the green state. In this case, reactive processing routes like reaction bonding of aluminium oxide (RBAO), sintered alumina aluminide alloys (3A) are good examples. These techniques have been developed at Advanced Ceramics Institute of the Technological University of Hamburg-Harburg (TUHH - Technische Universität Hamburg-Harburg) (CLAUSSEN, *et al.*, 1990), (CLAUSSEN and WU, 1992), (WU, *et al.*, 1993), (CLAUSSEN, *et al.*, 1996), (JANSSEN, *et al.*, 2002),(JANSSEN, *et al.*, 2008).

Fibre reinforcement of ceramics is a concept which has attracted a lot of interest, especially in the automotive and aerospace industry. The essential requirements for fibre reinforced ceramic matrix composites (FRCMC) are high temperature stability, oxidation resistance and damage tolerance (JANSSEN, *et al.*, 2008). For non-oxide matrices, reinforcement is especially performed with long-fibre (C_f-SiC)

composites with suitable rupture behaviour (JANSSEN, 2007). At high temperature and long time applications (i.e. burners, turbine components, structural insulations, etc.) the stability of those materials in oxygen atmosphere is still a feature that limit their broader application.
In the last few years, researches concentrated on complex coatings for oxidation protection of the components (internal) or of the entire prefabricated part (external), for use in oxygen rich atmospheres, such as for combustion processes. At present, it is not yet unequivocally clarified whether a damage tolerant fibre composite can actually be produced with these concepts. Therefore, most commercial applications of carbon fibre reinforced silicon carbide (C_f-SiC) are focused yet on systems where the average service temperature in air is quite moderate (i.e. brake disc rotors in advanced sport cars). Oxide-Oxide FRCMCs are therefore an attractive alternative.
Polycrystalline oxide fibres although are still limited in maximum service temperature when compared to carbon or (very expensive) silicon carbide fibres like High Nicalon. Therefore, research on these composites has been running for more than a decade (EVANS and ZOK, 1994). The production problems are yet not solved and only some oxide-oxide FRCMCs are produced in lab in a very small scale (WESTWOOD, *et al.*, 1996). This work will focus, therefore, on the development of a novel route for porous ceramic matrix production by combining features of proven effective techniques.

1.1 MOTIVATION

The motivation of this research project was the opportunity of combine features of two proven techniques for develop and adapt a novel route for production of porous ceramic materials. Particularly in this study the novel route was adapted for producing porous matrix material for composites, although the technique may be directed for some other applications. This work concerned in ensuring the successful development of the production steps for obtaining desired phases through within the processing cycles.

1.2 OBJECTIVES

The prime objective of this work is to develop a porous ceramic material to be used as porous ceramic matrix. This matrix has to present stable porosity and a specific microstructure to enable damage tolerant behaviour and also has to exhibit a desirable mechanical behaviour at high temperatures.

The following specific objectives are to be achieved:

- Development of a method for obtaining a ceramic matrix, in which a controlled porosity and a tailored microstructure are generated consisting on mullite particles surrounded by finer alumina particles. The desired porosity ranges from 20% to 50%. The desired mullite particle size ranges from 5 to 15 μm and the alumina particles are expected to be a finer particulate dispersed around the mullite particles.
- Definition of viscosity properties of the slurry to be used in the composite panel infiltration process;
- Definition of the setup of production route for reaction/oxidation/sintering thermal treatment;
- Evaluation of mechanical properties of the produced matrix by Weibull statics.
- Characterization of the matrix morphology in order to determine how particles of alumina are distributed within the matrix material.
- Determination of oxidation kinetics of the intermediate phase, i.e. activation energy of oxidation.

2 LITERATURE REVIEW

Reaction-bonding as well as ceramic composites fabrication techniques will be reviewed in this chapter.

2.1 REACTION BONDING TECHNIQUES

Ceramics are well known as brittle materials. Fracture toughness of most ceramics does not exceed values of 10 MPa$\sqrt{m}$. However, the application of sophisticated processing techniques, limiting typical flaw sizes, reducing heterogeneities to a micrometre scale, enables attainment of flexural strength up to a GPa range. According to Knechtel and co-wokers, the reliability of structural ceramics can be controlled by at least four mechanisms with dissimilar degrees of efficiency, e.g. distribution of defect size, R-curve effects, stress induced plasticity and reduced flaw size (KNECHTEL, *et al.*, 1995). Those controlling parameters are within reaction bonding techniques, which may produce very clear grain boundaries, with very fine dispersed grains.

The characteristic feature of reaction bonding techniques is the involved reaction, which occurs during the heat treatment schedule. Reaction-Bonded Aluminium Oxide (RBAO) and Reaction-Bonded Mullite (RBM) are examples of such techniques. The properties and processing of reaction-bonded ceramics are presented in the literature (CLAUSSEN and WU, 1992). RBAO and RBM compacts exhibit low shrinkage, and very distinctive mechanical properties due to their microstructure morphology. Reaction Bonding techniques can be modified to produce zirconia–toughened RBAO, for instance, among other composite ceramics. Nevertheless, the RB processes exhibit different fundaments and features in comparison with directed metal oxidation (CLAUSSEN and WU, 1992). While conventional sintered products present a shrinkage range from 15 to 20%, the RB techniques exhibit nearly zero shrinkage, which makes them suitable for application where near net shape plays an important role. The almost zero shrinkage feature comes from the expansion associated with the oxidation of the raw-materials, wherein metallic particles amounts of up to 60 vol.% are combined with the other raw materials. Some additives are employed so that the kinetics of oxidation is modified in order to ease the process. Those metallic particles may easily oxidize during milling, which may be avoided in a closed milling system. The same approach is applied to mechanical alloying of intermetallics, i.e. attrition milling. The milled powder is then dried and pressed, which cause the Al and Al_2O_3 particles to form

contacts by bridging. This is the reason why those compacts can present high green strength, e.g. 20-50 MPa, which are values far higher than those of conventional ceramic green bodies. In heating treatment, the compacts undergo not only sintering mechanisms, but also solid state oxidation, which balances and hinders compact shrinkage. In RB techniques where the near net shape is not a highlighted property, the shrinkage can reach at most 5%.
Completely reaction-bonded bodies usually exhibit 3 to 8% homogeneously distributed micropores with sizes lower than 1 μm. Those compacts can exhibit mechanical strength up to 500 MPa, 94.5% theoretical density and may present up to 20 vol.% ZrO_2 as reinforcing phase.
As previously mentioned, RB techniques can be modified in various way by either metal, e.g. Zr, Cr, Si etc, or ceramic additives, e.g. ZrO_2, Cr_2O_3, MgO, SiC etc. Depending on the selected modification the RB compact can either present a low shrinkage, e.g. RBAO or Zirconia-Toughened Alumina; a near net shape, e.g. Reaction Bonded Aluminium/Chromium Oxide; or even a slightly expansion, e.g. RBM (CLAUSSEN and WU, 1992).

2.1.1 RBAO technique

Authors in literature (CLAUSSEN, *et al.*, 1989) addressed the fabrication of reaction-bonded alumina with near zero shrinkages (<1%). In this case, the samples of attrition-milled Al/Al_2O_3 powder mixtures are heat treated at temperatures between 1200 and 1550°C, so that the expansion due to the $Al \rightarrow Al_2O_3$ reaction and the sintering shrinkage of Al_2O_3 are nearly balanced. Those authors also addressed a shrinkage of ~14% for samples made out of 100% Al_2O_3, regarding the same powder particles distribution and heat treatment schedule.
Later on (WU and CLAUSSEN, 1990) a reduction of mullite-zirconia ceramics was proposed by combining the RBAO reaction with the reaction of zircon ($ZrSiO_4$) with Al_2O_3adding metallic aluminium powder to the mixture. Although the produced compacts presented lower shrinkage, they showed higher porosity and lower toughness mechanical strength. The final properties were 350 MPa strength, 4.5 MPa$\sqrt{m}$ toughness and 13.5% porosity. On the other hand, modified samples presented 250 MPa, 2.5 MPa$\sqrt{m}$ and 5.5%, of strength, toughness and porosity, respectively.

Tailoring of reaction-bonded Al_2O_3 ceramics is reported in the literature (CLAUSSEN, *et al.*, 1990). Authors discussed possible mechanisms of microstructural development and of composite formation. Attrition milled Al/Al_2O_3 compacts with 50% and 35 vol.% of Al were heat treated and yielded theoretical density of 93% and strength of 350 MPa. The microstructure exhibited a homogeneous distribution of fine (>1μm) closed pores. They also addressed the hazard decreasing level of the process due to the passivation of the surface, which comes from the heavily comminuted Al particles (~1μm). This intensive milling of particles is carried out in organic media, i.e. acetone, at temperatures of 12°C. The small additions of zirconia, up to 5 vol.%, lead to considerably reducing in reaction bonding times. Even though Al powder presented some impurities, e.g. Si, Mn etc, no intergranular glass phase was observed by TEM (CLAUSSEN, *et al.*, 1990).
According to Claussen, Wu and Janssen, the RBAO process starts from precursor mixtures consisting of Al and Al_2O_3 (CLAUSSEN, *et al.*, 1989), (WU, *et al.*, 1993), (JANSSEN, *et al.*, 2002). In practically all cases, ZrO_2 is added to enhance oxidation and to improve microstructure and mechanical properties of the final product. The precursor mixtures are intensively milled in order to reduce the particle size, mainly that of Al, and to achieve a high degree of homogenization. Green bodies for RBAO contain about 30–45 vol. % of aluminium which bonds the alumina particles so that binder additions are not required. RBAO powder compacts reach substantially high-green strength, i.e., isostatic compaction at pressures as low as 170MPa is sufficient to obtain green bodies with high strength (20MPa in 4-point bending) that can be extensively green machined to complex shapes and down to very low wall thickness values below 50 μm. (JANSSEN, *et al.*, 2002) After machining, the green compacts are subjected to a two-step heat treatment in air in order to first oxidize Al and then sinter the material. The oxidation of Al is associated with a 28% volume expansion and together with the high-green densities (typically >60% T.D., up to 75% possible) this leads to a reduced sintering shrinkage of about 10–15%. The newly formed, very fine Al_2O_3 sinters and bonds the originally added Al_2O_3. The sintered material has typical grain sizes of 1–1.5 μm and 0.5 μm for Al_2O_3 and ZrO_2, respectively. RBAO composites tested without any machining, i.e., as fired, using a “Punch-on-Three-Equiaxed-Balls” test configuration exhibit typical strength values of 700 MPa after pressureless sintering and >1 GPa after HIPing. (JANSSEN, *et al.*, 2002).

The process can be modified in various ways, e.g. to form reaction-bonded mullite (RBM).

2.1.2 RBM technique

In the case of RBM process, SiC instead of Al_2O_3 is added to the precursor powder (WU and CLAUSSEN, 1990), (SCHEPPOKAT, *et al.*, 1998), (SCHEPPOKAT, *et al.*, 1999). The large volume increase (108%) associated to the SiC oxidation together with the 28% volume increase from Al oxidation make extremely low (<0.2% linear) sintering shrinkage possible, provided the green density is high (>72% T.D.). RBM may attain strength values of 250 MPa.

2.1.3 3A technique

As far as powder preparation is concerned, this process is similar to the RBAO process, however, it includes a redox reaction between aluminium and the oxide of another metal (CLAUSSEN, *et al.*, 1996), (GARCIA, *et al.*, 1998), (JANSSEN, *et al.*, 2002), (SCHEPPOKAT, *et al.*, 2005). The basic reaction can be written as

$$Al_{(s)} + Me_aO_{b(s)} \rightarrow MexAl_{y(s)} + Al_2O_{3(s)} \qquad 1$$

Sintering has to take place under vacuum or in an inert atmosphere to prevent reaction between Al with oxygen and nitrogen from atmosphere. Examples of application of oxides, which were found in literature, are Cr_2O_3, Fe_2O_3, Nb_2O_5, TiO_2, and ZrO_2(CLAUSSEN, *et al.*, 1996). The process can be modified by using a metallic material, such as Cr, Fe, or Mo, instead of the metal oxide, and adding only a small amount (≈1 wt. %) of Al for sinter kinetics assisting (JANSSEN, *et al.*, 2008). This version of the 3A process has the advantage that the highly exothermic redox reaction takes place only on a very small scale, i.e., between Al and the oxide layer on particles of the other metal, so that higher heating rates can be used. Advantages of the 3A process are high-green strength allowing green machining, pressureless sintering, and compositional flexibility (CLAUSSEN, *et al.*, 1996).

2.1.4 Other reaction bonding techniques

Other types of reaction bonding techniques are found in literature, for instance, Silicon Nitride (TRAVITZKY and CLAUSSEN, 1992), Aluminium Niobate and Cromate (GARCIA, *et al.*, 1998) (GARCIA, *et al.*, 1999). Applying reaction bonding route for silicon nitride causes the material to improve its mechanical properties, e.g. strength raised to 510

MPa, and when infiltrated with a Ti-39 wt% Al alloy the toughness raised to > 5 MPa$\sqrt{m}$.

2.2 ALUMINIUM CARBIDE

The creep strength of the aluminium carbide particles-reinforced silicon carbide matrix composites increases with the volume fraction of aluminium carbide particles dispersed in the matrix. It can be accounted for, almost exclusively, by the effect of this fraction on the threshold stress (ZHU, *et al.*, 2000). Aluminium carbide can be used as an abrasive in high-speed cutting tools due to its high hardness, i.e. approximately the hardness of topaz.(SAVEKER and BONNELL, 2000). Aluminium carbide is also suitable for grain refinement of Mg alloys with only 5% additions of Al_4C_3, which in turn act as nuclei for heterogeneous nucleation for Mg alloys phases (NIMITYONGSKUL, *et al.*, 2010). It is moreover used for strengthening Al alloys present a very particular creep behaviour, with a lower and a higher temperature variation, which in turn can be predicted by models found in literature (GURJAR, *et al.*, 1993) and follow a power law creep (DOBEŠ, *et al.*, 2012).
Wand and co-workers (WANG, *et al.*, 2004) evaluated the reaction between Al and C in binary alloys by means of Differential Scanning Calorimetry (DSC) and X-Ray Diffractometry (XRD), Figure 1.

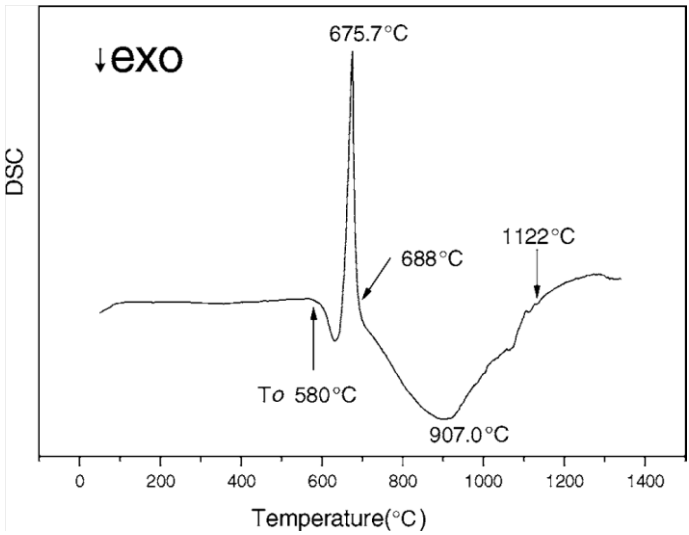

Figure 1 - DSC of non isothermal Al_4C_3 formation (WANG, *et al.*, 2004).

According to the authors the wide peak between 688°C and 1122°C is related to the aluminium carbide formation. The reaction between Al and C is dependent on the type of carbon structure. The higher the contact area, the more complete is the carbide reaction (BESTERCI and PARILÁK, 2004) (BESTERCI, 2006).

2.3 ALUMINIUM VAPOUR INFILTRATION

Aluminium vapour infiltration is a technique that provides final parts with well defined structures replicated from the original template (RAMBO and SIEBER, 2005). Although this technique is more suitable to build ceramic structures from biotemplates rather than other liquid infiltration techniques, it is also suitable to produce a very fine grain-size ceramic phase due to the chemical reaction among the aluminium and carbon powder. Some works report the final structure of those biotemplated ceramics (Figure 2).

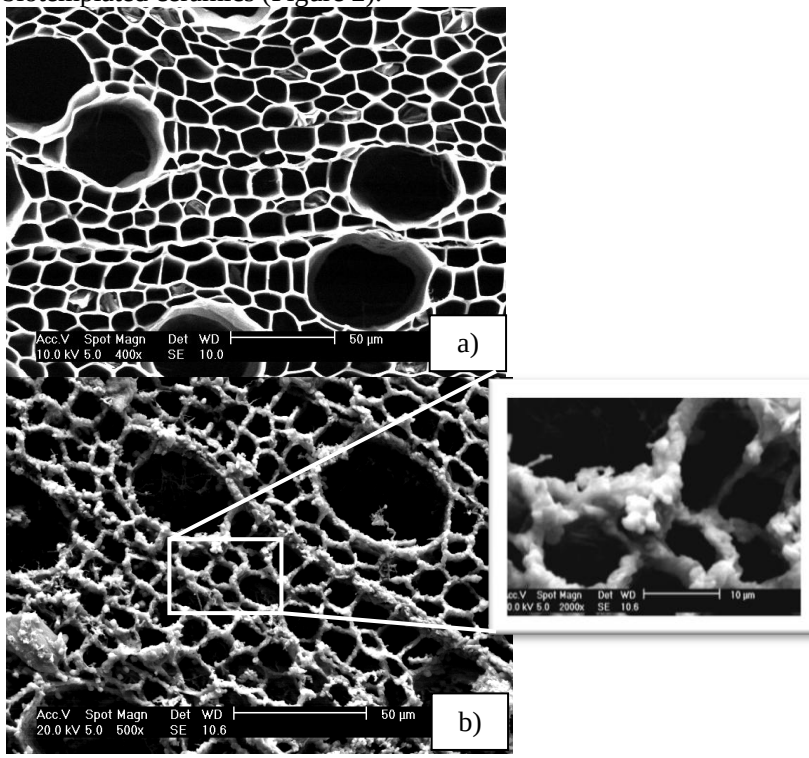

Figure 2 - Carbon preform used in aluminium vapour infiltration (a) and respective porous ceramic structure produced (b). (BERTI, 2008).

The carbon structure used in this technique presented bimodal pore size distribution with average pore size of 10 and 50 µm (see Figure 2 a) and b)). The resulted final structures showed a well defined replication of the carbon perform. The structure walls are formed by a very fine sized particle of alumina.

The reactions that take place during the heat treatment are carbide formation followed by oxidation. Those reactions convert aluminium powder in aluminium oxide, according to the following equations:

- Al_4C_3 formation (equation 2):

$$4Al_{(s)} + 3C_{(s)} \rightarrow Al_4C_{3(s)} \quad (2)$$

- Al_2O_3 formation by Al_4C_3 oxidation (equation 3):

$$Al_4C_{3(s)} + 9O_{2(g)} \rightarrow 4Al_2O_{3(s)} + 6CO_{(g)} \quad (3)$$

2.4 REACTION KINETICS

Reaction kinetics is determined by measuring either the amount of metal consumed or by the amount of oxygen consumed or even by the amount of oxide produced (BIRKS, *et al.*, 2006) (YOUNG, 2008). In practical terms only the oxygen comsuption can be continuously assessed. Thermogravimetry allows the metal comsuption to be measured. To determine the oxidation kinetics, any of above mentioned methods can provide quantitative parameters. The principal rate laws of reaction kinetics are (BIRKS, *et al.*, 2006):

- Linear law, for which the rate of reaction is independent of time, is found predominantly in reactions whose rate is controlled by a surface-reaction step or by diffusion through the gas phase.
- Parabolic law, for which the rate is inversely proportional to the square root of time, is found when diffusion through the scale is the rate-determining process.
- Logarithmic law, which is only observed for the formation of very thin films of oxide, i.e., between 2 and 4 nm, and is generally associated with low temperatures.

Additionally, some systems may even present combined reaction kinetics laws, e.g. oxidation of niobium in air, at 1000°C initially follows a parabolic law and later becomes linear.

2.4.1 Oxidation kinetics

In the last decade several materials have been studied regarding their oxidation kinetics, e.g. carbides (GOZZI, *et al.*, 1998), phosphated iron (REBEYRAT, *et al.*, 2000), nickel (NIKLASSON and KARMHAG, 2003), and nitrides (XINMEI and KUO-CHIH, 2009) among others. Moreover, mathematical models are also presented in literature (BROCK and PRYOR, 1973) (DOILNITSYNA, 2002) (CHOU, 2006).

Nickel particles with varying sizes were submitted to isothermal oxidation by thermogravimetric experiments (RASHIDI, 2011). In this study weight gain kinetics was evaluated regarding specific area. An activation energy of ~108 kJ/mol was found for both the nano and micro-sized particles. A theoretical modelling involving the contribution of grain boundary diffusion was in good agreement with experimental results. Oxidation kinetics of free and matrix enclosed nickel particles exhibited dissimilar activation energies of oxidation (BROCK and PRYOR, 1973), (KARMHAG, *et al.*, 2000).

Kinetic modelling of oxidation of aluminium in oxygen and its morphology has been extensively studied with heating rates of 1 to 40 K/min (BECK, *et al.*, 1966) (RAI, *et al.*, 2006) (SCHOENITZ, *et al.*, 2010). The activation energy of oxidation was found to occur in two stages, depending on the heating rates applied. Values found were 393±108 and 341±105 kJ/mol for the first and second oxidation stages, respectively, using 5 K/min. The higher the heating rates, the lower the activation energy of oxidation, both in the first and in the second stage. Additionally, the energy of activation value becomes more imprecise with the application of higher heating rates. Moreover, the activation energy for combustion of aluminium nanoparticles is smaller than that of a bulk aluminium sample (AUMANN, *et al.*, 1995). Corroborating to the last statement, the activation energy of oxidation reached 196.8±14.8 and 127.3±9.5 for micro- and nanosized aluminium particles, respectively (PIVKINA, *et al.*, 2004). Those values are not in agreement to those presented by (PARK, *et al.*, 2005).

Studies found in literature have evaluated the oxidation energy of oxidation of aluminium particles within RBAO mixtures (WU, *et al.*, 1993) (SUVACI, *et al.*, 2004). An oxidation activation energy of 222 kJ/mol was found (AARON, *et al.*, 2005) , and aluminium particle oxidation was claimed independent on particle size.

Boron carbide activation energy presented values of 209.4±11.4, 212.7±35.8 and 219.2±45.3 kJ/mol for fine, medium and coarse particle

sizes, respectively, as measured by isothermal thermogravimetric experiments (LI. and QIU, 2007).
Soot particles with size resolved oxidation kinetics presented values of 164 kJ/mol for activation energy of oxidation of nanosized particles (HIGGINS, *et al.*, 2002).
Silicon nitride oxidation kinetics was 310±25 kJ/mol and depending on the temperature it exhibiteds parabolic (lower than 1250°C) and non-parabolic rate law (higher than 1300°C) (PERSSON, *et al.*, 1993). Additionally, when impure silicon nitride is oxidized in dry air or dry oxygen, a protective oxide is formed, which retards further oxidation. Parabolic rate law is observed for such materials (HORTON, 1969).
In SiC particles-reinforced aluminium matrix composites, the interaction at high temperature between solid- or liquid aluminium and silicon carbide crystals always proceeded via dissolution-precipitation mechanisms (VIALA, *et al.*, 1993).
Direct oxidation of Al-Mg alloys in Mg matrices presented activation energy of 361 kJ/mol. That alloy firstly reacts with Al-Mg and then oxidized into spinel phases (VENUGOPALAN, *et al.*, 1996).
Silicon carbide activation energy of oxidation was found as 118 kJ/mol (HOU, *et al.*, 2009). In this study, a mathematical model was also suggested. The oxidation of such material also presented dependency on the vicinity material (LIU, 1997). The higher the amount of yttrium aluminium garnet, the lower the energy of activation of oxidation of silicon carbide particles(QUANLI, *et al.*, 2007).
In carbon long fibre-reinforced carbon matrix composites, silicon is infiltrated for enhancing oxidation. Those composites are dependent not only on the composite microstructure and fibre architecture, but also on the tensile strength in oxidizing environments (LAMOUROUX, *et al.*, 1995).

2.5 COMPOSITES

Composite materials have unique combination of properties, i.e. wear resistance, strength at high temperature, and damage tolerance. Composites are applied in several engineering fields, e.g. aerospace, gas turbines, automotive, and biomedical. The properties of composites are selected due to its very specific characteristics, which have to fit to the application, and simple comparisons between those properties might yield in wrong interpretation. If the ultimate bending strength of an oxide ceramic composite, i.e. ~200MPa, is compared to the ultimate bending strength of a monolithic ceramic, i.e. 1000MPa, it may be

considered that the composite has a fifth of the monolithic material value. This is true, however, it is not a fair material selection comparison. A composite material might present lower strength in comparison with its monolithic material, but it also show damage tolerance and it also present better mechanical properties at higher temperatures, i.e. strength, creep and fatigue properties. Therefore, the complete comparison must be taken into account for a correct interpretation.

Composites can be classified according to its matrix material type in:

- Metal Matrix Composites (MMC), in which a metal is a matrix phase, e.g. aluminium, magnesium, iron, cobalt, copper; and a dispersed ceramic or metallic phase, e.g. oxides, carbides, tungsten or molybdenum;
- Polymeric Matrix Composites (PMC), in which apply a thermoplastic or set polymer is the matrix phase, e.g. nylon, polysterene, unsaturated polyester, or epoxy; and a embedded glass, carbon, steel or Kevlar fibres as reinforcement. Fibres are commercially available in several patterns, which are selected according to the specific application;
- Ceramic Matrix Composites (CMC), in which a non-oxide or oxide ceramic is the matrix phase, e.g. silicon carbide, silicon nitride, alumina, or mullite; and a embedded non-oxide or oxide fibre reinforcement, such as carbon, carbides, sapphire, alumina, mullite, as reinforcement. Those fibres are also available in several patterns.

Further classification can be given to particulate composites according to geometrical and spatial characteristics (CALLISTER, 2000), (CALLISTER, 2006):

- Concentration;
- Size;
- Shape;
- Distribution, which relates how particles organize themselves with the matrix;
- Orientation, which relates how particles orientate themselves according to the frame axis.

The relation between reinforcement and matrix phase is also classified according to geometrical and spatial characteristics:

- Particle-reinforced composites, which may present large particles or dispersion-strengthened particles;

- Fibre-reinforced composites, which may present continuous and aligned fibres or discontinuous aligned and randomly oriented fibres.
- Structural composites, which may present laminates forms or sandwich panel.

The correct decision of which composite may be used in a specific application is a function of the combination of the composite properties, which are related to every material type, and to the requirements of the application. The mechanical properties of a composite represent a key factor for selection. Figure 3 presents composite strength values with volume fraction of fibres variation.

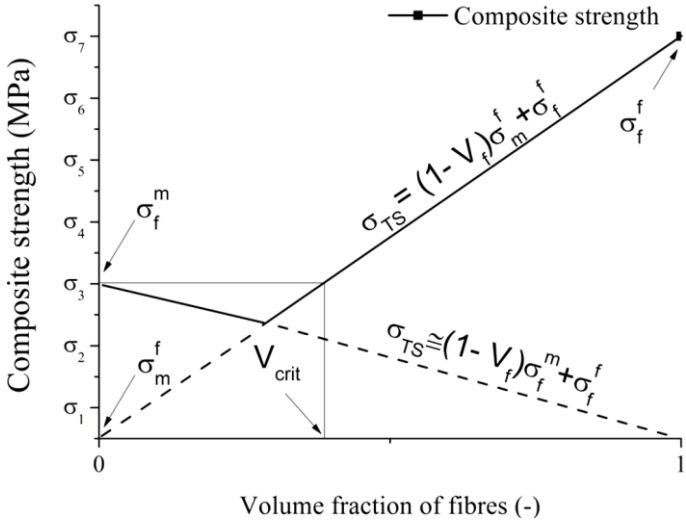

Figure 3 - Strength as a function of the volume fraction of fibres. (MARTIN, 2006)

In this case, it is indicated which phase is dominant regarding mechanical properties of the composite (continuous and dashed lines, where the first represents the dominant phase). When the fibres volume fraction, V_f, is lower than the critical fibres volume fraction, V_{crit}, then the composite mechanical properties are matrix dominated, which implies a composite with properties similar to the matrix phase. On the other hand, in cases of V_f values higher than the V_{crit} then the composite mechanical properties are fibre dominated, which implies a composite with properties similar to the fibre phase. One may observe that although

values in the lower vicinity of the V_f are indeed fibre dominant, due to the volume fraction of the matrix/fibre ratio, the overall composite mechanical properties yet present a matrix dominant phase behaviour. This observation implies that it is necessary more than a minimum V_f, where fibre phase is dominant, so that the mixture cause the composite to present a sensitive mechanical strength increasing. Therefore, in order to produce fibre-dominant mechanical properties composite, it is necessary to produce composites with a minimum volume fraction of fibre. This observation infers that fibre dominant mechanical behaviour composites are slightly sensitive to matrix mechanical properties variations, at least from a mechanical point of view.

Efforts have been made in order to develop low-cost alternative routes to produce CMC's (LUNDBERG and ECKERBOM, 1995), (JURF and BUTNER, 2000), (HASLAM, *et al.*, 2000), (HOLMQUIST, *et al.*, 2000). Some methods rely on multiple bundle/fabric infiltration which results in cost increasing due to the time-consuming process (HEGEDUS, 1991), (LANGE, *et al.*, 1995), (JOHNSON, *et al.*, 1998), (SHE, *et al.*, 2002) (SIMON, 2005). Figure 4 presents a schematic CMC process where fabric is infiltrated with slurry, and then laid-up, vacuum bagged and thermal treated.

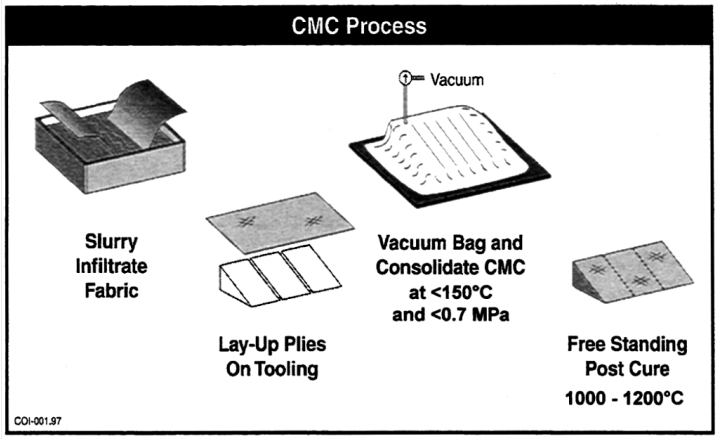

Figure 4 - CMC fabrication process (JURF and BUTNER, 2000).

2.5.1 Porous materials and porous matrices

Several sources in literature have related methods to obtain ceramics with porosity intentionally developed within the material. These materials are also known as ceramic with functional porosity. Those materials are used in wide fields of engineering.

A processing method to produce a carbon-fibre-reinforced silicon carbide with low-cost process was reported (MENTZ, *et al.*, 2006). That process yields a reaction-bonded silicon carbide matrix and avoids reactive damage of the carbon fibres with fibre-dominated behaviour and porous matrix.

Porous structures have been reported for fabricating of matrix composites. Weakly bonded particle mixtures of mullite and alumina were assessed as candidate matrices for use in porous matrix ceramic composites. Conditions for the deflection of a matrix crack at a fibre-matrix interface were used to identify the combinations of modulus and toughness of the fibres and the matrix for which damage-tolerant behaviour is expected to occur in the composite. For an aging temperature of 1200°C, the critical time exceeds 10000 h for mullite-rich mixtures (FUJITA, *et al.*, 2004). This reference reported variation in the porosity of pure mullite compacts with aging time (Figure 5). Despite the slight change in powder density, the porosity of the compacts remains essentially constant over the entire range of aging times, within 0.2% of its initial value.

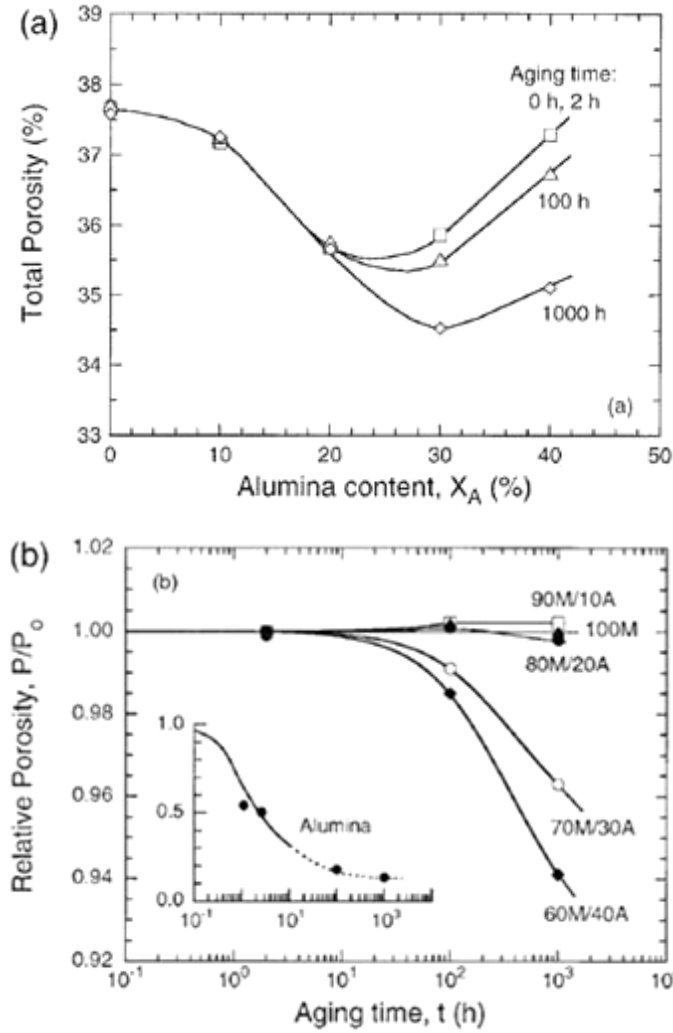

Figure 5 - (a) Effects of composition and aging time on compact porosity. (b) Results in (a), normalized by the initial (green) porosity at the same composition (FUJITA, *et al.*, 2004).

Mullite-alumina mixtures exhibit physical and mechanical characteristics that make them attractive for use as porous matrices in ceramic composites. The key attributes include stable porosity at the

targeted service temperatures of oxide composites, especially for alumina concentrations <20%, and combinations of modulus and toughness that should lead to deflection of a matrix crack at a fibre-matrix interface (FUJITA, *et al.*, 2004).
The composites Nextel fibres 610 and 720 with mullite porous matrix have been reported to present favourable mechanical properties both at room temperature and after high-temperature long-term aging. In this reference, the matrix was produced by colloidal processing (SIMON, 2005). This route provided a composite that exhibits damage-tolerance behaviour with fibres pull-out characteristics (Figure 6a and b). Highlighted in Figure 7a) and b) is the microstructure of the composite matrix. Nanometric particles of mullite surround micrometric mullite powder displaying core-shell structure.

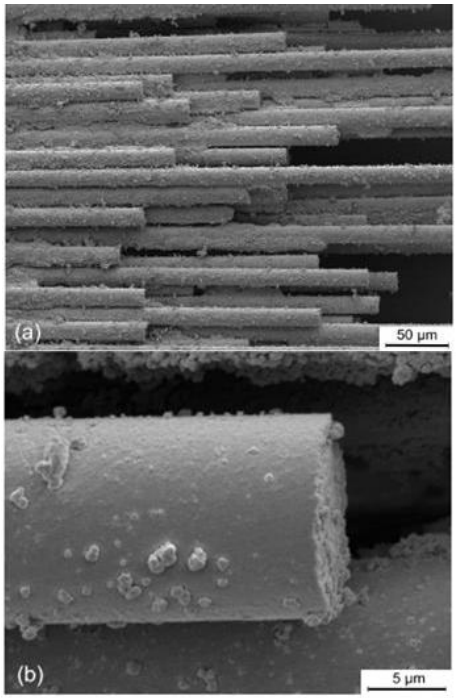

Figure 6 - (a) SEM micrographs of the fracture surfaces of N720/M composite tensile test specimens, displaying: (a) uncorrelated fracture of fibres within the fibre bundle and (b) fractured fibre after debonding from the porous mullite matrix. (SIMON, 2005)

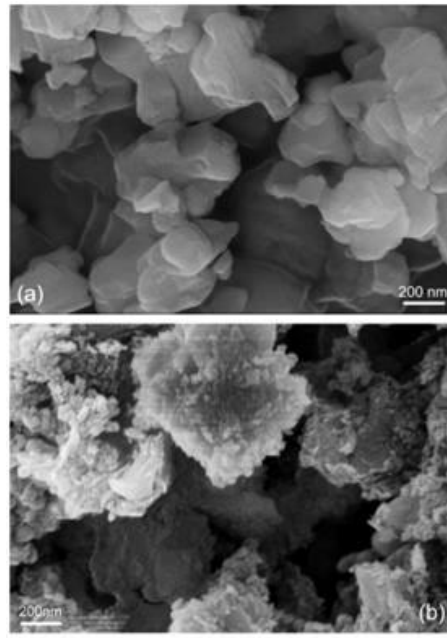

Figure 7 - SEM micrographs of the used ceramic powders: (a) mullite powder, and (b) mullite-nanopowder (M-N) mixture displaying composite particles with core-shell structure (SIMON, 2005).

More significant enhancements in stability have been achieved through the use of mullite as the main matrix constituent and alumina as the binder (LEVI, *et al.*, 1998) (CARELLI, *et al.*, 2002). In a common implementation, mullite powder is dispersed in aqueous slurry and infiltrated into a fibre preform via a vacuum-assisted technique. The two processing routes lead to distinctly different matrix topologies, shown schematically in Figure 8a. Compositional maps of two prototypical systems are presented in Figure 8 (b) (FUJITA, *et al.*, 2005), (ZOK, 2006).

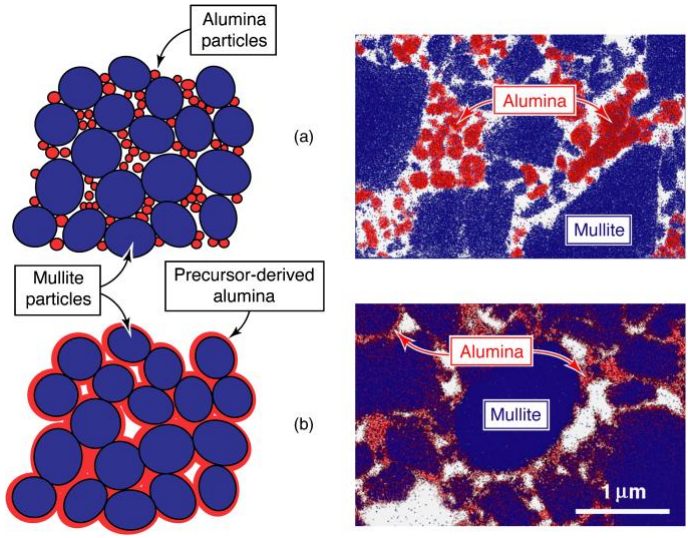

Figure 8 - Energy-dispersive spectroscopy/transmission electron microscope maps of thin foils of (a) 80% mullite/20% alumina (without precursor addition) and (b) pure mullite compact impregnated 10 times with the concentrated precursor (ZOK, 2006).

The preceding processing routes and the resulting microstructures are characterized by three attributes (ZOK, 2006):

- The mixed mullite/alumina slurry method allows both matrix phases to be infiltrated simultaneously. By contrast, the precursor route requires additional steps, beyond that of slurry infiltration, and is thus more costly.
- The presence of particulate alumina can compromise the stability of the mullite network, especially if its proportion exceeds the percolation threshold (FUJITA, *et al.*, 2004). Conversely, if the slurry is comprised of only mullite and the alumina is introduced subsequently via the precursor route, the contiguity of the mullite network is ensured.
- Because of limitations on the maximum fraction of alumina (to inhibit densification), the slurry route results in matrices that are relatively weak. Although essential for crack deflection, this weakness compromises the off-axis properties, especially the resistance to delamination. In contrast, the precursor allows filling of the void spaces

between the particles in the network (at least while the pores remain open), resulting in an increase in the mechanical integrity of the network. The latter route provides access to a broader range of matrix properties.

Other study related synthesis and characterization of porous mullite/alumina mixtures for use as matrices in oxide fibre composites (FUJITA, *et al.*, 2005). An assessment was made of the utility of a precursor-derived alumina (PDA) for controlling both the modulus and the toughness of mullite-rich particle mixtures. In this reference the PDA was Al powder slowly digested in a solution of $AlCl_3.6H_2O$ in deionised water at 85°C. Property changes are probed through models of mechanical behaviour of bonded particle aggregates. Consideration of the conditions for crack deflection at a fibre–matrix interface to ensure damage tolerance in a fibre composite was evaluated as well. Figure 9 presents some Fracture surfaces of three representative porous compacts.

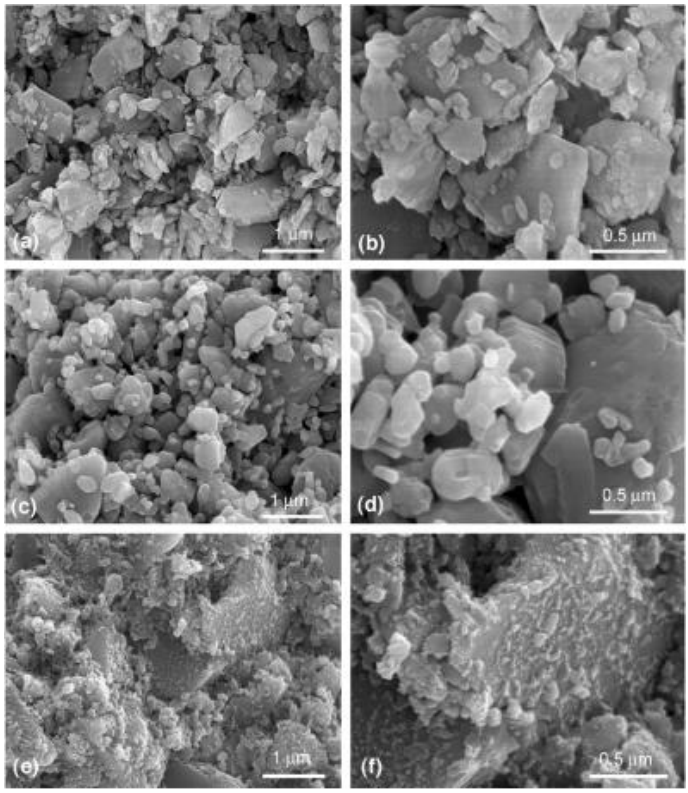

Figure 9 - Fracture surfaces of three representative porous compacts, all with pure mullite particle slurry, but with varying volumes of precursor derived alumina: (a, b) 0; (c, d) 8.3%; (e, f) 15.8%, after aging for 2h at 1200°C (FUJITA, *et al.*, 2005).

The precursor-derived route has the additional advantage over the mixed mullite/alumina particle route in that the contiguity of the mullite particle network is not compromised. Consequently, the structure is relatively immune from densification at the targeted upper use temperature for the corresponding fibre composites. Comparisons between predicted and measured properties suggest that the precursor-derived phase exhibits some degree of segregation to the particle junctions, yielding larger property elevations relative to that for a uniform precursor distribution (FUJITA, *et al.*, 2005). There are several commercial available fibres. Fabrics are produced by interweaving fibre tows in several satin sizing. Braiding is defined as "the process of

interlacing three or more threads in such a way that they cross one another and are laid in a diagonal formation, flat tubular or solid constructions may be formed in this way" (FARNFIELD and ALVEY, 1975).

2.5.2 Mechanical properties

Composites are known by their capability of enabling damage tolerance at room temperature, along with their ability of bearing load at high temperatures. Considering toughening mechanisms, there are a few that may be present in composite material, e.g. fibre pull out, fibre bridging, crack deflection etc. Figure 10 illustrates those toughening mechanisms.

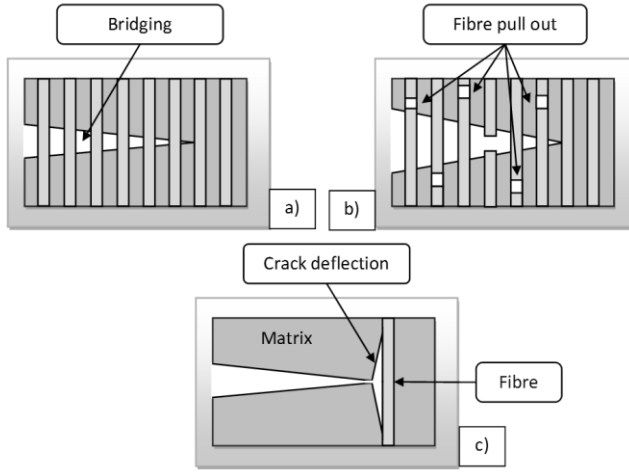

Figure 10 - Toughening mechanisms in composite materials.

Through bridging toughening mechanisms, fibres hinder crack propagation by preventing both upper and lower parts of crack from distancing from each other. When the crack extension crosses fibres deformation limit, then fibres start to fail. The intact part of the fibre starts to pull the failed part out of the matrix, in the fractured zone and the attrition between fibre and matrix surface is responsible for some energy consumption. An implicit toughening mechanism is present in the previously cited cases, which is crack deflection. Once the crack has to surround the fibre in order to keep the fibre intact for bearing loads, then crack deflection is a prerequisite for bridging and fibre pull out. Instead of it, if the crack moves through the fibre, than the composite

mechanical property comes closer to monolithic ceramic material and therefore presents no damage tolerance behaviour. In the literature there is an approach which gives a criterion for distinguishing whether the matrix/fibre combination will result in a penetration or a deflection of a moving crack through fibre/matrix interface (HE and HUTCHINSON, 1989), (HE, *et al.*, 1994). According to that theory, a combination of elastic mismatch and interfacial toughness between interface and matrix predicts whether the crack moves or not through the fibre (HE and HUTCHINSON, 1989). The zones, wherein penetration or deflection occurs, are presented in Figure 11.

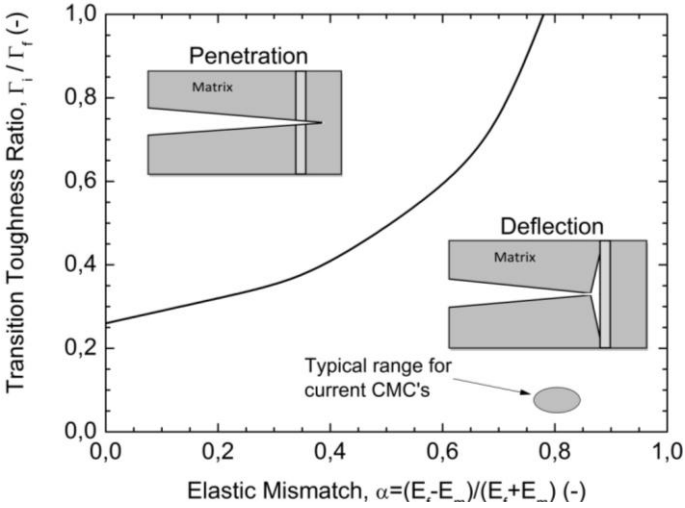

Figure 11 - He-Hutchinson criteria for crack deflection. (ZOK and LEVI, 2001).

The information in this graphic infers that a matrix/fibre interface with values closer to one, i.e. heavy bonded fibre and matrix, tends to cause the crack move through the fibre, which is not an interesting feature. In order to enable the deflection feature in a composite two alternatives are suggested: either by coating fibres (MORGAN, *et al.*, 1995), (BOAKYE, *et al.*, 1999), (KERANS and PARTHASARATHY, 1999), (CHAWLA, *et al.*, 2000) (JACKSON, 2006), (JACKSON, 2006) or introducing porosity within the matrix (ZOK and LEVI, 2001), (MATTONI, *et al.*, 2001), (FUJITA, *et al.*, 2004), (FUJITA, *et al.*, 2005).

2.5.3 High Temperature Properties of Composites

The most notable feature contrasting monolithic and composite ceramic materials lays on the fact that composite materials can bear similar magnitudes of load both at room and at high temperatures and can also withstand damage without brittle fracture. In this section, some data concerning these composite features are introduced.

Porous-matrix oxide/oxide CMCs exhibit several behaviour trends that are distinctly different from those exhibited by traditional CMCs with a fibre–matrix interface. Most SiC-fibre-containing CMCs exhibit longer life under static loading and shorter life under cyclic loading. For these materials, fatigue is significantly more damaging than creep.

The high-temperature mechanical behaviour of a porous matrix Nextel 610/aluminosilicate composite was investigated (LEE, *et al.*, 1998) (ZAWADA, *et al.*, 2003). Results revealed low creep resistance limiting the use of that CMC to temperatures below 1000°C. Because creep was shown to be much more damaging than cyclic loading to oxide–oxide CMCs with porous matrix, high temperature creep resistance remains among the key issues that must be addressed before using these materials in advanced aero space applications (RUGGLES-WRENN, *et al.*, 2006), (MEHRMAN, *et al.*, 2007), (RUGGLES-WRENN and BRAUN, 2007).

Ceramic matrix composites, capable of maintaining high strength and fracture toughness at high temperatures are prime candidate materials for aerospace applications. Additionally, the low density of CMCs and their higher service temperatures, together with a reduced need for cooling air, contributes for improving high-temperature performance when compared to conventional nickel-based superalloys (ZAWADA, *et al.*, 2003). Concurrent efforts in optimization of CMCs and in design of combustion chambers are expected to accelerate the insertion of the CMCs into aerospace turbine engine applications, such as combustor walls of turbines (PARLIER and RITTI, 2003) (MATTONI, *et al.*, 2005), (PARTHASARATHY, *et al.*, 2005). Up to date, the majority of CMCs development has been driven by the continuous will to improve the performance of military and commercial aircrafts (PARLIER and RITTI, 2003). CMC are suitable for applications up to 1100°C such as flame-holder, exhaust cone and inner flaps for convergent nozzles (see Figure 12).

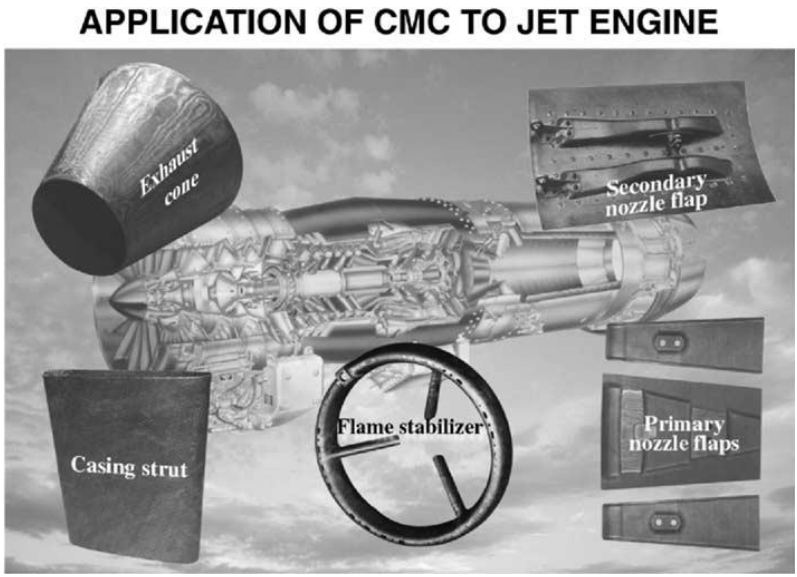

Figure 12 - Typical CMC projects on Jet Engines (PARLIER and RITTI, 2003).

Because these applications require exposure to oxidizing environments, the thermodynamic stability and oxidation resistance of CMCs are vital issues. The need for environmentally stable composites motivated the development of CMCs based on environmentally stable oxide constituents (LANGE, *et al.*, 1995) (MOUCHON and COLOMBAN, 1995), (TU, *et al.*, 1996), (SZWEDA, *et al.*, 1997).

From a decade ago, oxide composites have emerged as viable candidates for high-temperature thermostructural applications. Their rapid evolution is attributable to recent developments in materials and microstructural concepts, both for enabling damage tolerance and for ensuring long-term morphological stability at the targeted service temperatures. These are expected to play a significant role in future material designs and their implementation in engineering systems (ZOK, 2006).

The advantages for the developers are obvious: the low specific weight and the high specific strength over a large temperature range. Since the start of development, test times of 8900 s (approx. 2,5 h) at wall temperatures of up to 2000 K and combustion-chamber pressures of 10-11 bars were reached within the scope of various test campaigns. Advanced reusable space launch vehicles will likely incorporate fibre-

reinforced CMCs in critical propulsion components (SCHMIDT, *et al.*, 2004).

The application of two oxide–oxide composites, Nextel 720/aluminosilicate and Nextel 720/alumina, in the design of a combustor was evaluated using a combination of rig testing and numerical analysis. The rig tests showed the alumina-matrix composites to survive up to ten hours of use, while the alumniosilicate matrix composites suffered radial cracks in the ±45° oriented regions (Figure 13). The use of appropriate fibre architecture to meet the combustion design needs is suggested (PARTHASARATHY, *et al.*, 2005)

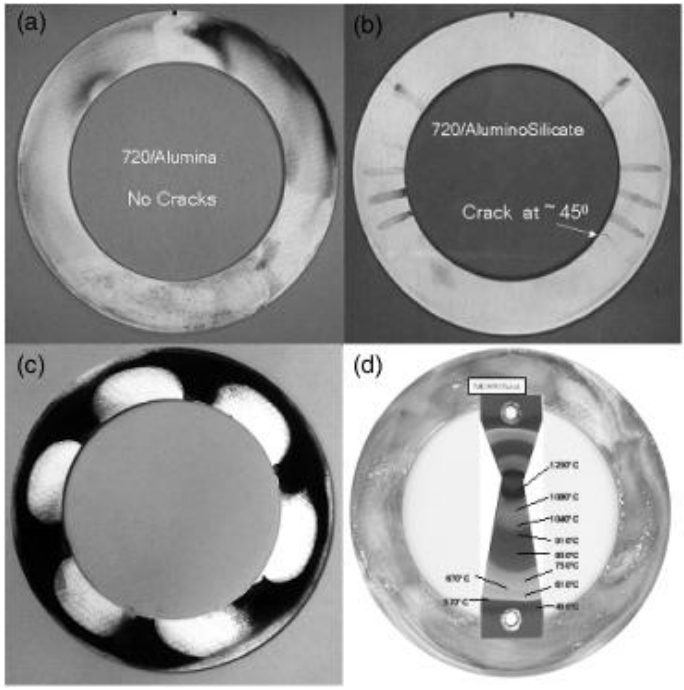

Figure 13 - Tests in a combustor: (a) alumina matrix composites with no cracks; (b) aluminosilicate matrix composites exhibiting cracks at the same location. (c) combustor under conditions for soot formation, . (d) maximum temperature reached to be around 1200°C.(PARTHASARATHY, *et al.*, 2005)

3 MATERIALS AND METHODS

The experimental procedure of this work can be summarized as:

- Slurry preparation and characterization;
- Composite panel production;
- Thermal treatment development;
- Physical and mechanical properties characterization of both the composite panel and the matrix material;
- Oxidation kinetics determination.

3.1 MATERIALS

For the RBMAO process development the used raw materials were aluminium powder (Eckart-Werke, Ecka AS 081 – <45 µm), mullite powder (Treibacher, WFM 0.08 – 80 µm) and phenolic resin powder (novolac, Hexion corp., PF 0227 SP 01). For adjusting the slurry viscosity, a phosphate ester (PE) dispersant (Zschimmer & Schwarz, Dolacol D1001) was used. In order to produce composites from RBMAO matrix, a reinforcement was added (Nextel 720 ™ woven fibre, 3M) into eight-harness satin woven fabrics. For the oxidation kinetics experiment commercial aluminium carbide (99% Al_4C_3, Sigma Aldrich, USA, 325#mesh) was used.

3.2 POWDER PREPARATION

The slurry for infiltrating the fibre fabric woven was prepared by combining the ceramic powder, i.e. mullite, and the metallic powder, i.e. aluminium, and milling the mixture using an attritor mill (NFT PE 075), balls and jar of Zirconia and using acetone as milling media without atmosphere controlling. For each mill batch the mixture consisted of 88.6 g of mullite and 11.4 g of aluminium powder. In order to evaluate relationship of particle size and milling time a standard mixture was loaded into the mill jar and samples of the slurry were taken out in intervals of every hour. The particle size distributions of these samples were measured (Mastersizer, Malvern MS5). The measuring procedure consisted of braking agglomeration by dipping an ultrasonic probe into the collected sample for 1 min and proceeding the measuring right afterwards.

3.3 VISCOSITY DETERMINATION OF THE SLURRY

The viscosity determination of the slurry to be used in the fibre fabric woven infiltration was split in three steps: optimising dispersant amount (in the range from 0.6 to 2.0% of solid content, according to the supplier); finding the maximum slurry solid content; and measuring the effect of the phenolic resin addition. Moreover, before any viscosity measurement, the slurry was dispersed by dipping an ultrasonic probe into the slurry container for 1 min. A cup/rotor set was used in the viscometer (MV1, Haake RV 20). The shearing stresses measured were in the range from 1 to 400 s^{-1}, with a dwelling time of 1 min and then returning to 1 s^{-1} according to Figure 14:

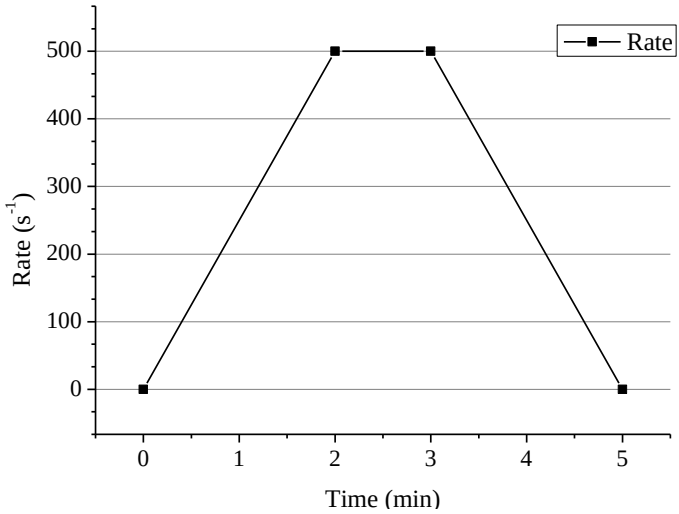

Figure 14 - Viscosity measurement set points

A calibration test was done previously to the viscosity measurements. It consisted of measuring the viscosity of a standard fluid (Brookfield standard fluid with nominally 50 mPa.s) within the rate variation range.
The first step consisted in preparing samples with 40 ml slurry (45 wt.%) in different containers and varying the dispersant amount for each one, which will be tagged as PE%.
The second step consisted in preparing samples with 40 ml slurry (with the PE% optmised) in different containers with stoichiometric amount of

phenolic resin in relation to the aluminium content and varying the particle volume fraction for each one.
The third step consisted of prepare samples with 40ml of slurry (with the better PE%) in different containers with stoichiometric amount of carbon graphite in relation to the aluminium content and varying the particle volume fraction for each one.

3.4 THERMAL TREATMENT CYCLE DETERMINATION

In order to determine the set points of the thermal treatment to which the composite panel would be submitted, a characterization of the raw material mixture of the matrix was carried out. The whole thermal treatment process consisted of two programmed steps, one in inert atmosphere and the other in oxidizing atmosphere. The purpose of the first thermal treatment is to form the intermediate carbide phase, which is a product from the reaction of the pyrolysed carbon with the aluminium powder. The second thermal treatment is to oxidize the previously formed carbide phase and to convert it in to an oxide ceramic. Therefore to characterize the thermal treatment cycles some differential thermal (DTA) and thermogravimetric (TG) analyses (Netzsch DTA/TG STA 409) were performed. Phase analyses (Bruker AXS D8 Discovery) were based in powder X-Ray diffraction. The XRD was set to a step of 0.02° and reading time of 2 s using k_α ($\lambda = 1{,}5418$ Å).
Those characterization techniques may be divided in three parts:

- reaction thermal treatment;
- oxidation thermal treatment and;
- TG of mixtures in excess and in stoichiometrical additions, in relation to the carbon and aluminium content.

For the reaction thermal treatment characterization, three different analyses were performed. Firstly, a sample of the phenolic resin underwent an inert atmosphere DTA/TG analysis with heating rate of 10°C/min until 1450°C. Subsequently, a sample of the dried slurry powder containing mullite, aluminium and resin underwent an inert atmosphere DTA/TG analysis with same heating cycle of the first DTA/TG test. Then, the present phases of a powder sample, which were submitted to the first thermal treatment, were detected by means of XRD analysis.
For the oxidation thermal treatment characterization, three different analyses were done. Firstly, a sample containing mullite and aluminium powder underwent an oxidizing atmosphere DTA/TG analysis with heating rate of 10°C/min until 1450°C. Afterwards a sample of the

mullite and aluminium powder and phenolic resin underwent a DTA/TG analysis at the same heating cycle. Then, the present phases of powder sample, which were submitted to the second and final thermal treatment, were determined by XRD.
Additionally, two samples of mullite and aluminium powder were analysed by DTA/TG. The difference between samples was the amount of resin: the first one had a stoichiometric ratio and the second one had 50%mol more than the stoichiometric ratio.
The stoichiometric ratio was determined according to equation 4:

$$\begin{array}{lll} 4Al_{(s)} + 3C_{(g)} & \leftrightarrow & Al_4C_{3(s)} \\ 4 \cdot 27g + 3 \cdot 12g & \leftrightarrow & 144g \end{array} \quad \textbf{4}$$

Considering that the mixture was prepared with 88.6 g mullite and 11.4 g aluminium, the stoichiometric value was 6.9 g and the value in excess was 9.9 g, respectively for the phenolic resin. The latest value corresponds to the suggested set point for the oxidation thermal treatment.

3.5 FIBRE FABRIC WOVEN INFILTRATION

In order to produce the composite panel according to the developed matrix route suggested in this work, the fibre fabric woven had to be prepared, since it is provided with a sizing from the supplier. Before the infiltration process, therefore, a desizing thermal treatment was performed, following the procedure established by the supplier (3M); heating rate of 7°C/min until 700°C with dwell of 30 min for small samples and 2 h for large samples.
The tools required for the infiltrations process are presented in Figure 15.

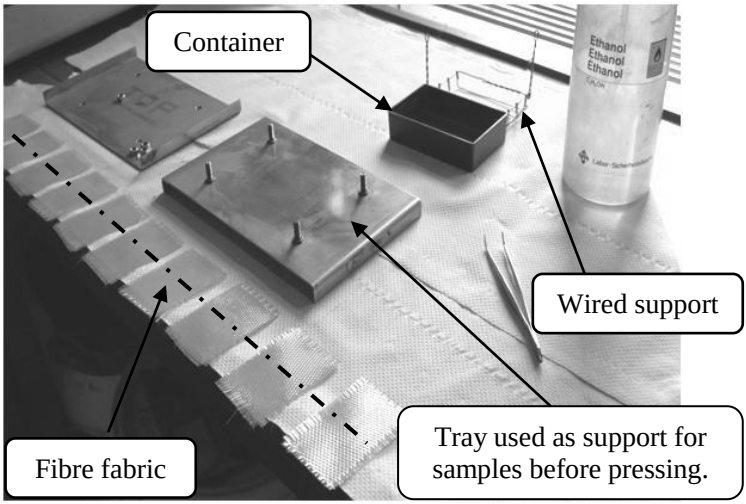

Figure 15 - Set-up of infiltration process.

The milled powder containing 88.4g mullite, 11.6 g aluminium and 6.9 g of phenolic resin was mixed with ethanol to produce a slurry for infiltrating the fabric woven of 720 Nextel fibres. In this slurry 0.6 wt.% phosphate ester dispersant was also added. The slurry was mixed for 30 min in a magnetic stirrer. The slurry was then poured into a container with a wired support, which holds the fabrics and helps the extraction of the fibre fabrics out of slurry container. Finally, fibres were dipped into the slurry, and the infiltration process was assisted by an ultrasonic bath (Figure 16).

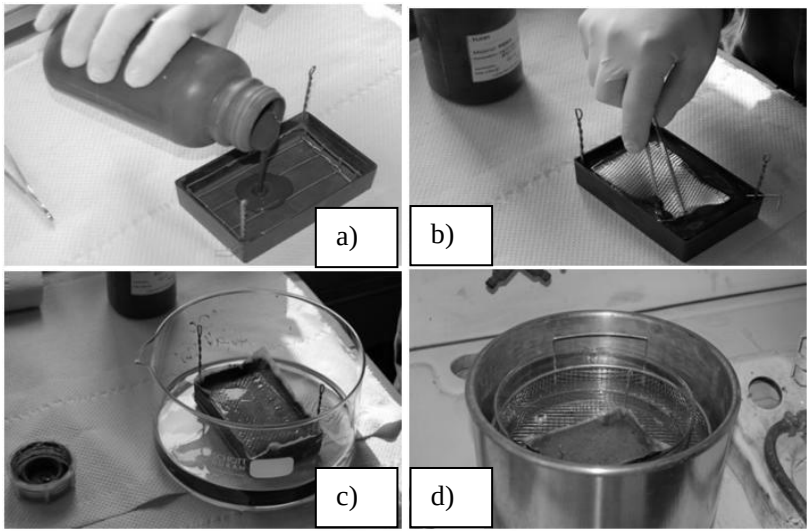

Figure 16 - Infiltration process: (a) slurry poured into the container; (b) fibre fabric woven dipped in the slurry; (c) slurry container in a becker; (d) becker in an ultrasonic bath.

In Figure 16 (c and d), the green cover placed over the container with slurry is wetted with ethanol in order to cause the slurry not to dry along the infiltration process. After 10 min infiltration process, the fibres were taken out of the slurry and placed onto the support tray in order to cast off the excess slurry, by pressing the whole set with trays and fibre fabric woven with pressure of 0.7 MPa for 30 s. After this time, nuts were then finger tightened in order to keep the fibres together; and only later on the pressure was released.

A cylinder was placed over the tray to better distribute the pressure onto the tray and therefore to compact fibres with homogeneity. Then, in order to dry the infiltrated fibre fabric, the tray set was placed in a vacuum chamber for 24h.

3.6 POROSITY

For the porosity measurement two types of samples were considered:

- Dried slurry; and
- Compacted monolithic bars (as used for the mechanical test).

In the first case, samples were prepared by drying the slurry so that only the respective solid contents, 50 and 60 wt.% were evaluated. Due to the

irregular dimensions, those samples were measured by Archimedes' principle.
In the case of pressed samples, the density was first geometrically determined and converted to porosity.
In both cases, the experimental plan was designed in two levels. Firstly, the composition varied:, just mullite and aluminium powder with the same content of the slurry for infiltration with exception of resin content. With these samples the pressure for compaction was varied in two points, i.e. 50 and 200 MPa.
In the second case, the samples had the same composition of the slurry for infiltration, and compaction pressure was 50 MPa. Moreover, the powder for the pressed samples was prepared by drying a slurry batch with composition of 88.4 g mullite and 11.6 g aluminium powder, with addition of 6.9 g phenolic resin, and sieved in 200 #mesh. All samples were weighted (2 g) prior to feeding the compaction mould. Those samples are described in Table 1:

Table 1 - Experimental plan for porosity measurement.

Method	Variation	
Archimedes	50 wt.% solid content	60 wt.% solid content
Geometrical	Without resin 50 (WOR50) and 200 MPa (WOR200)	With resin 50MPa (WR50)

For measuring the samples weight a balance with a 0.001 g resolution was used (R200D, Sartorius). The theoretical density was obtained by calculating the density of a solid with 80 wt.% mullite and 20 wt.% alumina using the rule of mixture, considering the theoretical density of each component.

3.7 LINEAR SHRINKAGE

For the linear shrinkage determination, the same features applied in geometrical porosity measurement were used, i.e. monolithic bars with and without resin and pressed either with 50 MPa or 200MPa. The initial dimensions of the samples are presented in the Table 2.

Table 2 - Experimental plan for linear shrinkage measurement.

Samples	Dimensions (LxWxH) [mm]
Without Resin 50 MPa (WOR50)	47.2x6.7x4.6
Without Resin 200 MPa (WOR200)	42.2x6.7x3.8
With Resin 50 MPa (WR50)	47.2x6.7x4.4

The largest dimension (length) was considered to determine the linear shrinkage. Then 30 samples of each group were prepared and underwent a two-stage thermal treatment. The length of the samples was measured after oxidation for both groups and after every thermal treatment for the group with resin.

3.8 DENSITY

For density determination the samples had the same configuration used for the linear shrinkage. Nevertheless, only 10 samples were considered for measuring density, which was performed geometrically.

3.9 MECHANICAL BEHAVIOUR OF MATRIX AND COMPOSITE

For the mechanical test of the matrix material bars with same characteristics used for linear shrinkage determination, were applied. In this case, 30 bars were considered. The mechanical tests were done according to the ASTM C1161 – 02c and 1341 - 00 standards (ASTM - C 1341 - 00, 2003)(ASTM - C 1161 - 02C, 2003). Considering the samples dimensions, the used rate in the test was 2mm/min. For measuring the flexural load, a universal testing machine (ATS, model 27-z-0007-D96) was used (see Figure 17).

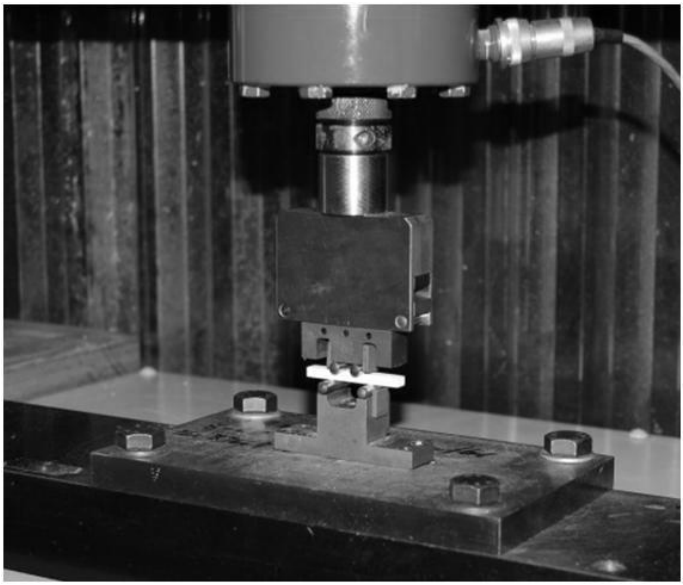

Figure 17 - Apparatus for measuring the flexural strength.

A four-point flexural mechanical testing set was applied, with a span of 20 mm and a bearing roller with 4 mm diameter. The bearing roller was fixed with the help of magnets to ensure a degree of freedom for the tested samples during test. In Figure 17 the magnets are the squared plates right on side of the bearing roller, in accordance with ASTM C1161 – 02c and 1341 - 00. A Weibull approach was fitted to the strength results in order to determine the mechanical properties of each group.
Additionally, the mechanical behaviour of a composite panel produced from 720™ Nextel fibre fabric woven was evaluated using the same testing set, with dimensions according to ASTM C1161 and 1341. The panel configuration corresponded to eight infiltrated layers of fibre fabrics with 45x6x3mm (LxWxH, respectively).

3.10 MICROSTRUCTURAL ANALYSES

The microstructure was examined by scanning electron microscopy (SEM, Philips XL 30, FEI CO.; JEOL JSM-6390LV), field emission gun scanning electron microscopy (FE-SEM, Leo Gemini 1530) and optical microscopy (OM, Aristomet) with a CCD camera.

First characterizations were carried out for samples taken out of the composite panel with the aim of evaluating the flaw density after thermal treatment cycles. Those images were also considered for evaluation of fibre surface quality after thermal treatment. Additionally, three groups of matrix samples were considered. Those samples were analogue to those used in the linear shrinkage with some additional compaction pressure values, i.e. without resin, pressed at 25, 50, 75 100 and 200 MPa and with resin, at 50 MPa. The microstructure of the composite panel was also evaluated in SEM and OM. SEM images in SE (secondary electron detection) were considered under several magnifications.

3.11 OXIDATION KINETICS

The oxidation kinetics was evaluated in order to determine the activation energy for the oxidation of aluminium carbide. In this context, two experiments were suggested. The first one is related to the oxidation kinetic of the aluminium carbide with a mixture of 50 wt.% mullite and aluminium powder with the stoichiometric amount of resin to provide carbon for the carbide formation. This mixture underwent the reaction thermal treatment proposed in this work without the oxidation thermal treatment to produce a mixture with non-oxidized carbide. This powder mixture was then submitted to a TG analysis in isothermal dwells at 600°C to 1200°C, with a heating time schedule of 1h up to the dwelling temperature.

The second experiment was the determination of the apparent activation energy of oxidation process of a commercially available aluminium carbide powder (Aluminium Carbide 99%, Sigma Aldrich, 325#mesh). In this context, the commercial powder underwent the same test configuration of the first experiment.

Prior to these evaluations, two different samples were submitted to a DTA/TG analysis in order to qualitatively evaluate the oxidation kinetics. The difference between those samples was the presence of carbide phase. They consisted of 50/50% mullite/aluminium; in the case of carbide phase then phenolic resin was added to the mixture and it underwent the reaction thermal treatment. Therefore, this experiment was planned to evaluate the oxidation kinetics of aluminium and aluminium carbide powder in a qualitative way.

4 RESULTS

The presentation of results was organized according to fabrication process steps, i.e., powder preparation, panel production, thermal treatment and characterization. All results are first presented and then discussed at the end of the section.

4.1 POWDER PREPARATION

Figure 18 presents the evolution of the particle size as the milling time increases.

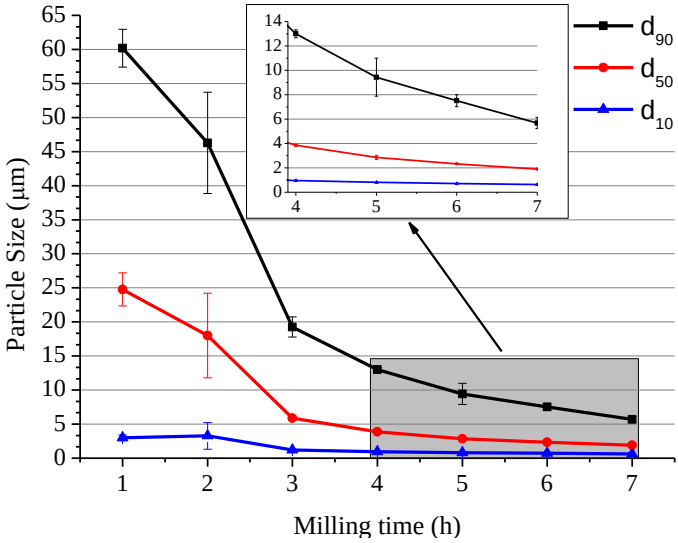

Figure 18 - Evolution of the mean particle size according to milling time.

The presented curves show different particle sizes. According to the literature for reaction bonding processes, mean particle sizes, i.e. d_{50}, lower than 2 µm are acceptable for producing final parts without flaws arising from the thermal treatment. The milling time from the mixture used in this work was, therefore, fixed in 7 h.

4.2 VISCOSITY

The slurry viscosity variation regarding the dispersant agent is presented in Figure 19, for a fixed shear rate of $400s^{-1}$.

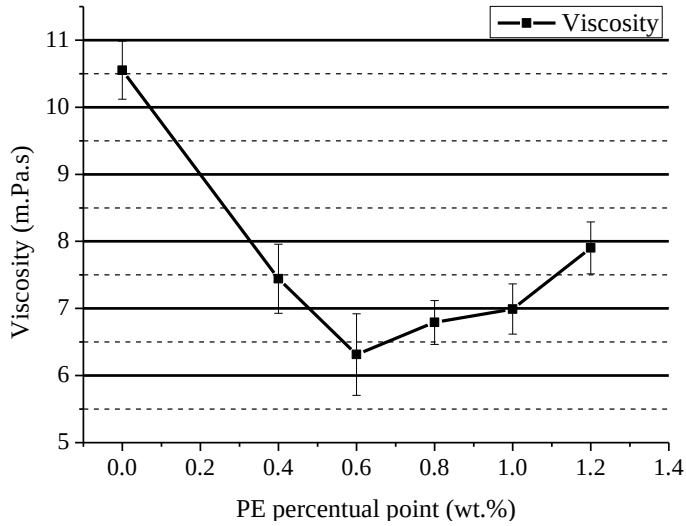

Figure 19 - Slurry viscosity as a function of the dispersant amount.

The viscosity presents a minimum value at 0.6 wt.% dispersant with regard to the solid weight percentage. This was the set value in order to perform further characterization of the slurry. Moreover, the viscosity and shearing stress of the slurry containing 0.6% as a function of the shear rate is presented in Figure 20.

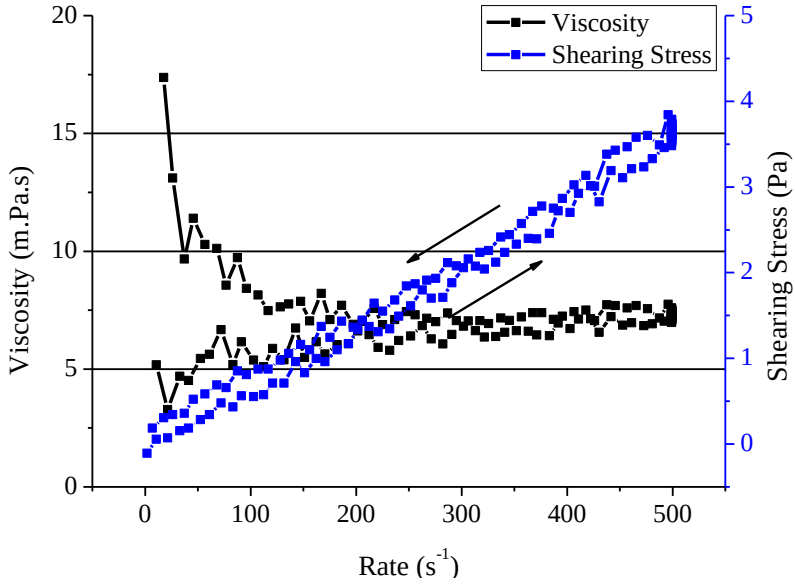

Figure 20 - Shearing stress and viscosity of a slurry with 0.6 PE%

Although the slurry viscosity presented a slightly rheopexic behaviour (area of 72.1 $Pa.s^{-1}$), it showed a quasi Newtonian fluid behaviour (blue curve in Figure 20). The rheopexic behaviour found may be associated with the time it dwelled at $500s^{-1}$, which may have caused the slurry to dry, since ethanol was the solvent. The slurry viscosity presented values of 6.31± 0.77 mPa.s which can be verified in the black curve of Figure 20.

The second step of characterization was the slurry viscosity variation with regard to the solid content (Figure 21). Table 3 presents log values of the non-linear curve fitting.

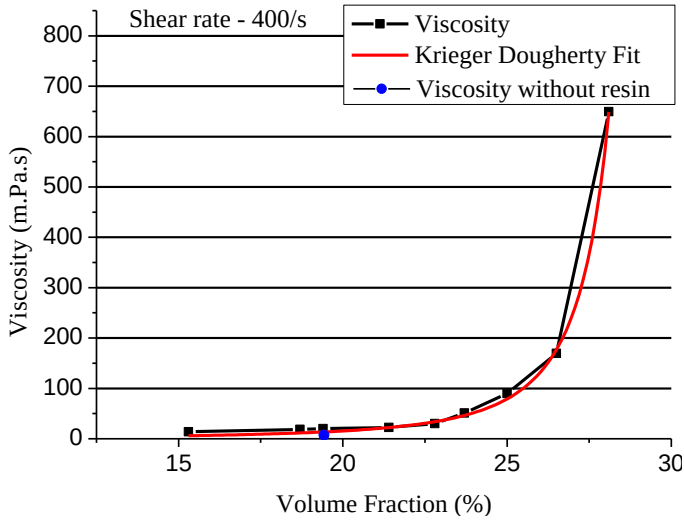

Figure 21 - Viscosity as a function of the particle volume fraction in a slurry with phenolic resin addition.

Table 3 - Log values of the non-linear curve fitting.

Model	**Krieger – Dougherty**		
Equation	$\eta_r = \left(1 - \frac{\phi}{\phi_m}\right)^{-\eta\phi_m}$		**5**
Reduced Chi-Sqr		45.18328	
Adj. R-Square		0.99893	
		Value	Standard Error
Maximum Volume Fraction of particles [-]	Φ_m	0.304	$1.45*10^{-4}$
Intrinsic Viscosity [Pa.s]	η	8.2	-
Solvent Viscosity [Pa.s]	η_s	1.074	-

According to Figure 21 and Table 3, the maximum volume fraction of particles, which can be achieved with this slurry, is approximately 30%. This value is not reasonable when compared to literature values for similar suspensions with ceramic particles, which have similar shapes (RAHAMAN, 2003). The found intrinsic viscosity was 8.2 Pa.s, which

is more related to fibre-shaped particles. Spherical particles tend to present intrinsic viscosity values of about 2.5 Pa.s. Additionally, the slurry with the highest solid content presented shear thinning behaviour. The second step of characterization was the slurry viscosity as a function of solid content with addition of carbon powder (Figure 22). Table 4 presents log values of the non-linear curve fitting.

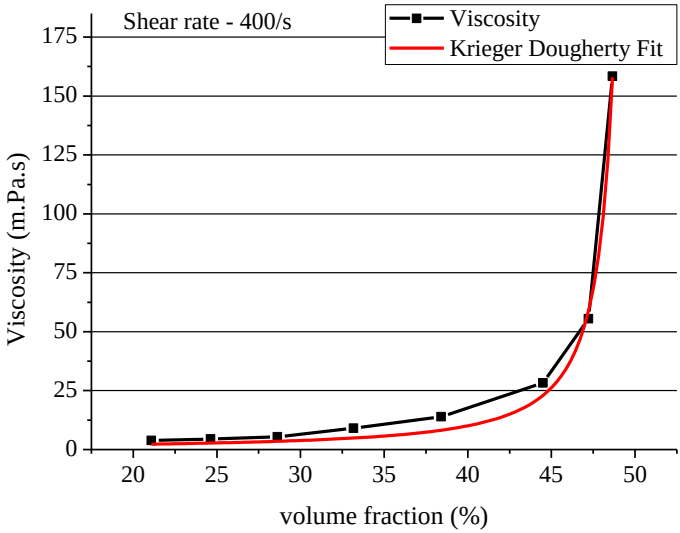

Figure 22 - Viscosity as a function of the particle volume fraction of slurry with graphite addition.

Table 4 - Log values of the non-linear curve fitting.

Model		**Krieger – Dougherty**	
Reduced Chi-Sqr		13.9298	
Adj. R-Square		0.99502	
		Value	Standard Error
Maximum Volume Fraction of particles [-]	Φ_m	0.501	$3.22*10^{-4}$
Intrinsic Viscosity [Pa.s]	η	2.785	-
Solvent Viscosity [Pa.s]	η_s	1.074	-

According to Figure 22 and, the maximum volume fraction of particles, which can be achieved with this slurry, is approximately 50%. This is a reasonable value when compared to literature values for similar suspensions of ceramic particles with similar shapes (RAHAMAN, 2003). The intrinsic viscosity found was 2.8 Pa.s, which is also related to spherical particles (RAHAMAN, 2003).

Concerning the results in this section, the set points for producing a stable suspension of the raw material mixture with addition of phenolic resin in ethanol were:

- 0.6 wt.% phosphate ester dispersant;
- 45 wt.% solid content slurry.

Some slurries were then produced, in which fibre fabric woven were infiltrated and composite panel were produced. To produce composite panels using phenolic resin for both prepreg consolidation and for carbon source to the carbide reaction, this resin was applied to the slurries. Although the slurry exhibited enough stability for going through the infiltration process without any phase segregation or precipitation, the slurry presented neither high solid content nor low viscosity. Those properties are required for a desirable fibre fabric woven infiltration and composite panel production, which means composites with desired mechanical strength. Lower viscosity, i.e. 50mPa.s, and higher solid content, i.e. approximately 45 vol. %, or ~80 wt.%, are desirable slurry properties for fibre fabric woven infiltration (MACHRY, 2010),(WAMSER, 2010).

In order to evaluate the slurry properties with the phenolic resin replacement, an evaluation of the slurry viscosity with graphite powder was carried out. According to the results of Figure 22, which are summarized in Table 4, the application of graphite as an alternative source for carbon to be used in the carbide reaction is a promising way for lowering the slurry viscosity. Detrimentally, the composite route production might lose the potential for producing prepregs with enough green handling strength, once the phenolic resin is not only the carbon source, but also it consolidates the infiltrated fabric woven by solvent drying. Nonetheless, small additions of phenolic resin for this purpose may not harm the low viscosity of the slurry, which was achieved with the application of the graphite powder. Consequently, a combination of graphite powder with small contents of phenolic resin is suggested. Therefore, a mixture combining 3 g graphite powder and 0.7 g phenolic resin might be used in order to produce a slurry, which not only presents low viscosity, but can also consolidates the fibre fabrics into prepregs.

4.3 THERMAL TREATMENT

Figure 23 presents DTA/TG analyses of phenolic resin in an inert atmosphere (Argon).

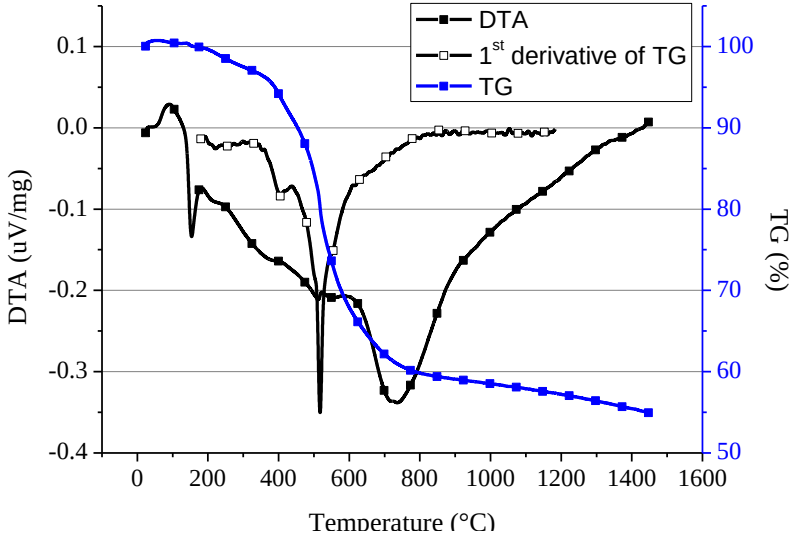

Figure 23 - DTA/TG analysis of phenolic resin in an inert atmosphere.

Novolac-Type phenolic resins are normally used in applications which require high amounts of residual carbon after pyrolysis. The 1st derivative curve of the TG analysis shows a sharp peak at a ~500°C and a smaller peak at ~400°C. This sample presented a residual carbon amount of 55% (last point of TG blue curve). The first dwell temperature was considered as 400°C, followed by another dwell temperature at 500°C.

Figure 24 presents DTA/TG analyses of raw materials mixture in an inert atmosphere.

/

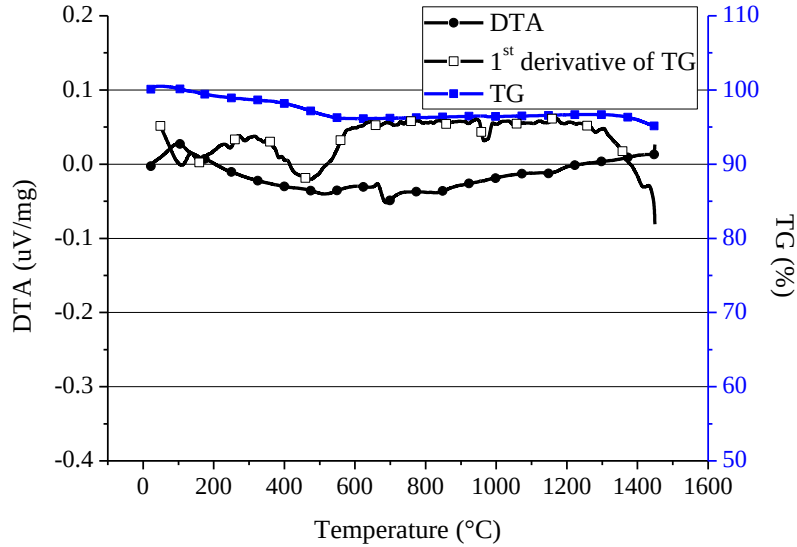

Figure 24 - DTA/TG analysis of raw materials mixture in inert atmosphere.

The 1st derivative curve of TG analysis shows a peak in the same temperature range of that presented in Figure 23, although in a smaller intensity. It is associated with the available pyrolysing material which is losing mass. The reason behind this analysis was to evaluate whether the resin with the mixture of raw material would behave the same way it did non-combined . This hypothesis was confirmed by the presence of the peak in the same temperature range. Moreover, in this TG curve, no weight change regarding to oxidation of the metallic aluminium powder was observed due to the non-oxidizing atmosphere.
Figure 25 presents XRD analysis of raw materials mixture after thermal treatment.

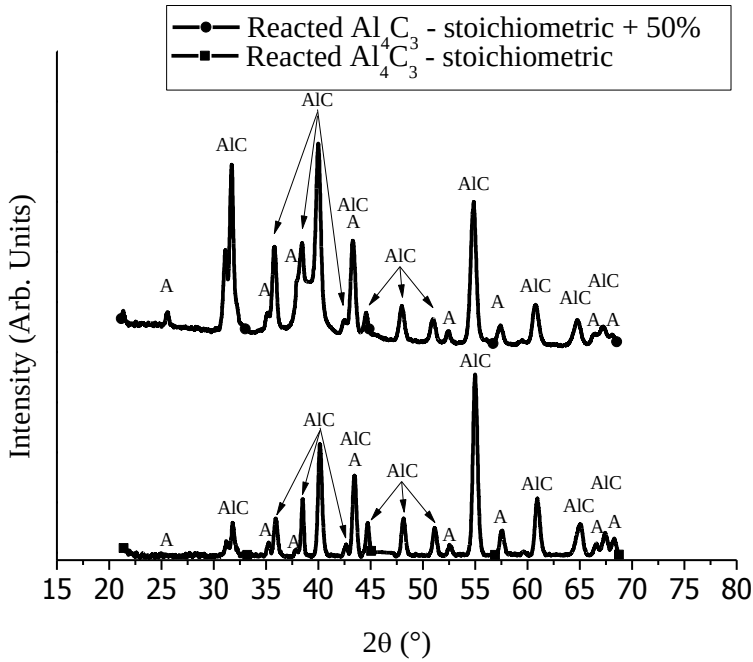

Figure 25 - XRD after reaction thermal treatment, with stoichiometric and 50%mol excess resin content.

This figure shows results of two distinct samples. The upper curve presents XRD patterns for the sample with composition of the combined raw materials with the addition of resin in excess of 50%mol in relation to the stoichiometry amount for aluminium carbide formation. T the lower curve presents patterns for the sample with stoichiometric amount of resin. In both XRD curves the after the suggested reaction thermal treatment the intermediate carbide phase was formed. The Figure 26 presents the suggested set points for the thermal treatment.

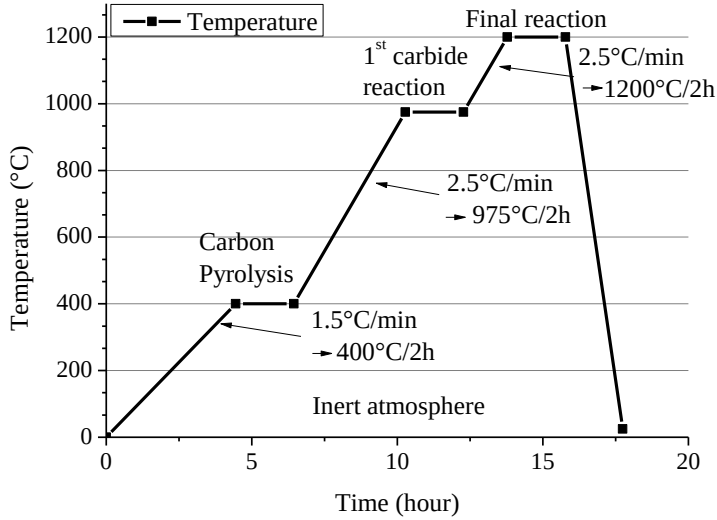

Figure 26 - Reaction thermal treatment set points suggested in this work.

In this figure dwelling temperatures are 400°C, 975°C and 1200°C, for the carbon pyrolysis, first carbide reaction and final carbide reaction, respectively. Argon provided the inert atmosphere characteristic for this thermal treatment.

Following the analyses, the DTA/TG of raw material mixtures without resin is then presented in Figure 27.

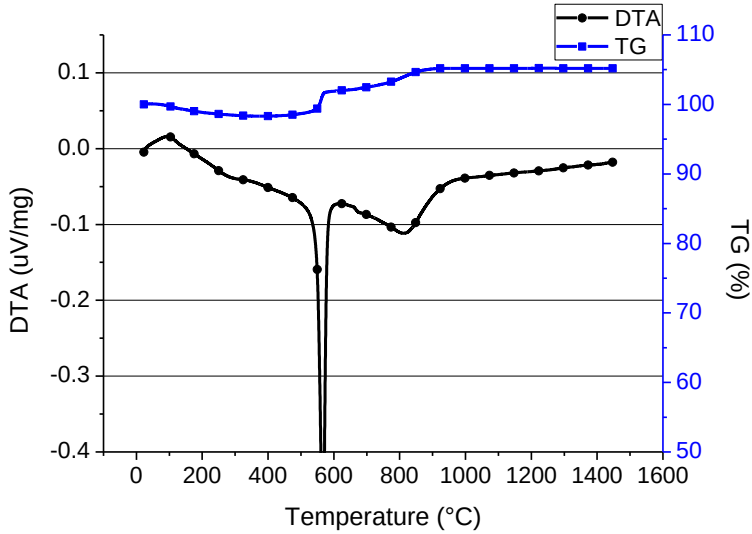

Figure 27 - DTA/TG analysis of raw materials mixture without resin in oxidizing atmosphere.

Two different behaviours may be detected in comparison to those in the inert atmosphere (DTA/TG), which is the weight gain, with starting temperature in the range of 600°C and a very well defined exothermal peak associated to this weight gain. Considering the sample composition, those two features are associated to the oxidation of the metallic aluminium powder, since in this analysis, there was neither the reaction thermal treatment nor the resin content in the mixture, and therefore no carbide reaction could have taken place. Therefore, the single available component for oxidation reaction was the aluminium powder. Moreover, the presented curves are consistent with the available RBAO literature data: not only the extremely defined peak in the DTA curve at 600°C, but also the weight gain in two steps depicted in the TG curve.

The DTA/TG of raw material mixture with resin result is then presented in Figure 28.

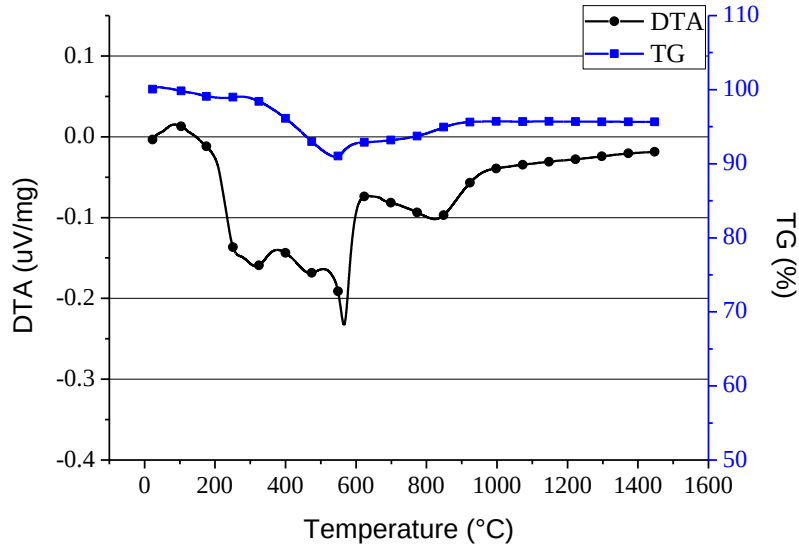

Figure 28 - DTA/TG analysis of raw materials mixture with resin in oxidizing atmosphere.

The TG curve presents weight loss in the temperature range of 300-500°C, associated to the pyrolysis of resin and consistent with the temperature range of weight loss presented in Figure 23. With increasing temperature a weight gain is observed, associated with oxidation of aluminium powder.

Figure 29 presents XRD analysis of raw materials mixture after reaction and oxidation thermal treatment.

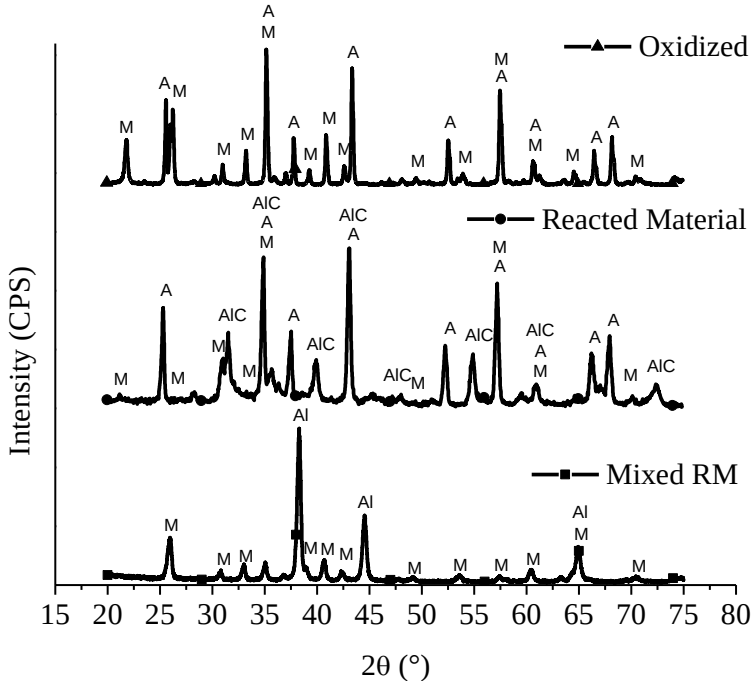

Figure 29 - XRD analysis of raw materials mixture after oxidation- and reaction thermal treatment and as prepared samples.

In the pattern curve of the mixed raw material (MRM), i.e. the bottom part of graph, the present phases are only mullite and aluminium, indicated as M and Al, respectively. This sample after undergoing the reaction thermal treatment yielded a product, from which the pattern curve of reacted material was carried out. In this pattern curve, alumina and aluminium carbide phases are present, both indicated as A and AlC, respectively. The alumina phase can be justified due to the premature oxidation of the metallic aluminium powder, once the MRM contained an oxide ceramic component, which is able to supply oxygen for the oxidation reaction even though the furnace atmosphere where the reaction took place was inert. The top curve presents a XRD pattern of sample after all thermal treatments. The present phases are only mullite and alumina.

Figure 30 presents DTA/TG analyses of raw materials mixture in oxidizing atmosphere. In this figure, two sample compositions were

considered: with resin in stoichiometric amount, and with excess of 50%mol.

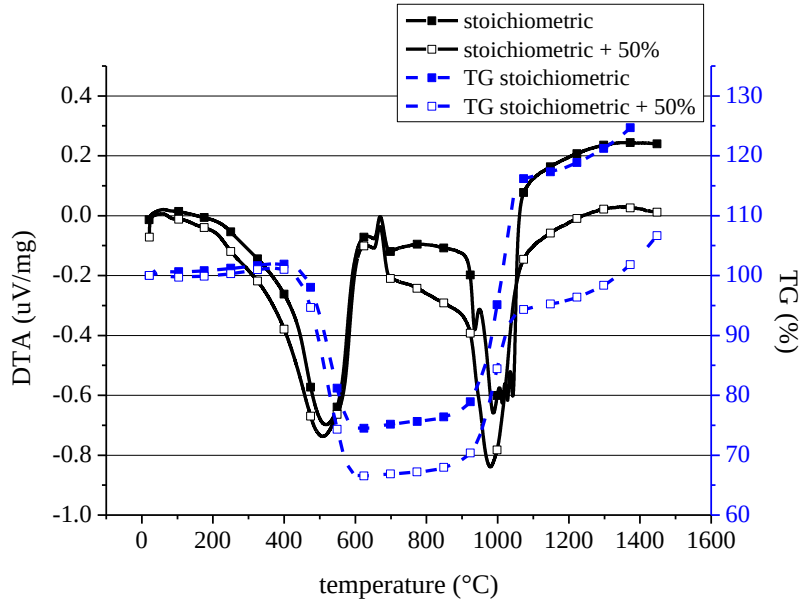

Figure 30 - DTA/TG analysis of sample without reaction thermal treatment of raw materials mixture with resin, with stoichiometric- and 50% excess resin content in oxidizing atmosphere.

Those two samples were prepared with the mixture of the ceramic raw material and the addition of phenolic resin both in stoichiometric and in 50% excess amount without reaction thermal treatment.

Both TG and DTA curve results present an analogous behaviour, wherein weight loss takes first place from 400 to 550°C and afterwards weight gain takes place at > 900°C, achieving quasi stable weight value for >1050°C. Although the sample with 50% excess achieved a lower final mass amount, the weight gain profile is similar to the other sample.

The Figure 31 presents the suggested set points for the oxidation thermal treatment.

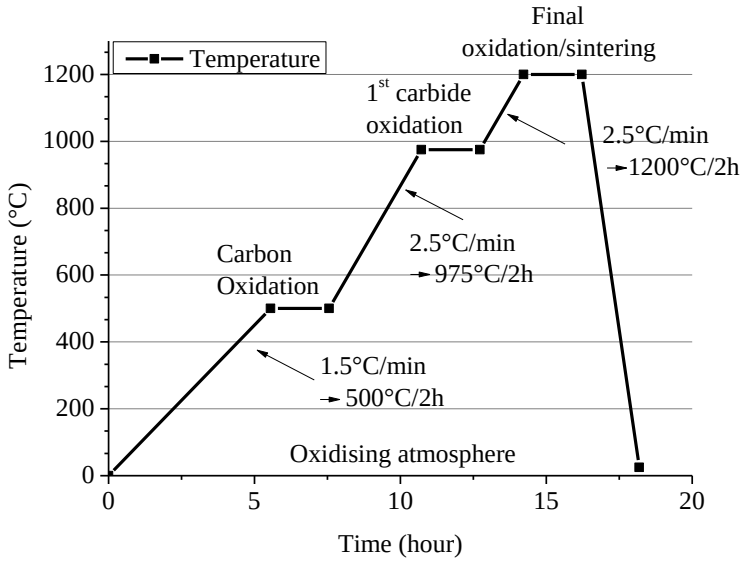

Figure 31 - Oxidation thermal treatment set points suggested in this work.

In this figure dwelling temperatures are 500°C, 975°C and 1200°C, for the carbon oxidation, first carbide oxidation and final carbide oxidation, respectively. Laboratory air provided the oxidising atmosphere characteristic.

Regarding the presented results of this section, the set points for the thermal treatment are presented in Figure 26 and Figure 31. Rates of 1.5 and 2.5°C/min, the heating rate until the first and second dwell time, respectively, were selected in order to prevent excessive degassing formation, so that the material presents neither collapse nor crack formation and therefore enabling the formation of low flaw density, which is a prerequisite for the suggested novel route production.

Considering the reaction thermal treatment set points, the first dwelling temperature was selected in order to give time for gases, which originate from phenolic resin pyrolysis, to flow out from the internal microstructure without causing flaws to the sample. The second dwelling temperature was selected in order to give time so the carbide reaction can occur. According to Wang and co-workers the maximum DSC peak of aluminium carbide occurs at 975°C; therefore, it was the second fixed dwelling temperature (WANG, *et al.*, 2004). The last dwelling temperature was constrained from the maximum temperature, wherein

the fibres have its internal microstructures modified, i.e. grain-growth or phase segregation (GOUSHEGIR, *et al.*, 2012).
Considering the oxidation thermal treatment set points, the first dwelling temperature was selected in order to give time for gases resulted from carbon pyrolysis, to flow out from the internal microstructure without causing internal flaws. The second dwelling temperature was selected in order to give time for the carbide oxidation to occur. In Figure 57, the DTA curve of mullite Al_4C_3, i.e., black curve with open square symbol, a wide peak, which has a maximum at ~950°C, is associated to the aluminium carbide oxidation. The second dwelling point was therefore fixed, for convenience, at the second dwelling temperature of the reaction thermal treatment, i.e., 975°C. The last dwelling temperature is 1200°C and it is constrained from the maximum temperature.
In Figure 29, the top curve presents the XRD pattern of a sample after all thermal treatments. The present phases are only mullite and alumina, what confirms that is possible to achieve a final mixture of phases consisting of mullite and alumina, with an intermediate carbide phase.

4.4 FIBRE FABRIC WOVEN INFILTRATION

For producing composite panel slurries with resin, mullite and 45 wt.% aluminium powder were used for infiltrating the fabric woven with precursors of the matrix material. The infiltration process can be illustrated in the flowchart presented in Figure 32

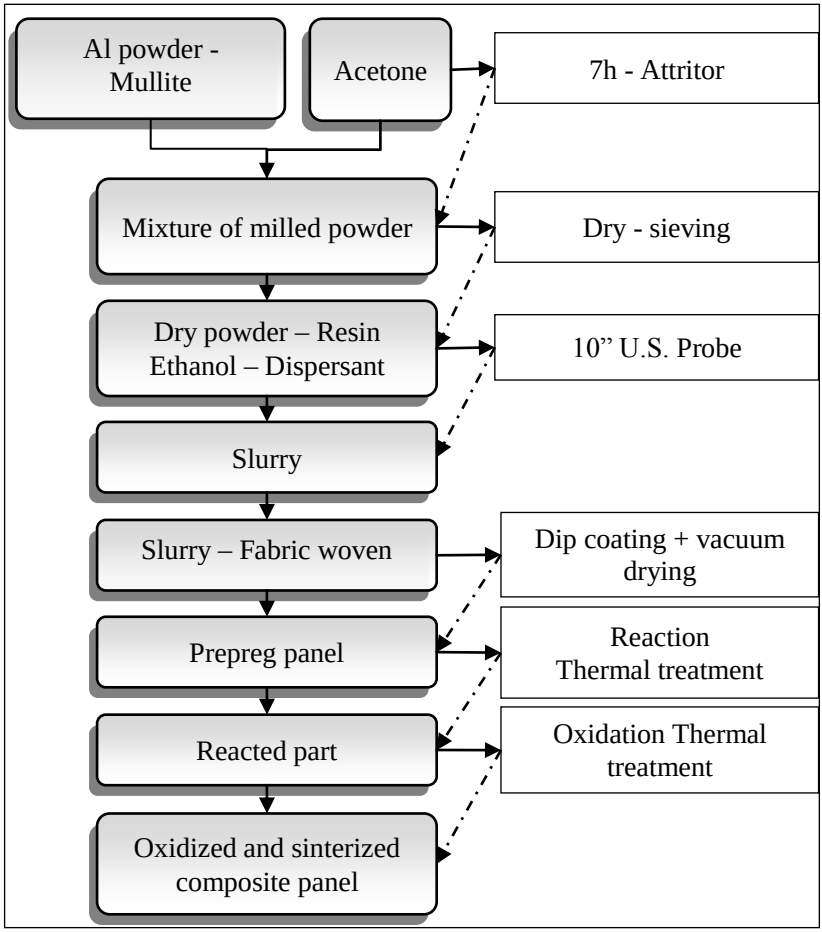

Figure 32 - Flowchart of infiltration - and thermal treatment processes.

After infiltrating fibre fabric woven with slurry and pilling them up in stacks, the prepreg panel was produced, presenting a greyish colour due to the amount of aluminium powder within the mixture. An example of prepreg panel is shown in Figure 33.

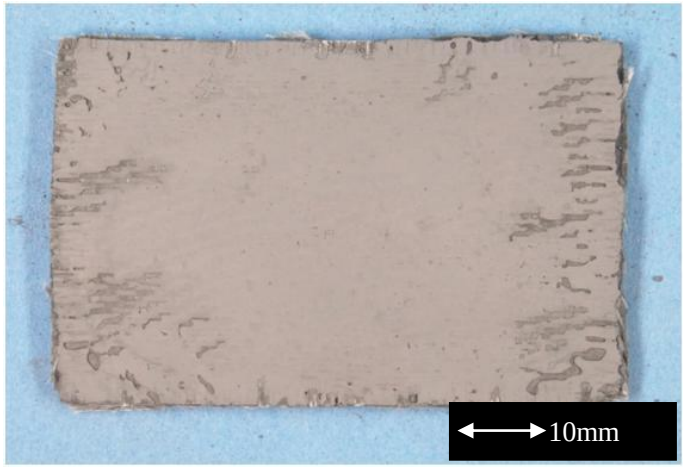

Figure 33 - Infiltrated prepreg panel.

The sample is just dried and, due to the resin content, it presents strength enough for dry cutting in the required dimensions. Afterwards, the prepreg underwent the two-stage thermal treatment (Figure 26 and Figure 31). Right after this treatment, the sample presented dark colour, associated to the pyrolysed resin. In this thermal treatment, inert atmosphere was assured by pressurizing Argon at 1 bar inside the furnace tube. If any connection of the gas tubes or even the tube tap would have presented any leakage, then any oxygen/oxidant gas from outside would not be able to enter within the tube due to its internal higher pressure. After the reaction thermal treatment, then the reacted composite panel underwent the oxidation thermal cycles in a muffle furnace. In this process, oxidizing atmosphere ensured the oxidation reaction of the newly formed intermediate carbide phase in order to produce the final ceramic oxide phase, i.e. alumina. Inside the muffle, the samples were carefully placed over ceramic foams to ensure a flowing path for the oxygen required in the oxidation reaction. Ceramic bricks were also used to place samples in a region of the muffle with more homogenous temperature distribution and higher access for the oxygen to reach the sample.
After finishing this last thermal treatment, the sample presented a whitish colour (Figure 34) due to the content of oxide ceramic, i.e. mullite and alumina.

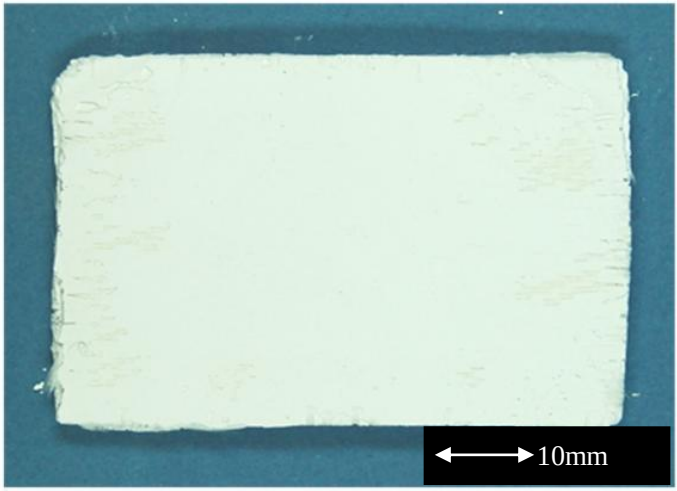

Figure 34 - Composite panel after oxidation TT.

4.5 POROSITY

The results of the two experiment methods for porosity determination are presented in Table 5.

Table 5 - Matrix porosity values.

Samples	Porosity [%]		
	Green	Reacted	Sintered
Dried 50 wt.%	-	-	56.5±0.5
Dried 60 wt.%	-	-	56.6±0.7
Without Resin 200 MPa (WOR200)	-	-	31.7±0.5
Without Resin 50 MPa (WOR50)	-	-	53.4±0.4
With Resin 50 MPa (WR50)	52.8±0.4	54.0±0.7	50.9±1

The values of porosities obtained from Archimedes' principle, i.e., dried 50% and 60%, are very similar. Pressed samples, i.e., WOR200 and 50 and WR50, presented porosity more consistent with the compaction pressure. The sample with compaction pressure of 200 MPa presented lower porosity than samples compacted at 50MPa. This is expected, but

when samples pressed with 50 MPa are compared, then samples which have resin addition in their composition presented lower porosity values. In this case, resin also acts as a lubricant and provides better compaction of raw materials. Nevertheless, the difference between the porosities is within the range of the standard deviation. Other important characteristic is the stable porosity value along the thermal treatment cycle. It started with 53%, changed to 54% and finished with 51%, which gives a final change of approximately two percentage points.

4.6 LINEAR SHRINKAGE

The results for linear shrinkage of pressed samples are presented in Table 6.

Table 6 -Matrix linear shrinkage values.

Samples	Linear shrinkage [%]		
	Reacted	Sintered	Sum
Without Resin 200 MPa (WOR200)	-	-0.27±0.12	-0.27±0.12
Without Resin 50 MPa (WOR50)	-	-0.55±0.1	-0.55±0.1
With Resin 50 MPa (WR50)	-1.71±0.1	-0.39±0.06	2.1±0.1

From those densities all porosity values were calculated with respect to the theoretical density of a mixture of 80% mullite and 20% alumina, i.e., 3.21 g/cm³. This last value do not

4.7 DENSITY

The results of the two experiment methods for porosity determination are presented in Table 7.

Table 7 - Matrix density values.

Samples	Density [%]		
	Green	Reacted	Sintered
Dried 50 wt.%	-	-	1.40±0.02
Dried 60 wt.%	-	-	1.39±0.02
Without Resin 200 MPa (WOR200)	-	-	2.19±0.03
Without Resin 50 MPa (WOR50)	-	-	1.5±0.01
With Resin 50 MPa (WR50)	1.52±0.01	1.48±0.03	1.58±0.04

In this table all densities are presented, with these value all the porosity values were calculated with respect to the theoretical density of a mixture of 80% mullite and 20% alumina, i.e. 3.21 g/cm³.

4.8 MECHANICAL BEHAVIOUR OF MATRIX AND COMPOSITE

Mechanical properties are presented in this section. The first characterization was carried out with square cross section bars of the matrix material after it underwent the two-stage thermal treatment and the polishing process. In order to evaluate the effect of the compacting pressure on mechanical properties of the matrix, Weibull analysis was undertaken on the results from the four-point bending test. Figure 35 presents the Weibull analysis of the mechanical test carried out with bars of WOR50 and WOR200 and WR50. This figure presents values of $ln\big(ln(1/1-\text{failure probability})\big)$ in abscissa axis and natural logarithm of ultimate flexural stress values in ordinate axis.

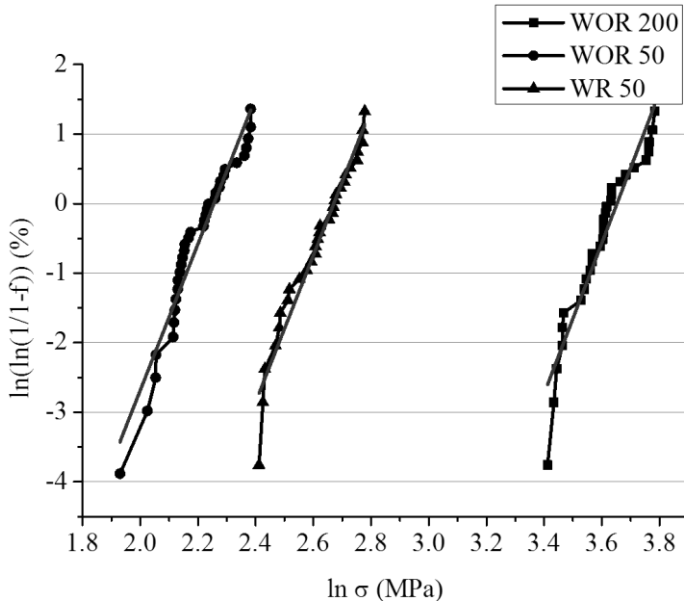

Figure 35 - Weibull analyses of matrix samples.

In Figure 35 all set of results present similar values of curve slope, i.e. Weibull parameter *m*, which was ~10.5. Samples without resin presented the higher and the lower set of mechanical strength, and the samples with resin presented higher values than the WOR50 samples, which were compacted at the same pressure, i.e., 50MPa, and lower values than WOR200, pressed at higher pressure, i.e., 200MPa. Table 8 presents a summary of the mechanical properties of the tested samples.

Table 8 - Mechanical behaviour of reaction-bonded aluminium oxide/mullite.

Samples	Mechanical properties [%]		
	σ_0 [MPa]	m	σ_{max}[MPa]
RBAO (WOR50)	9.24	10.52	10.85
RBMAO (WR50)	14.15	10.54	16.10
RBAO (WOR200)	38.55	10.82	43.95

The second characterization was carried out with the composite panel after the two-stage thermal treatment and the cutting process. Figure 36

presents the result curve of mechanical test carried out with 720™ Nextel long fibre reinforcement using the RBMAO route for matrix consolidation.

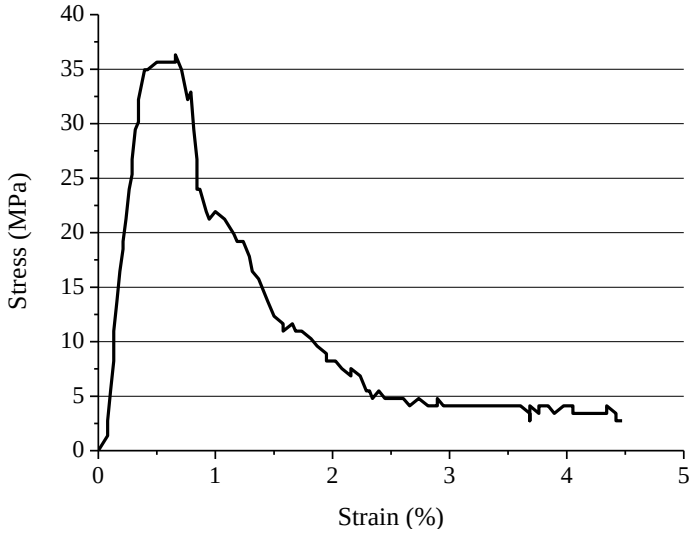

Figure 36 - Four point bending test of NEXTEL 720® panel.

Deformations of ~2% without brittle fracture behaviour may be observed along with the capability of bearing loads after ultimate flexural stress, a.k.a. damage tolerance. Although this data corresponded to a damage tolerant behaviour, the ultimate flexural strength is lower than the expected, ~200 MPa(RUGGLES-WRENN, *et al.*, 2006)(RUGGLES-WRENN, *et al.*, 2008), which implies that more development in the infiltration process in order to get better composites is yet demanded.

According to the Weibull fitting, which is presented in Figure 35, the samples without resin pressed at 200 MPa presented higher σ_0 than the samples with resin pressed at 50 MPa, which showed in turn higher σ_0 than the samples without resin pressed at 50MPa. This may be associated to the presence of sintering characteristics in samples WR50 in comparison to the samples WOR50 (cf. Figures of WR50 samples, i.e. Figure 38 a) and b), with Figures of WOR50 samples, i.e. Figure 42a) and b); Figure 41 and Figure 47).

Although WR and WOR samples presented dissimilar σ_0, they showed Weibull parameters *m* with similar values. In this case, WOR, which represents RBAO, and WR, which represents RBMAO, are indeed

production routes with comparable reliability and since RBAO is a feasible and reliable route, then RBMAO can be fitted in this classification.

4.9 MICROSTRUCTURAL ANALYSES

The images presented in Figure 37; Figure 38;Figure 39; and Figure 40 were collected in FE-SEM with 50.000X and 100.000X magnification of samples produced without resin by compacting them with pressures corresponding to 25, 50, 75 and 100 MPa.

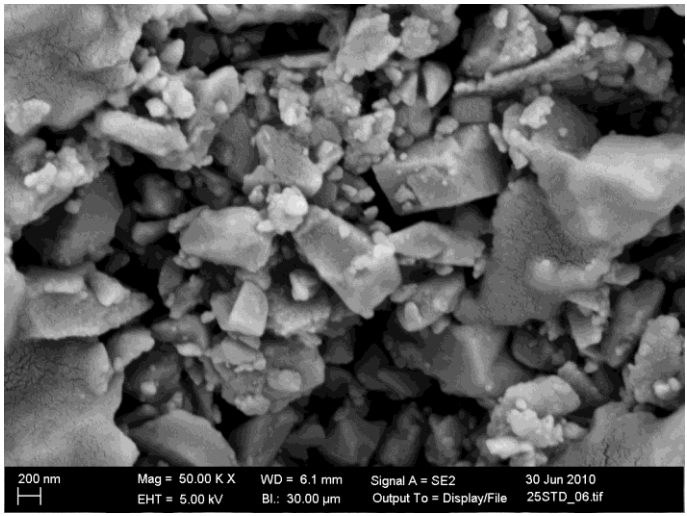

Figure 37 - Sample without resin pressed at 25 MPa with 50.000X magnification.

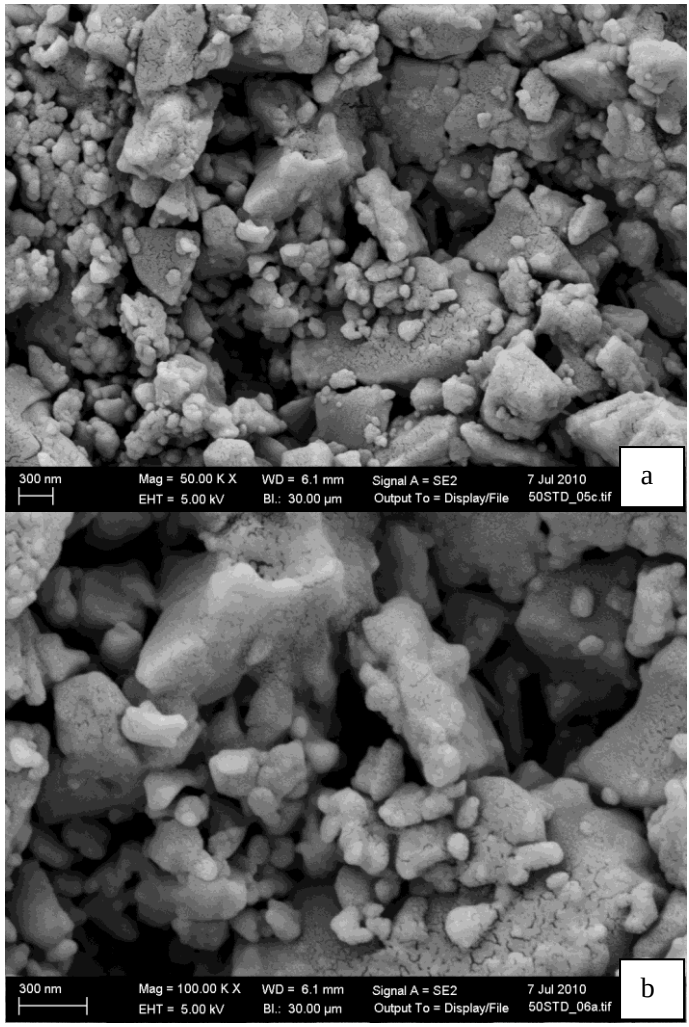

Figure 38 - Sample without resin pressed at 50 MPa with 50.000X (a) and 100.000X (b) magnification.

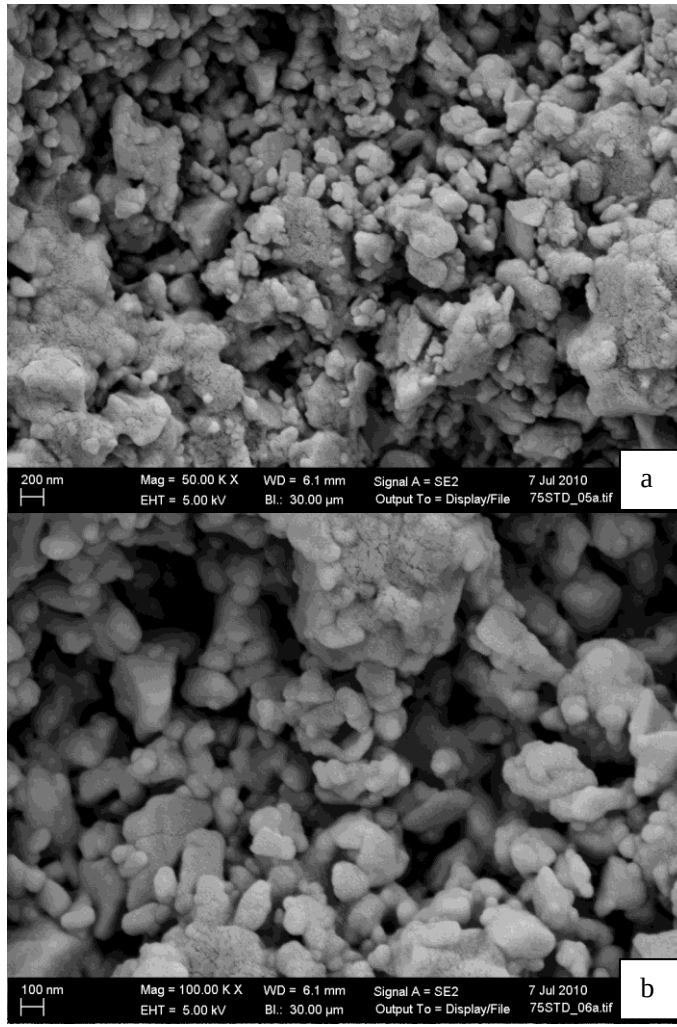

Figure 39 - Sample without resin pressed at 75 MPa with 50.000X (a) and 100.000X (b) magnification.

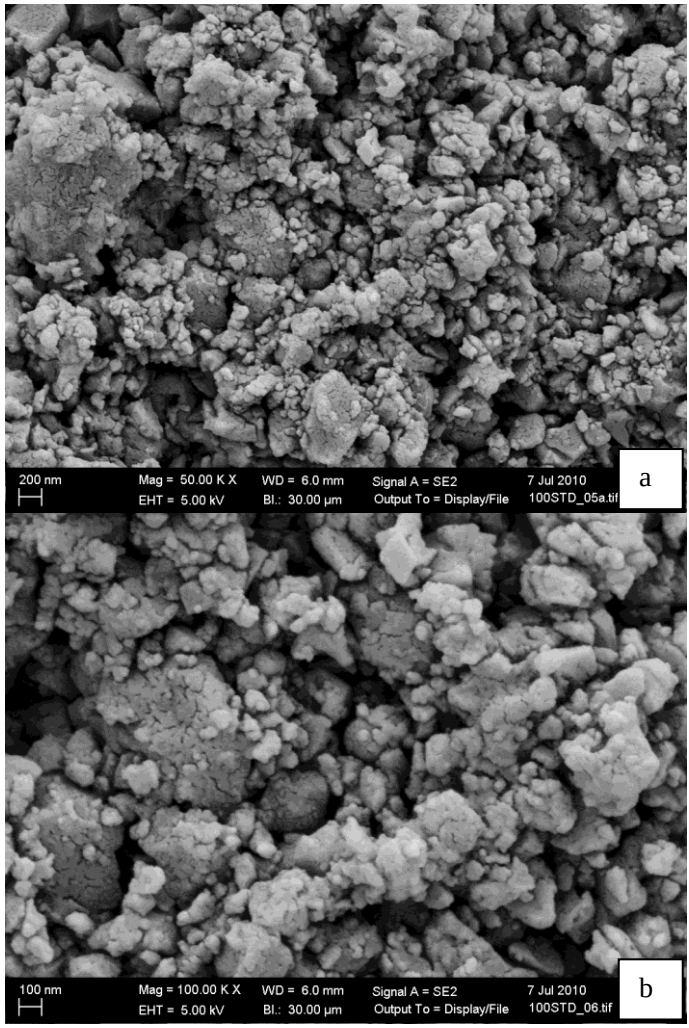

Figure 40 - Sample without resin pressed at 100 MPa with 50.000X (a) and 100.000X (b) magnification.

In all those images the brighter region represents ceramic particles with submicrometric size. Samples pressed at 25 MPa (Figure 37) present grains that still show features of the particles, which gave form to them, even after they underwent the thermal treatment at 1200°C. This behaviour is less evident as the compaction pressure rises, as expected.

Samples pressed at 100 MPa presented denser microstructures than 25 MPa samples and the sintering features are more evident as well. Samples compacted at 50 MPa slightly differ from 25 MPa samples. In turn, 75 MPa samples present the same feature in comparison with 100 MPa samples. On the other hand, in a comparison to 75 and 25 MPa samples, the 75 MPa samples showed denser microstructure with grains more evident. The densest samples were those compacted at 100 MPa.
In Figure 41 to Figure 43, SEM images, the samples were the same used in mechanical test, i.e., WR50 and WOR50 and 200. The image analysis was performed in fractured surfaces and polished surfaces.

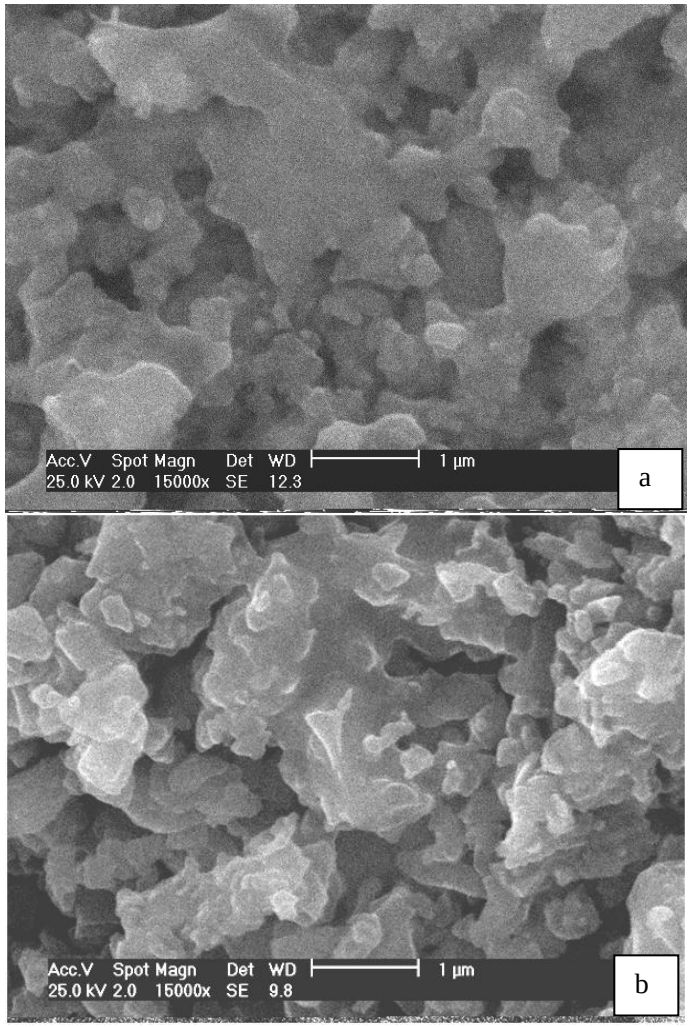

Figure 41 - Micrograph of 15.000X of matrix material - WR50 - polished (a) and fractured surface (b).

In both WR samples, it is possible to observe grain formation from sintering. This feature is verified by the rounded edges of the grains and the formation of continuity through the grains (top of Figure 41 a)). In those figures, the gray region represents ceramic grains, which were formed after the two-stage thermal treatment.

Figure 42 and Figure 43 show SEM micrographs of samples produced without resin.

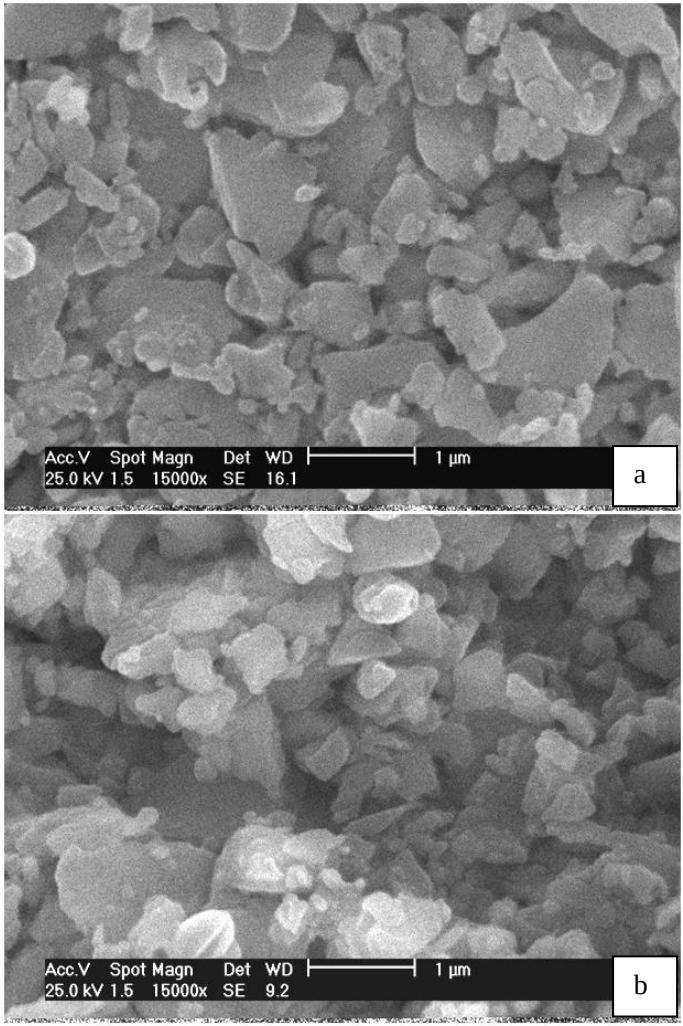

Figure 42 - Micrograph 15.000X of matrix material - WOR50 - polished (a) fractured surface (b).

Figure 42 a) and b) show the same surface appearance of sample presented in Figure 37, and Figure 38, where lacks of sintering

characteristics were observed and the grains are similar to the original particles of the raw material.

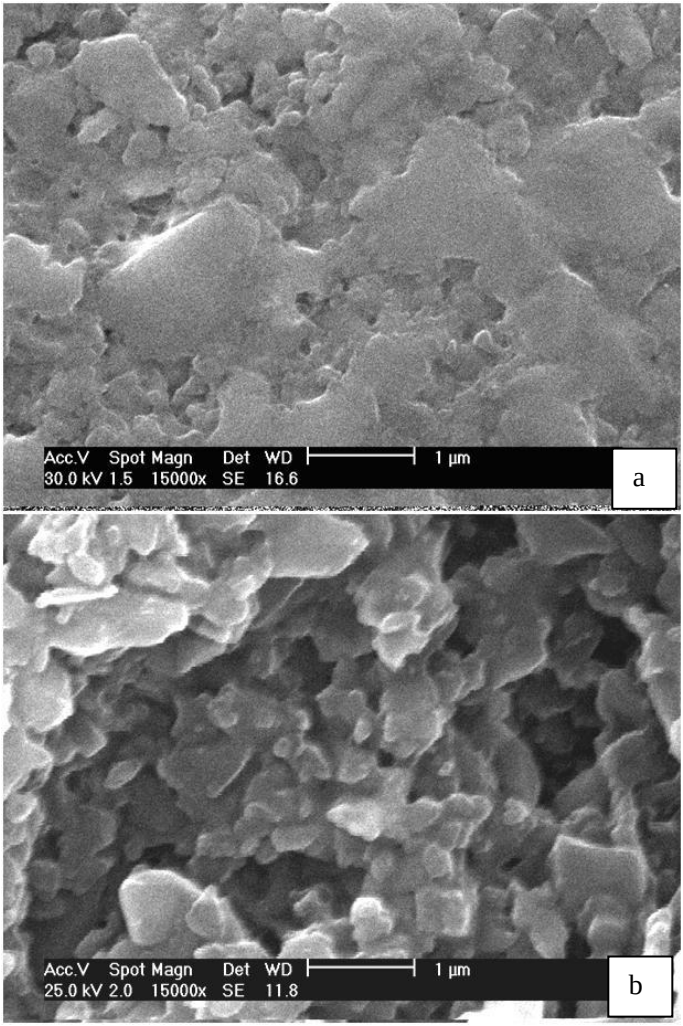

Figure 43 - Micrograph 15.000X of matrix material - WOR200 - polished (a) fractured surface (b).

In turn, in the last two images for both fractured and polished surface (Figure 43 a) and b)) the sintering features are more evidenced by the continuity of the grains and rounded particle edges. SEM images in

Figure 44 and Figure 45, are from the composite panel sample produced with a reinforcement comprising of eight layers of 720™ fibre fabric woven infiltrated with the RBMAO matrix.

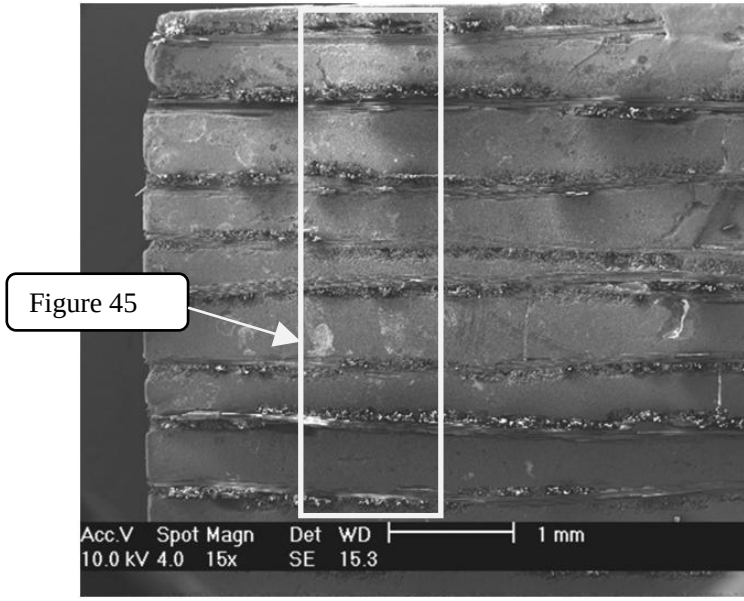

Figure 44 - Micrograph 15X of a composite panel of 720 NEXTEL® and RBMAO matrix.

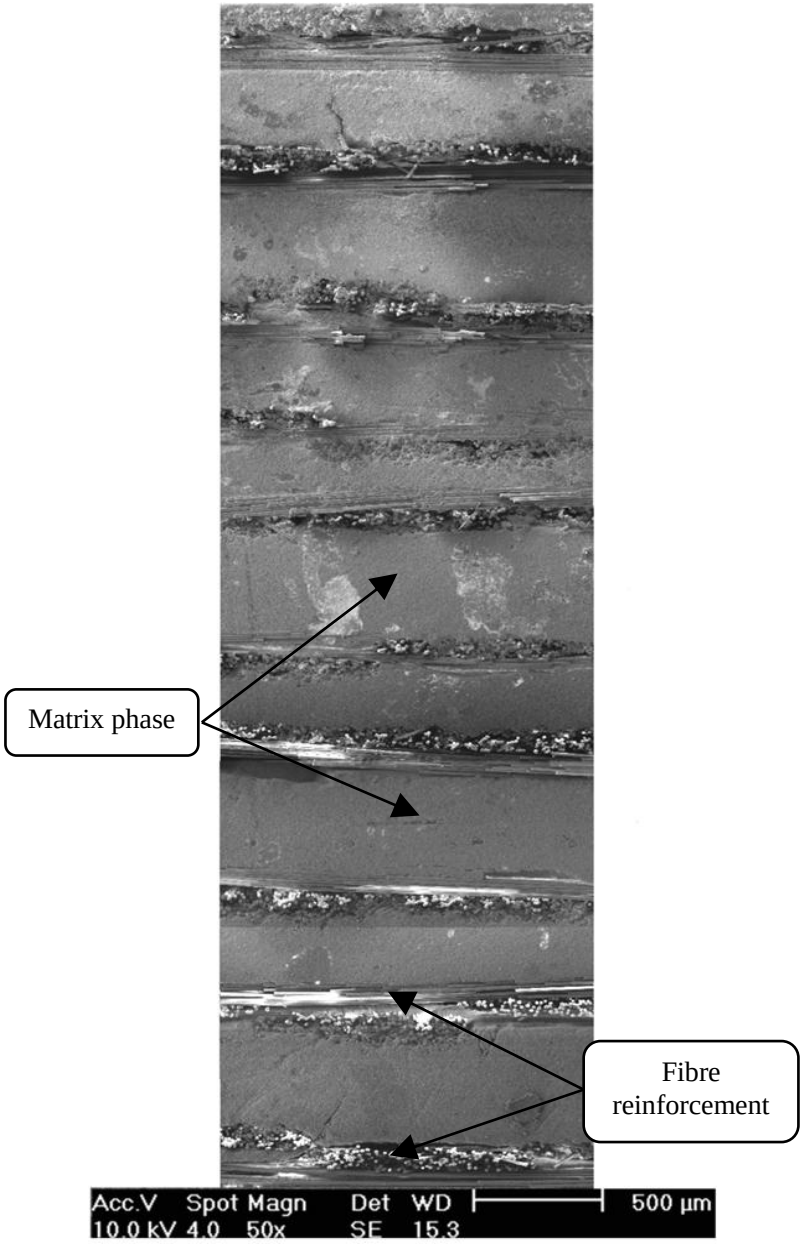

Figure 45 - SEM micrograph 50X composite panel of 720 NEXTEL® and RBMAO matrix.

These two previous figures are images of panel cross section and fibres shown between the homogenous gray phases, which represent the matrix phase. The lower density of flaw, which is not normally present in those kind of composite materials (YANG, *et al.*, 2009). Low flaw density enhances composite properties, e.g. permeability, electrical and thermal properties, by producing a composite with more homogeneous matrix morphology. Although those properties are increased due to the matrix homogeneity, the ultimate tensile strength is not sensibly modified, which is expected once the composite is fibre-phase dominant, from a "mechanical property" point of view. Low flaw density is also present in the image collected from a similar sample in a conventional optical microscope (Figure 46).

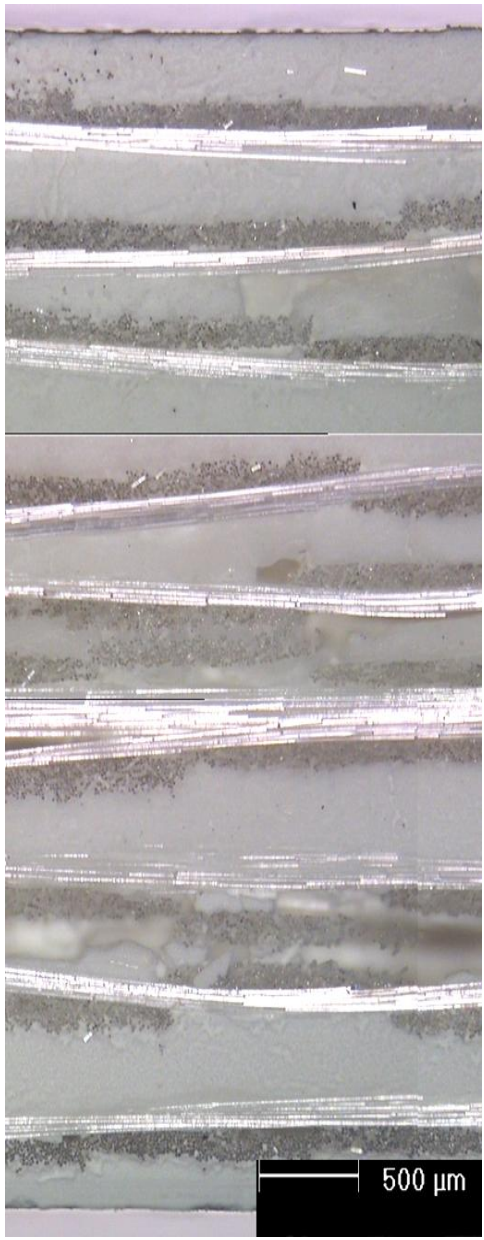

Figure 46 - OM micrograph 50X of a composite panel of 720 NEXTEL® and RBMAO matrix.

Figure 47 presents longitudinal surface cross section of a composite panel sample.

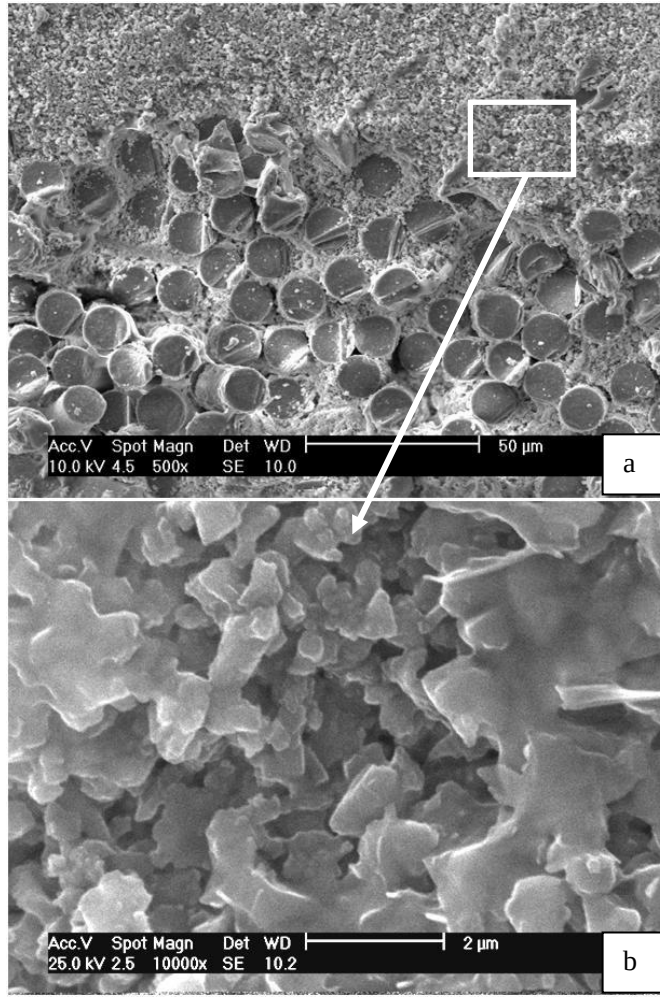

Figure 47 - Micrograph 500X (a) and 10.000X (b) composite panel of 720 NEXTEL® and RBMAO matrix.

In Figure 47 a) the cylindrical shape patterns represent the fibre fabrics woven reinforcement with very homogenous diameter distribution, as specified by the supplier (3M), and the matrix is infiltrating the space

among fibres. In the magnification extension of the matrix part of the Figure 47 b), grains present rounded edge particles and a continuity, with similar appearance and shape of those micrograph which were collected from pressed monolithic bar (cf. Figure 41 a) and b) with Figure 47 b)). Figure 48 presents the outer surface of a composite panel (Leo FESEM).

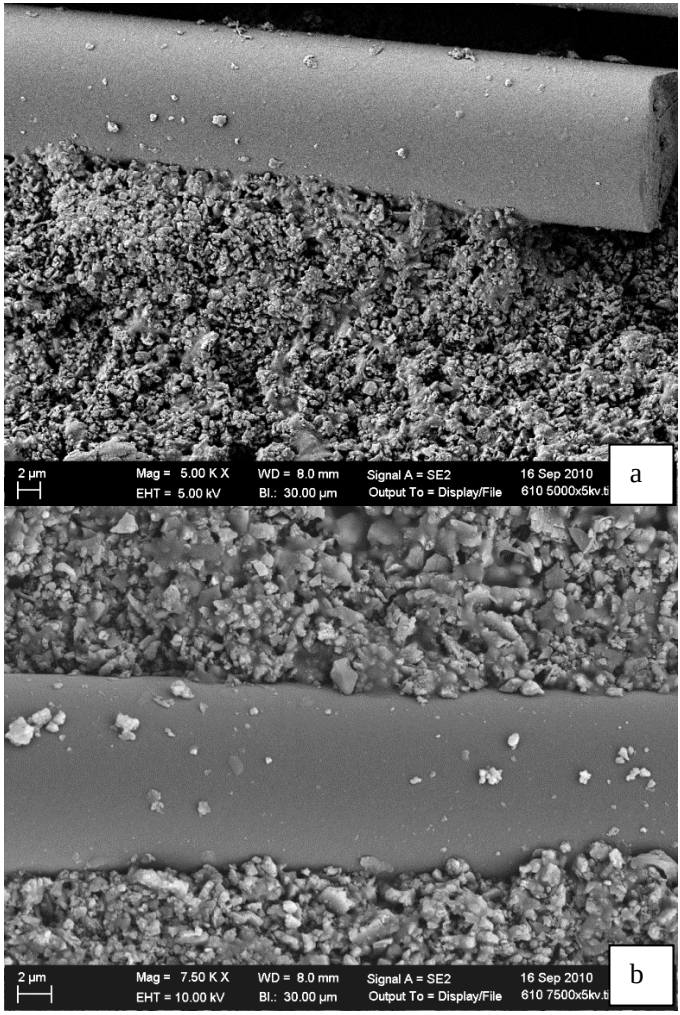

Figure 48 - Micrograph 5.000X (a) and 10.000X (b) of a composite panel of 720 NEXTEL™ and RBMAO matrix.

In Figure 48, the fibre surface quality is not affected after the suggested thermal treatment. Although the thermal treatment involves two kinds of reaction, i.e. carbide formation and oxidation reaction, the process does not affect the fibres and therefore it does not harm their properties. Moreover, a recent work pointed out a maximum temperature, i.e. 1300°C, wherein fibre grains do not coalesce (GOUSHEGIR, *et al.*, 2012). A batch consisting of the same raw material mixture but with different particle sizes was prepared so that the phase could be visually identified due to the bigger mullite particle size and smaller alumina newly formed phase. The samples of this batch are presented in Figure 49.

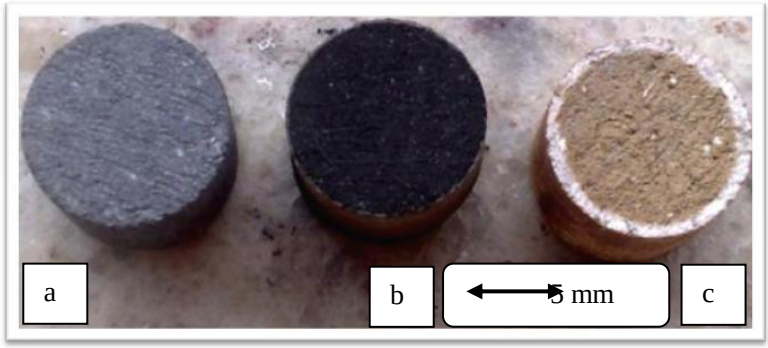

Figure 49 - Samples visual aspect: (a) as processed (b) reacted in inert atmosphere at 1200°C (c) oxidized at 1200°C.

The green body presented gray coloration due to the amount of aluminium powder added as raw material (Figure 49a). The strength of green body was high enough to allow handling and cutting. The dark aspect of the reacted samples (Figure 49b) refers to the carbon originated during the carbonization step. The oxidized sample presented an external region where oxidation took place while the inner region preserved the reacted composition (i.e. aluminium carbide). It remained unreacted due to the small dwell period (Figure 49c). In images of Figure 50 to Figure 54, which were collected in SEM (Jeol), are the same samples of the side group batch.

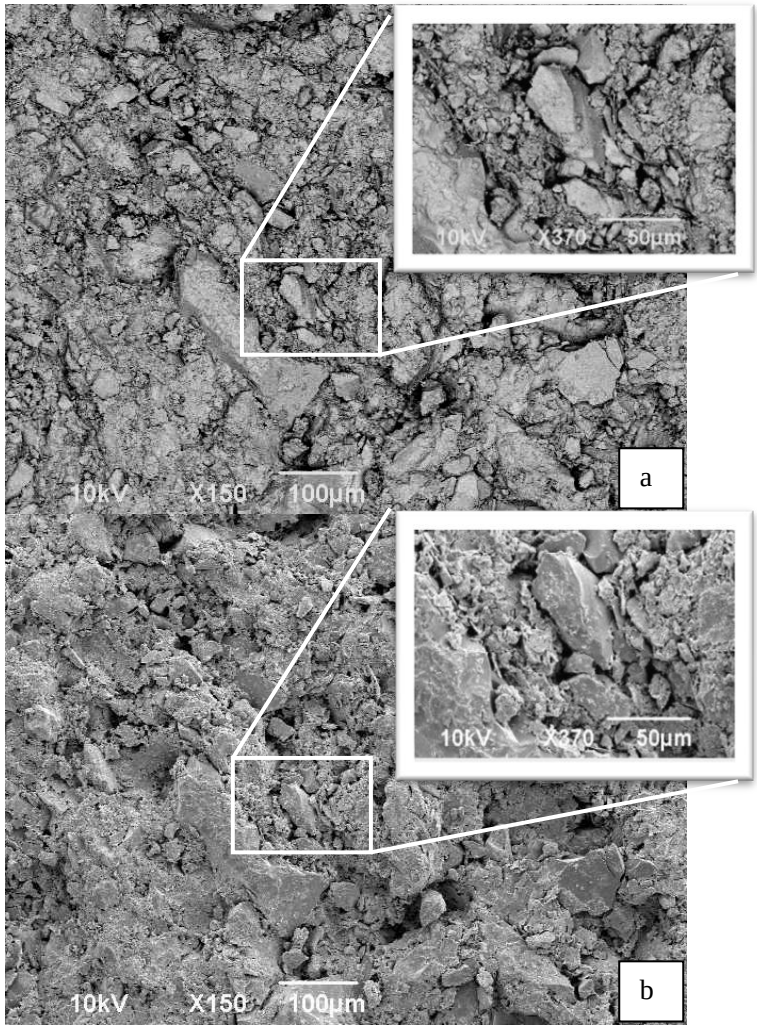

Figure 50 - Green body microstructure in BSE (a) and SE (b).

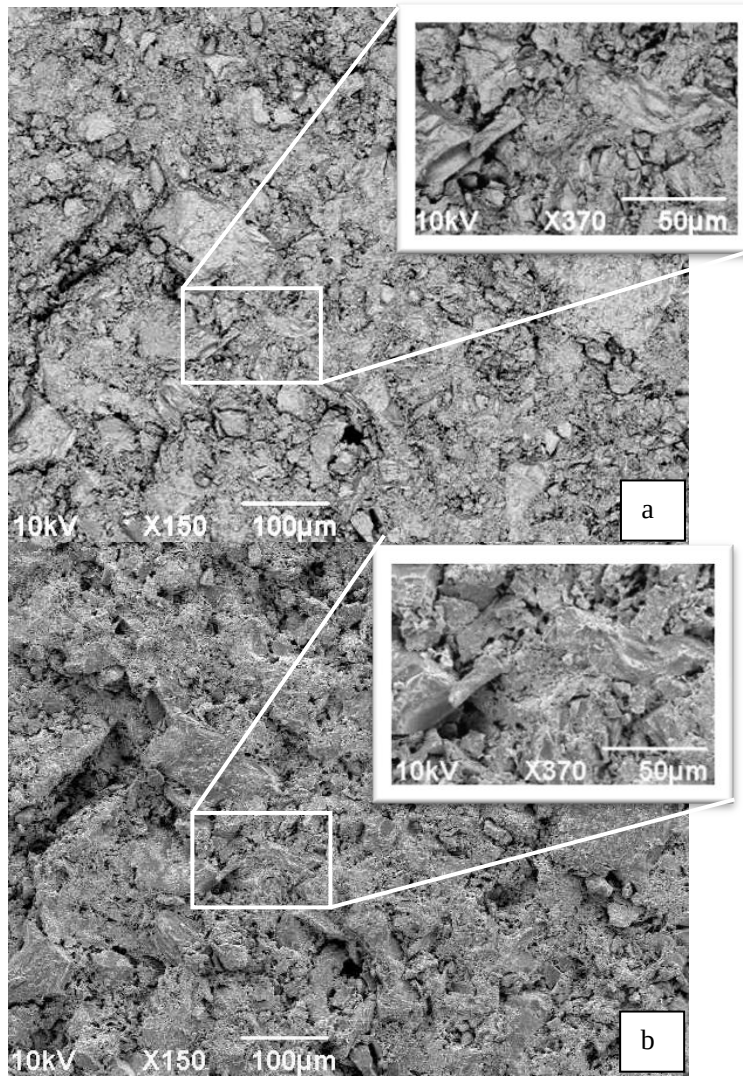

Figure 51 - Reacted sample microstructure in BSE (a) and SE (b).

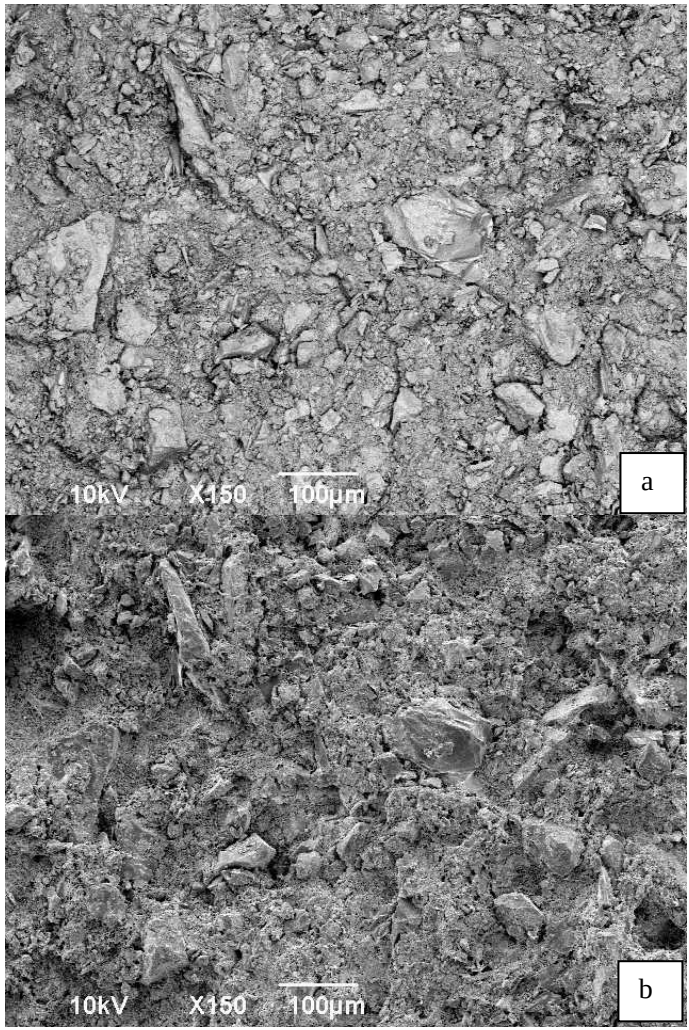

Figure 52 - Oxidized sample microstructure in BSE (a) and SE (b).

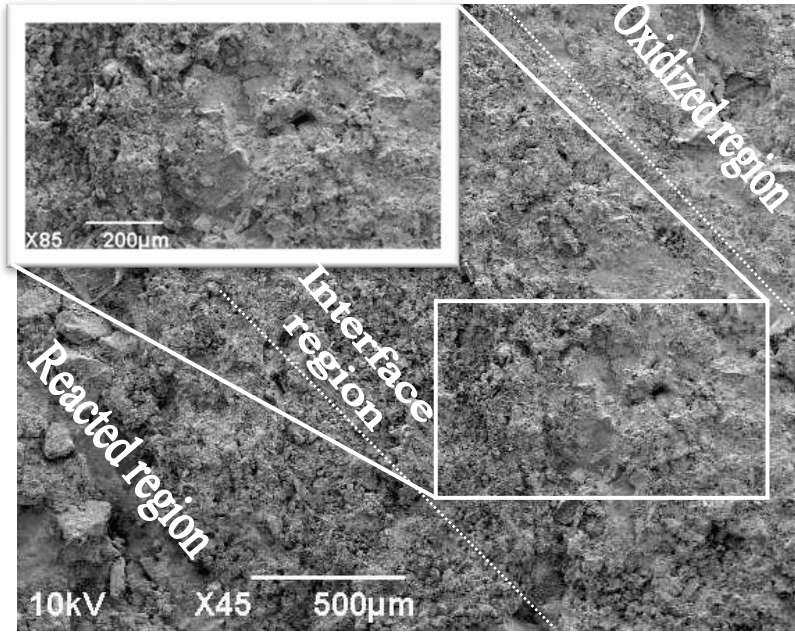

Figure 53 - Microstructure at interface between reacted and oxidized.

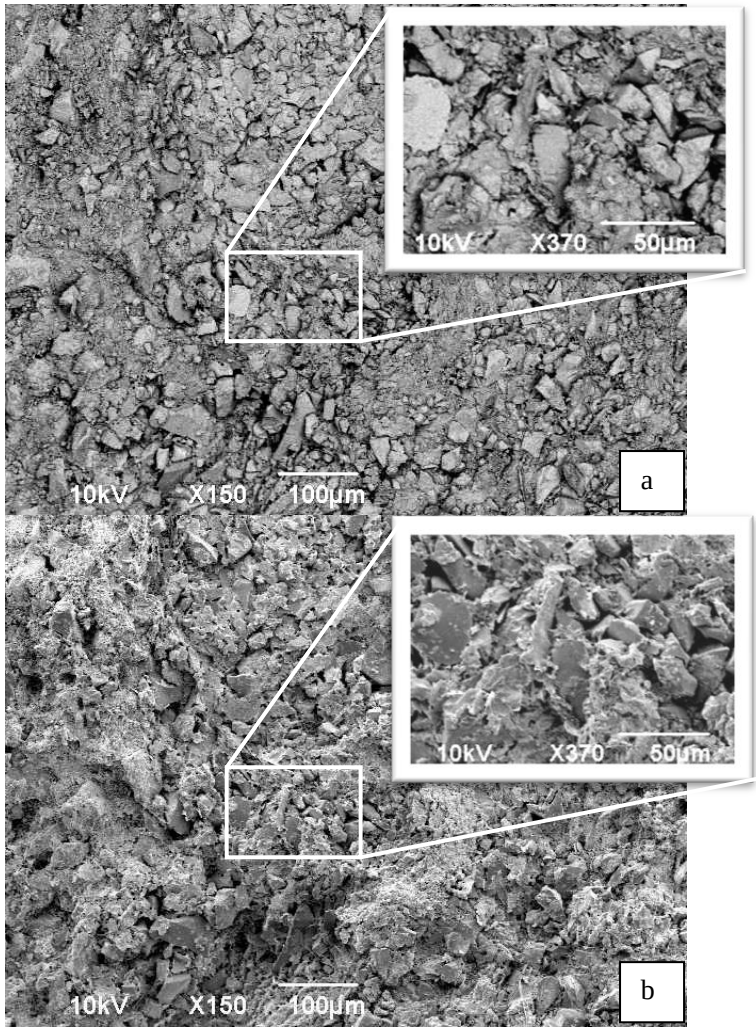

Figure 54 - Aluminium carbide phase within the partially oxidized sample microstructure in BSE (a) and SE (b).

SEM micrographs of green body exhibited microstructures, where mullite particles are surrounded by small particles associated to aluminium and resin particles (see Figure 50a and b). Pressing process resulted in a microstructure where aluminium particles and resin particles are yet present. The higher magnified images of Figure 50a and b clearly show small particles originated from used raw material. It is

actually expected to happen in order to provide a fine alumina layer surrounding the surface of mullite particles (Figure 51a and b). The reacted region is represented in the Figure 49b by the dark coloured region. After oxidation thermal treatment, the oxidized region presented a microstructure where coarse mullite particles are homogeneously distributed in microstructure surrounded by a finer particulate (Figure 52a and b). The interface between reacted/oxidized phases was displayed in a single image to evaluate the microstructure differences. It can clearly be seen that in the oxidized region finer particles are present (see Figure 53). The particles of the reacted region without carbon content, i.e. yellow brown in Figure 49, are coarser but exhibit a different microstructure from the green body (see Figure 54a and b). The reacted region is represented in the Figure 49b by the yellow brown coloured region.

In images in Figure 55 and Figure 56, which were collected in FE-SEM (Leo), are the same samples of the side group batch which differ by the image detection type used, wherein Figure 55a is SE; Figure 55b is *inless* and Figure 55c is BSE and Figure 56 is in SE. The last image is for highlighting the morphology of the newly formed phase, which is the very fine dispersed phase.

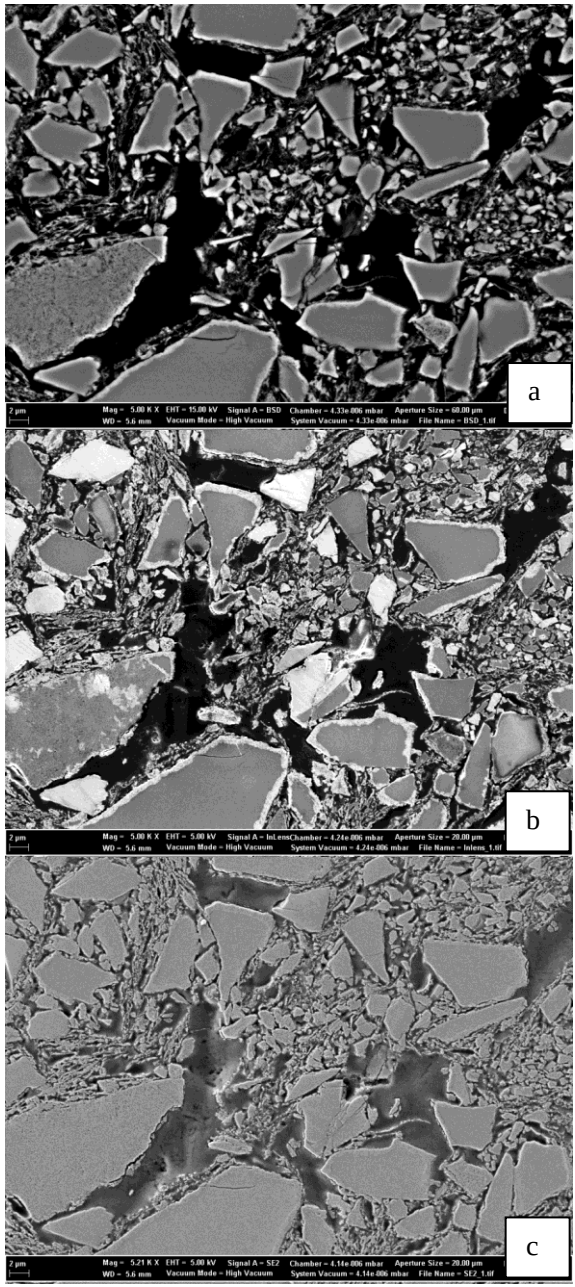

Figure 55 - Embedded oxidized samples in BSE (a) *inlens* (b) and SE (c).

In Figure 55 the several applied detection method present data related to composition, (a), topography (c), and mixed information (b). In Figure 55, the sample was embedded with epoxy resin in vacuum so that the void parts can be identified as the darker regions, which represents the porosity of the part, and brighter regions can be associated with the ceramic material. Mass contrast information is useful in order to observe that the inner particle composition is different from the outer shell layer. In this context, one can associate this different composition with the formation of an outer shell of alumina, although it was not evaluated in this study. Topography information image exhibits the epoxy resin filling in the void regions. From topography information image, the microstructure of mullite particles surrounded by fine dispersed alumina is also highlighted in Figure 56.

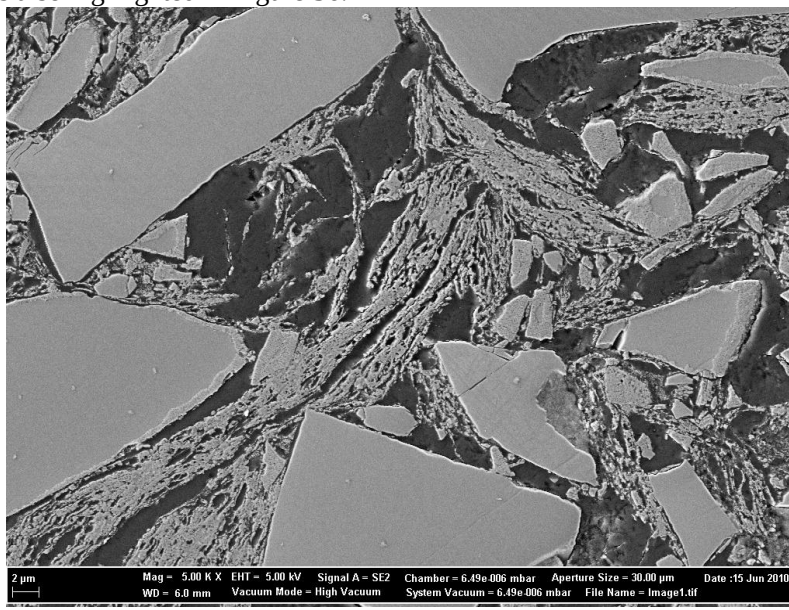

Figure 56 - Embedded oxidized samples in SE showing the newly formed alumina phase.

This microstructure present similarity with the optimal morphology pointed out in literature by (ZOK, 2006) and is also present in the Figure 8.

4.10 OXIDATION KINETICS

The first evaluation, in order to qualitatively evaluate oxidation kinetics of the aluminium carbide, was carried out with a DTA/TG of two different samples. The first type of sample consisted of a mixture of mullite and aluminium and the second type of sample consisted of a mixture of mullite and aluminium carbide, the one produced from the two-stage thermal treatment suggested in this work. Figure 57 presents DTA/TG analyses of aluminium and aluminium carbide samples for evaluation in oxidizing atmosphere.

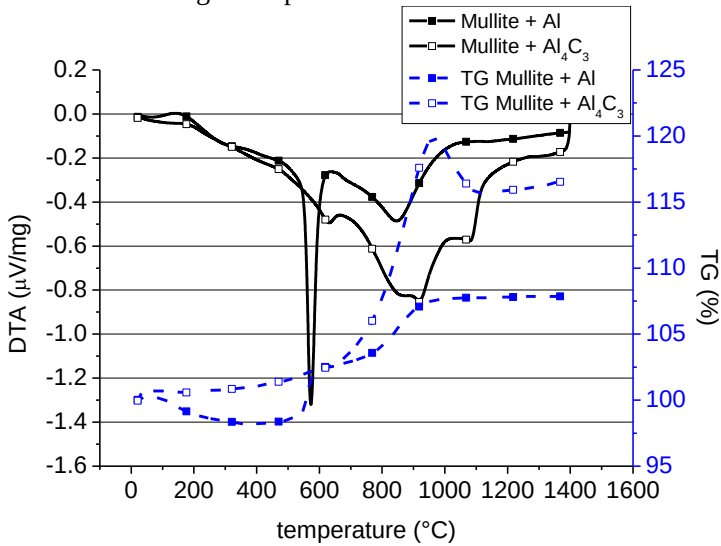

Figure 57 - DTA/TG analysis of RBMAO precursor mixture with samples reacted and not reacted.

Curves of both samples have dissimilar behaviour both for TG and DTA evaluation. In TG resulted curve for sample which contains aluminium carbide, it presents a single region of weight gain, which takes place in the range from approximately 650°C to 950°C with subsequent weight loss, resulted from oxidation of some residual carbon which was not completely reacted with the aluminium powder. In TG resulted curve for sample which contains aluminium powder, it presents the already presented oxidation behaviour of this type of material. In DTA resulted curve for sample which contains aluminium carbide, it presents a wide exothermal peak in temperature range from approximately 600°C to 1200°C. These peaks, i.e. peaks of oxidation of aluminium carbide,

contrast with the peaks presented in the oxidation of the aluminium powder, were only a very narrow peak at 570°C and a wider peak in 870°C were present. Therefore, in qualitative terms it is possible to state that aluminium and aluminium carbide powder possess dissimilar oxidation behaviour. In order to get more quantitative terms information of this difference, then mass gain evaluations experiments of those two materials were carried out.

An overlap of Figure 23 and Figure 27 results in Figure 30 and comparing the latest with the curve of the samples consisting of mullite and carbide, i.e. Figure 57, it is evident that those samples are dissimilar regarding their TG profile behaviour. Since the TG profile behaviour of Figure 57 is associated with the carbide oxidation TG profile, then it might be concluded that without the reaction thermal treatment it is not possible to produce the intermediate carbide phase. It is worthy reminding that Figure 30 is an evaluation wherein samples consisted of mullite, aluminium powder and resin. A result of this observation implies that if the simple heating of the raw material might produce the intermediate carbide phase, then in this evaluation, i.e. Figure 30, the TG profiles should present same TG profile associated with the carbide oxidation, i.e. Figure 57, which was not the observed behaviour.

Figure 58 present weight gain of commercially available aluminium carbide powder yielded from different temperature range of isothermal mass gain.

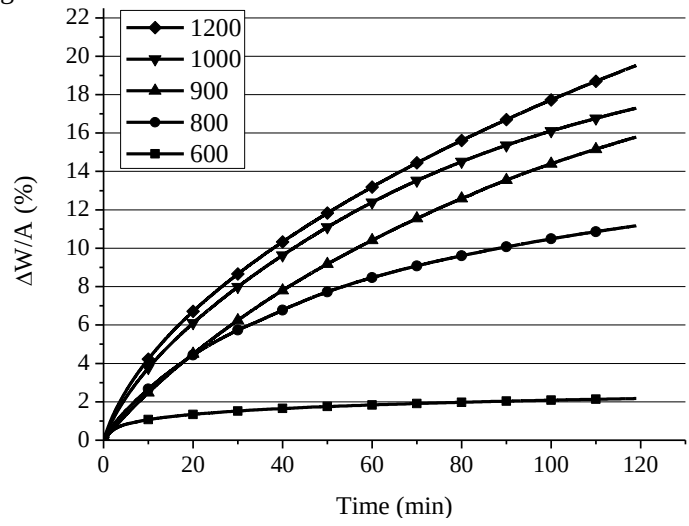

Figure 58 - Weight gain along the time for commercial Al_4C_3 - Aldrich®.

The parabolic trend present in these curves, for which the rate is inversely proportional to the square root of time, is found to be obeyed when diffusion through the scale is the rate-determining process. It follows the parabolic law when it fits to equation 6 (BIRKS, *et al.*, 2006).

$$\left(\frac{\Delta W}{\mathrm{A}}\right)^2 = k \cdot t \qquad 6$$

where ΔW is weight variation, A is specific area, t is elapsed time and k is oxidation kinetics parameter. Figure 59 present $(\Delta W/A)^2$ of the commercially available aluminium carbide powder.

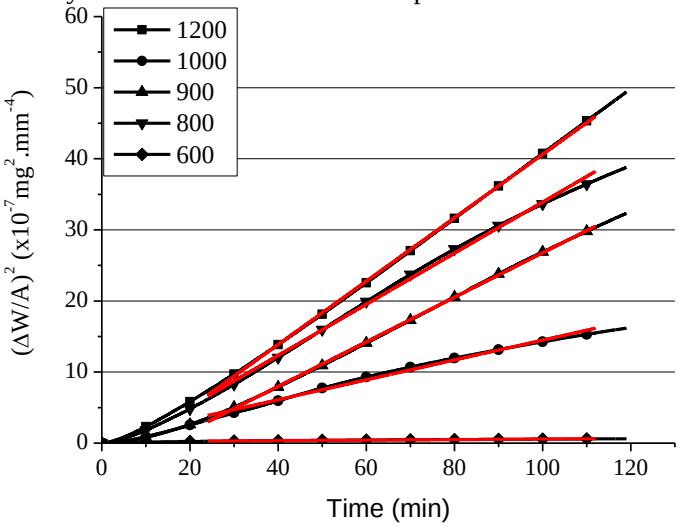

Figure 59 - Square Weight gain along the time for commercial Al_4C_3 – Aldrich®.

From this figure the linear trend curves (red curves in Figure 59) are evident, which corroborate the affirmation that this type of sample obeys parabolic rate law. In those curves the parameter of kinetic oxidation, k, is determined with the curve slope. In order to obtain the apparent activation energy of these samples an Arrhenius plot of ln(k) versus reciprocal elapsed time was recorded (see Figure 60).

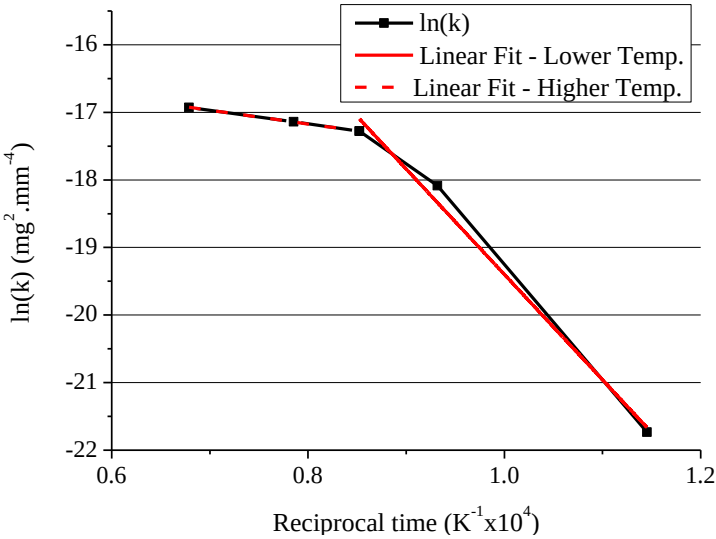

Figure 60 - Parameter of kinetic oxidation of commercial Al_4C_3 – Aldrich®.

From this curve the slope is the kinetics parameter oxidation, which is proportional to $-\Delta E_{activation}/R$. This curve has evidently two oxidation behaviours, one at lower temperature, i.e. below 900°C, and other at higher temperatures, i.e. above 900°C. The apparent activation energy until 900°C is 129.65 kJ/mol and above 900°C, when it decreases to 16.91 kJ/mol. This observation implies that until 900°C aluminium carbide oxidizes with slower rates than above the mentioned temperature.

Table 9 presents a summary of the experimental values for aluminium carbide oxidation kinetics evaluation of the commercially available.

Table 9 - Oxidation kinetic parameters of commercial Al_4C_3.

Samples		Oxidation Kinetics Parameter		
	BET	Temperature	k	ΔE_{oxid}
	[m²/g]	°C	mg^2mm^{-4}	kJ/mol
Al_4C_3 – Commercial	8.255±0.03	600	3.65E-10	129.65
		800	1.40E-8	129.65
		900	3.13E-8	129.65
		1000	3.60E-8	16.91
		1200	4.46E-8	16.91

An evaluation of the oxidation kinetics of aluminium carbide, which is produced through the RBMAO process, was considered in order to quantitatively determining oxidation parameters of the aluminium carbide in this environment. Figure 61 presents weight gain of aluminium carbide produced with RBMAO process. This figure shows the weight versus elapsed time and the five presented curve yielded from different temperature range of isothermal mass gain.

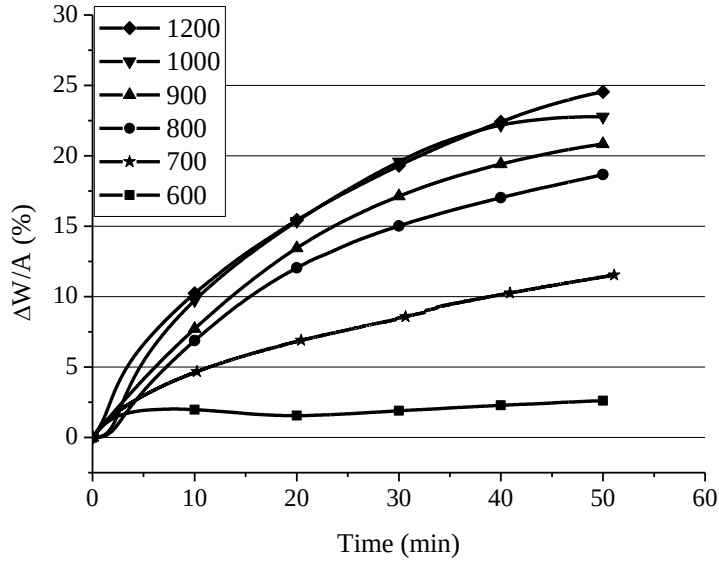

Figure 61 - Weight gain along the time for Al_4C_3 RBMAO sample.

The parabolic trend is also present in these curves, which also enabled the data treatment through equation 6 in order to evaluate the oxidation kinetics parameter of this sample.
Figure 62 presents $(\Delta W/A)^2$ of the aluminium carbide produced with the RBMAO process versus elapsed time.

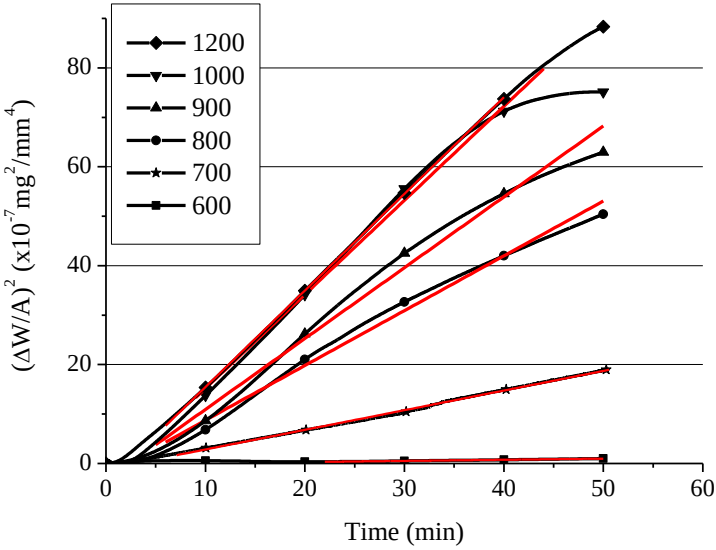

Figure 62 - Square Weight gain along the time for Al_4C_3 RBMAO sample.

The curves also presented linearity required from the evaluation with the equation 6 and in order to determine the parameter of kinetic oxidation the Arrhenius plot was also recorded for these data. Figure 63 presents ln(k) versus reciprocal temperature.

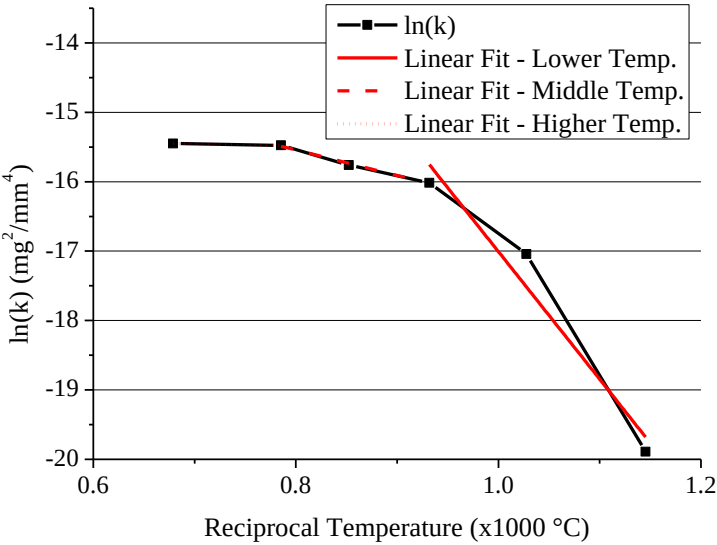

Figure 63 - Parameter of kinetic oxidation of Al_4C_3 RBMAO sample.

This curve has evidently three oxidation behaviours, one more than the observed in Figure 60. The first on is at low temperature, one between 800 and 1000°C and finally one at high temperature. At 800°C a change in the behaviour is observed. The apparent activation energy until 800°C is 156.72 kJ/mol and above 800°C it decreases to 30.51 kJ/mol and decreases even more above 1000°C to 2.10 kJ/mol. This observation implies that due to change in the environment, i.e. presence of mullite, the aluminium carbide oxidizes not only with higher rates in both lower and high temperature, but also changes oxidation behaviour in lower temperatures, i.e. 800°C, than the observed with the Aldrich™ powder. Table 10 presents a summary of the experiment for aluminium carbide oxidation kinetics evaluation of the commercially available.

Table 10 - Oxidation kinetic parameters of RBMAO Al_4C_3.

Samples		Oxidation Kinetic Parameter		
	BET	Temperature	k	ΔE_{oxid}
	[m²/g]	°C	mg^2mm^{-4}	kJ/mol
Al_4C_3 – RBMAO	8.781±0.07	600	2.30E-9	156.72
		700	3.97 E-8	156.72
		800	1.11E-7	156.72
		900	1.43E-7	30.51
		1000	1.90E-7	30.51
		1200	1.95E-7	2.10

The evaluation of the oxidation kinetics of the aluminium carbide stands for the justification of the production of the intermediate carbide phase with its oxidation afterwards, which represents RBMAO route, instead of oxidizing aluminium particles directly, which represents the RBAO route.

In this context, firstly an oxidation kinetics experiment with commercially available aluminium carbide was carried out and then in a second moment, an experiment where the aluminium carbide produced throughout the RBMAO route was carried out.

An observation in both carbide materials was that they have two values of apparent activation energy of oxidation, one at lower temperatures and other at higher temperatures. This observation infers that aluminium carbide presents a feature that it is not easily oxidized at lower temperatures but it is easily oxidized at higher temperatures. In comparison with metallic aluminium particle, it presents an oxidation reaction in narrow first range of temperature, as showed in Figure 27, wherein the aluminium particles oxidize in temperature range from 550°C to 600°C, and finish its oxidation reaction in a second wider range of temperature, wherein the aluminium particles oxidize in temperature range from 750°C to 900°C. The apparent activation energy of oxidation of metallic aluminium powder is found to be placed in a range of 112-152 kJ/mol for temperatures lower 660°C, and 26-33 kJ/mol for temperature above 660°C (WU, *et al.*, 1993).

Because the carbide oxidation is kind of a shifting reaction, then it presents a slower rate reaction in comparison with the direct oxidation. A general aluminium carbide oxidation is expressed in equation 7

$$Al_4C_3 + \alpha O_2 \leftrightarrow Al_2O_3 + \beta CO_x \quad (7)$$

where Greek letters and "*x*" leave place for the variations in such kind of reaction, which is not the focus of this discussion.
A general metallic aluminium is expressed in equation 8.

$$4Al + 3O_2 \leftrightarrow 2Al_2O_3 \quad \textbf{8}$$

According to the equations 7 and 8, carbide oxidation demands a shift reaction between the "C" positions with the oxygen specimens in order to form the oxide, nonetheless, in the metallic oxidation these shifts are not required. This shift behaviour may be, therefore, addressed to the higher apparent activation energy of oxidation of the carbide phase.
The presented oxidation behaviour of the aluminium carbide has a promising application of matrix production route of all-oxide ceramics, due to the fact that it oxidizes with low oxidation rates at lower temperatures preventing the microstructure to form high flaw density and at high temperature the oxidation rate increases ensuring the fully oxidation of the carbide phase, which leaves no residual carbide phase to the final matrix material.
Moreover, another observation within the results, which corroborates with the affirmation that carbide particles oxidize with dissimilar behaviour of the metallic particles, is the oxidation profile behaviour presented in Figure 57. In this figure, aluminium particles oxidize in a two-stage process, wherein the first step is featured with a very high exothermal reaction followed by a wider peak exothermal reaction, and aluminium carbide oxidized in a single stage oxidation, wherein the oxidation step is featured with a very wider exothermal peak. Those two behaviours promote dissimilar heat load to the neighbourhood of the particles. Since the metallic particles have very exothermal oxidation reaction, they generate localized temperatures up to 2000°K, which may be responsible for increasing the flaw density formation. The oxidation reaction of the carbide particle presents a wider peak, and then the localized temperatures are lower in comparison with the first mentioned.
Additionally, the temperature, where the transition of the apparent activation energy of oxidation occurs, was observed at 900°C for the commercially available aluminium carbide and at 800°C for the RBMAO produced aluminium carbide. This behaviour may be associated to the mullite content, which can act as oxygen donor for the oxidation reaction and therefore improving the diffusion of the oxygen supply for the reaction.

5 DISCUSSION

This thesis focused mainly on the feasibility of the RBMAO as an alternative route for production of porous materials. Discussions are presented in this section in order to better understand this novel route in its fundamental aspects.

5.1 SLURRY RHEOLOGY

As a concluding remark of section 4.2, in page 38, the usage of phenolic resin is at same time beneficial and detrimental. Its usage is advantageous due to its potential of yielding high residual carbon after pyrolysis and producing prepregs with enough green handling strength. However, it is detrimental due to its characteristic of form organized structure between the resin and the raw material particles, which results in increasing viscosity. Alternatively, the replacement of most phenolic resin by graphite powder is a promising way to keep the slurry within the desired features for using in composite panel production.

5.2 THERMAL TREATMENT

As a concluding remark in section 4.3, in page 44, the two-stage thermal treatment proved its necessity to be performed in two steps. In this way, the reaction thermal treatment produces the intermediate carbide phase and the oxidation thermal treatment oxidizes subsequently this carbide phase. Therefore, the two-stage thermal treatment enables the production of the final oxide ceramic phase through and intermediate carbide phase, which will be discussed further in section 5.4 the importance its application.

5.3 MECHANICAL STRENGTH

As concluding remarks in section 4.8, in page 58, the RBMAO can be classified in the same reliable category of the RBAO process, due to its Weibull parameter similarity the last mentioned group. Moreover, in comparison of samples same compaction setup, the RBMAO samples presented higher strength than the adapted RBAO samples.

5.4 OXIDATION KINETICS

As a concluding remark in section 4.10, in page 84, the usage of the intermediate phase is justified due to the lower oxidation rate at lower temperatures, which contributes with the lower formation of flaw

density, and the increasing of the oxidation rate at higher temperature, which ensures complete carbide oxidation.

6 CONCLUSION

A summary of the concluding remarks is:

- According to the presented features of the RBMAO novel route and to the particular requirements for composite production, hence the route can be considered successfully developed.
- The use of phosphate ester as dispersant for such slurry is a promising alternative;
- The replacement of the phenolic resin by graphite powder produces a sensible viscosity decreasing, which allows the solid content to increase up to 47 vol. % without crossing the viscosity value of 50 MPa.s;
- The application of DTA/TG analyses for the thermal treatment set points was as promising tool. The two-stage thermal treatment was properly proposed and after analysis of present final phases, then the two-stage thermal treatment can be considered successfully developed, since it promoted the formation of the intermediate carbide phase and the final oxide ceramic phase;
- The ceramic matrix mechanical properties were evaluated and Weibull parameter was determined, i.e., 10.54, and σ_0 , i.e. 14,15 MPa, with σ_{max}, i.e. 16.1 MPa, which are placed in between the group of WOR50 and WOR200. This mechanical behaviour is addressed with the more evident sintering features presented by the WR50 samples.
- The observation of the SEM and FE-SEM images of the composite panel cross section shown a microstructure with low flaw density.
- Further viscosity evaluations are required for producing slurry with correct parameters to be used for infiltration process of the fibres bundles.
- Kinetics parameters of commercially available and RBMAO process produced Al_4C_3 were determined. It was found a two regimes oxidation kinetics for Aldrich™ Al_4C_3 and three regimes for RBMAO Al_4C_3, wherein oxidizes with lower rates at lower temperature in comparison with the metallic particle and oxidizes with high rates at higher temperatures, which ensure the total oxidation of the carbide yielding in an entirely oxidizes ceramic phase.

- The novel ceramic production route for application in porous matrix of all-oxide ceramic composite was suggested and proven as a promising alternative.
- RBMAO presents dissimilar features in comparison with other reaction bonding techniques due to two facts, first of all, it produced an intermediate phase and second due to the directly addition of mullite within the raw materials.

7 SUGGESTION FOR FUTURE WORK

7.1 IDEAL VISCOSITY FOR FIBRE FABRIC WOVEN INFILTRATION:

Although the main target of this work was to develop a route for all-oxide composites matrix production, which was successfully achieved, the proper composite panel was not produced due to the slurry viscosity characteristic. Nevertheless, some interim results in this field bring up some possibilities for solving the high viscosity problem, which comprised the replacement of the major amount of phenolic resin by graphite powder. Additionally, for the resin it is in charge not only to supply carbon, but also to consolidate the prepregs. It was also suggested that the addition of small part of phenolic resin may enable prepregs consolidation. In order to produce a proper composite panel, therefore, more infiltrations experiments applying the modified slurry are yet required.

7.2 POROUS WICK STRUCTURES FOR CAPILLARY EVAPORATORS

The technique may be adapted for production of porous wicks structure to be used in capillary evaporators. The parts produced out from the RBMAO exhibit desirable mechanical strength for the particular application and may be pressed in order to manufacture flat cylinder shaped parts, which is suitable for flat capillary evaporators. Researches in this field are already been undertaken.

8 LIST OF PUBLICATIONS

8.1 HT-CMC 7 - 7TH INTERNATIONAL CONFERENCE ON HIGH TEMPERATURE CERAMIC MATRIX COMPOSITES

BERTI, L.F., et al. **Novel synthesis route for porous matrix of ceramic oxide composites**. Proceedings of the 7th International Conference on High Temperature Ceramic Materials and Composites, Bayreuth 2010. Oral presentation.

8.2 8TH PTECH - EIGHTH INTERNATIONAL LATIN AMERICAN CONFERENCE ON POWDER TECHNOLOGY

BERTI, L.F., et al. **RBMAO: A novel route for porous matrix composites**. Proceeding of the Eighth International Latin American Conference on Powder Technology. Florianópolis, 2011. Oral presentation

8.3 MATERIALS SCIENCE FORUM – PUBLICATION BY NOV 2012. JCR – 0.399

BERTI, L.F. et al. RBMAO: A novel route for porous matrix composites**. Materials Science Forum**. v. 727-728, p. 568-573, Nov. 2012. DOI: 10.4028/www.scientific.net/MSF.727-728.568.

8.3 J. APPLIED THERMAL ENGINEERING – PUBLISHED IN MAY 2011. JCR – 1.823

BERTI, L.F. et al. Evaluation of permeability of ceramic wick structures for two phase heat transfer devices. **Journal of Applied Thermal Engineering**. v. 31, n. 6-7, p. 1076-1081, May 2011. DOI: 10.1016/j.applthermaleng.2010.12.001.

9 REFERENCES

AARON, J. M.; CHAN, H. M.; HARMER, M. P.; ABPAMANO, M.; CARAM, H. A phenomenological description of the rate of the aluminum/oxygen reaction in the reaction-bonding of alumina. **Journal of the European Ceramic Society**, v. 25, n. 15, p. 3413-3425, October 2005. ISSN 0955-2219. DOI: 10.1016/j.jeurceramsoc.2004.09.012.

ASTM - C 1161 - 02C. **Standard Test Method for Flexural Strength of Advanced Ceramics at Ambient Temperature**. American Society for Testing and Materials. [S.l.]. 2003.

ASTM - C 1341 - 00. **Standard Test Method for Flexural Properties of Continuous Fibre-Reinforced Advanced Ceramc Composites**. American Society for Testing and Materials. [S.l.]. 2003.

AUMANN, C. E.; SKOFRONICK, G. L.; MARTIN, J. A. Oxidation behavior of aluminum nanopowders. **Journal of Vacuum Science & Technology B**, v. 13, n. 3, p. 1178-1183, June 1995. DOI:10.1116/1.588232.

BECK, A. F.; HEINE, M. A.; CAULE, E. J.; PRYOR, M. J. The kinetics of the oxidation of Al in oxygen at high temperature. **Corrosion Science**, v. 7, n. 1, p. 11-22, June 1966. DOI:10.1016/S0010-938X(67)80066-0.

BERTI, L. F. **Caracterização de cerâmicas porosas para aplicação em sistemas de bombeamento capilar (Characterization of ceramic porous wicks for capillary pumped loop application)**. Federal University of Santa Catarina. Florianopolis, SC, p. 110. 2008. (CETD UFSC PCEM 0182). MS Thesis.

BESTERCI, M. Preparation, microstructure and properties of Al–Al4C3. **Materials & Design**, v. 27, n. 5, p. 416-421, JAN 2006. DOI: 10.1016/j.matdes.2004.11.012.

BESTERCI, M.; PARILÁK, L. Microstructure and Mechanical Properties of Al-Al4C3 Materials. In: SENKOV, O. N.; MIRACLE, D. B.; FIRSTOV, S. A.; FIRSTOV, S. A. **Metallic Materials With High Structural Efficiency**. Dordrecht: Kluwer Academic Publisher, v. 146, 2004. p. 195-202. NATO science series.

BIRKS, N.; MEIER, G. H.; PETTIT, F. S. **Introduction to the High Temperature Oxidation of Metals**. 2ª. ed. [S.l.]: Cambridge University Press, 2006. ISBN 978-0521480420.

BOAKYE, E. E.; HAY, R. S.; PETRY, M. D. Continuous Coating of Oxide Fiber Tows Using Liquid Precursors: Monazite Coatings on Nextel 720™. **Journal of the American Ceramic Society**, v. 82, n. 9, p. 2321–2331, 1999.

BROCK, A. J.; PRYOR, M. J. The kinetics of the oxidation of aluminum—copper alloys in oxygen at high temperature. **Corrosion Science**, v. 13, n. 3, p. 199-202, 1973. ISSN 0010-938X. 10.1016/0010-938X(73)90015-2.

CALLISTER, W. D. **Fundamentals of Materials Science and Engineering:** An Interactive e.Text. 5ª. ed. [S.l.]: Wiley, 2000.

CALLISTER, W. D. **Materials Science and Engineering:** An Introduction. 7ª. ed. [S.l.]: Wiley, 2006.

CARELLI, E. A. V.; FUJITA, H.; YANG, J. Y.; ZOK, F. W. Effects of Thermal Aging on the Mechanical Properties of a Porous-Matrix Ceramic Composite. **Journal of the American Ceramic Society**, v. 85, n. 3, p. 595 - 602, 2002.

CHAWLA, K. K. **Ceramic Matrix Composites**. London: Chapman & Hall, 1993.

CHAWLA, K. K.; LIU, H.; JANCZAK-RUSCH, J.; SAMBASIVAN, S. Microstructure and properties of monazite (LaPO4) coated saphikon fiber/alumina matrix composites. **Journal of the European Ceramic Society**, v. 20, n. 5, p. 551–559, 2000.

CHOU, K. A Kinetic Model for Oxidation of Si–Al–O–N Materials. **Journal of the American Ceramic Society**, v. 89, n. 5, p. 1568–1576, May 2006. ISSN 1551-2916. DOI:10.1111/j.1551-2916.2006.00959.x.

CLAUSSEN, N.; GARCIA, D. E.; JANSSEN, R. Reaction sintering of alumina– aluminide alloys (3A). **Journal of Materials Research**, v. 11, n. 11, p. 2884–2888, 1996.

CLAUSSEN, N.; JAHN, J. Mechanical Properties of Sintered, In Situ-Reacted Mullite-Zirconia Composites. **Journal of the American Ceramic Society**, v. 63, n. 3-4, p. 228-229, March 1980. DOI: 10.1111/j.1151-2916.1980.tb10700.x.

CLAUSSEN, N.; LE, T.; WU, S. Low-shrinkage reaction-bonded alumina. **Journal of the European Ceramic Society**, v. 5, n. 1, p. 29–35, 1989.

CLAUSSEN, N.; TRAVITZKY, N. A.; WU, S. Tailoring of Reaction-Bonded Al2O3 (RBAO) Ceramics. In: _____ **A Collection of Papers Presented at the 14th Annual Conference on Composites and Advanced Ceramic Materials:** Ceramic Engineering and Science Proceedings. 7-8. ed. [S.l.]: John Wiley & Sons, Inc., v. 11, 1990. Cap. 22, p. 806-820. DOI: 10.1002/9780470313008.ch22 - [online version 2008].

CLAUSSEN, N.; WU, S. Processing and Properties of Reaction-Bonded Al2O3 (RBAO) and Mullite Ceramics. In: HIRANO, T.; MESSING, G.;

HAUSNER, H. **Ceramic transactions**. Westerville: [s.n.], v. 22, 1992. p. 631-646.

DOBEŠ, F.; BESTERCI, M.; BALLÓKOVÁ, B.; SŰLLEIOVÁ, K.; DYMÁČEK, P. Analysis of creep fracture in Al–Al4C3 composite after ECAP. **Materials Science and Engineering: A**, v. 532, n. 0, p. 567-572, JAN 2012.

DOILNITSYNA, V. V. General diffusion-kinetic model of metallic oxidation. **Corrosion Science**, v. 44, n. 5, p. 1113-1131, May 2002. ISSN 0010-938X. DOI:10.1016/S0010-938X(01)00127-5.

EVANS, A. G.; ZOK, F. W. Review: The physics and mechanics of fibre-reinforced brittle matrix composites. **Journal of Materials Science**, v. 29, n. 1, p. 3857-3896, 1994.

FARNFIELD, C. A.; ALVEY, P. J. **Textile Terms and Definitions**. 7ª. ed. Manchester: The Textile Institute, 1975. ISBN 0-900739-17-7.

FUJITA, H.; JEFFERSON, G.; MCMEEKING, R. M.; ZOK, F. W. Mullite/alumina mixtures for use as porous matrices in oxide fiber composites. **Journal of the American Ceramic Society**, v. 87, n. 2, 2004.

FUJITA, H.; LEVI, C. G.; ZOK, F. W.; JEFFERSON, G. Controlling mechanical properties of porous mullite/alumina mixtures via precursor-derived alumina. **Journal of the American Ceramic Society**, v. 88, n. 2, 2005.

GARCIA, D. E.; JANSSEN, R.; CLAUSSEN, N.; BRITO, M. E. Effect of heating rate on grain morphology of in situ reinforced reaction bonded aluminium niobate-based composites. **Journal of Materials Science**, v. 34, n. 4, p. 769– 772, 1999. DOI: 10.1023/A:1004572913358.

GARCIA, D. E.; SCHICKER, S.; JANSSEN, R.; CLAUSSEN, N. Nb– and Cr–Al2O3 composites with interpenetrating networks. **Journal of the European Ceramic Society**, v. 18, n. 6, p. 601–605, 1998.

GOUSHEGIR, S. M.; GUGLIELMI, P. O.; DA SILVA, J. G. P.; HABLITZEL, M. P.; HOTZA, D.; AL-QURESHI, H. A. et al. Fiber-Matrix Compatibility in an All-Oxide Ceramic Composite with RBAO Matrix. **Journal of the American Ceramic Society**, v. 95, n. 1, p. 159-164, JAN 2012. DOI: 10.1111/j.1551-2916.2011.04863.x.

GOZZI, D.; GUZZARDI, G.; MONTOZZIA, M.; CIGNINI, P. L. Kinetics of high temperature oxidation of refractory carbides. **Solid State Ionics**, v. 101-103, n. 2, p. 1243–1250, May 1998. DOI:10.1016/S0167-2738(97)00413-X.

GURJAR, M. V.; MURTY, G. S.; UPADHYAYA, G. S. Elevated-temperature strengthening in carbide (Al4C3)-dispersed aluminium.

Journal of Materials Science, v. 28, n. 20, p. 5654-5657, 1993. DOI: 10.1007/BF00367842.

HASLAM, J. J.; BERROTH, K. E.; LANGE, F. F. Processing and properties of an all-oxide composite with a porous matrix. **Journal of the European Ceramic Society**, v. 20, n. 5, p. 607-618, 2000.

HE, M. Y.; EVANS, A. G.; HUTCHINSON, J. W. Crack deflection at an interface between dissimilar elastic materials: Role of residual stresses. **International Journal of Solids and Structures**, v. 31, n. 24, p. 3443-3455, December 1994. ISSN 0020-7683. DOI: 10.1016/0020-7683(94)90025-6.

HE, M. Y.; HUTCHINSON, J. W. Crack deflection at an interface between dissimilar elastic materials. **International Journal of Solids Structures**, v. 25, n. 9, p. 1053-1067, 1989. ISSN 0020-7683. DOI:10.1016/0020-7683(89)90021-8.

HEGEDUS, A. G. **Ceramic bodies of controlled porosity and process for making same**. 5.0177.522, 1991.

HIGGINS, K. J.; JUNG, H.; KITTELSON, D. B.; ROBERTS, J. T.; ZACHARIAH, M. R. Size-Selected Nanoparticle Chemistry: Kinetics of Soot Oxidation. **The Journal of Physical Chemistry A**, v. 106, n. 1, p. 96-103, January 2002. ISSN 10895639. DOI: 10.1021/jp004466f.

HOLMQUIST, M.; ADLERBORN, J.; RAZZELL, T.; SUDRE, O.; MOLLIEX, L. Processing and properties of oxide matrix/oxide fibre composite. **British Ceramic Transactions**, v. 99, n. 6, p. 266-269, 2000.

HORTON, R. M. Oxidation Kinetics of Powdered Silicon Nitride. **Journal of the American Ceramic Society**, v. 52, n. 3, p. 121-124, Jun 1969. ISSN 1551-2916. DOI:10.1111/j.1151-2916.1969.tb11195.x - [online version 2006].

HOU, X.; CHOU, K.; LI, F. A new treatment for kinetics of oxidation of silicon carbide. **Ceramics International**, v. 35, n. 2, p. 603-607, March 2009. ISSN 0272-8842. DOI:10.1016/j.ceramint.2008.01.015.

JACKSON, P. R. **Characterization of Compressive Creep Behavior of Oxide/Oxide Composite with Monazite Coating at Elevated Temperature**. Air Force Institute of Technology (AU). Wright-Patterson AFB OH. 2006. (AFIT/GAE/ENY/06-M17.). MS thesis.

JANSSEN, R. Faserverbundwerkstoffe. In: SALMANG, H.; SCHOLZA, H. **Keramik**. [S.l.]: [s.n.], 2007. p. 954-966.

JANSSEN, R.; CLAUSSEN, N.; SCHEPPOKAT, S.; ROGER, M. Reaction bonding and reaction sintering—a way to low cost manufacturing of alumina bases components. **Intermaterial**, v. 15, n. 4, p. 75–79, 2002.

JANSSEN, R.; SCHEPPOKAT, S.; CLAUSSEN, N. Tailor-made ceramic-based components - Advantages by reactive processing and advanced shaping techniques. **Journal of the European Ceramic Society**, v. 28, n. 7, p. 1369-1379, 2008. ISSN 0955-2219. DOI: 10.1016/j.jeurceramsoc.2007.12.022.

JOHNSON, S. M.; BLUM, Y.; KANAZAWA, C.; WU, H. J. Low-cost matrix development for an Oxide-Oxide composite. **Metals and Materials International**, v. 4, n. 6, p. 1119-1125, 1998.

JURF, R. A.; BUTNER, S. C. Advances in Oxide-Oxide CMC. **Journal of Engineering for Gas Turbines and Power**, v. 122, n. 2, p. 202–205, 2000.

KARMHAG, R.; TESFAMICHAEL, T.; WÄCKELGÅRD, E.; NIKLASSON, G. A.; NYGREN, M. Oxidation Kinetics of Nickel Particles: Comparison Between Free Particles and Particles in an Oxide Matrix. **Solar Energy**, v. 68, n. 4, p. 329-333, 2000. ISSN 0038-092X. DOIi: 10.1016/S0038-092X(00)00025-6.

KERANS, R. J.; PARTHASARATHY, T. A. Crack deflection in ceramic composites and fiber coating design criteria. **Composites Part A: Applied Science and Manufacturing**, v. 30, n. 4, p. 521-524, 1999.

KLOCKE, F. **Journal of the European Ceramic Society**, v. 17, n. 2-3, p. 457-465, 1997.

KNECHTEL, M.; CLAUSSEN, N.; CAHN, R. Reliability of structural ceramics [and discussion]. **Philosophical Transactions: Physical Sciences and Engineering**, v. 352, n. 1697, p. 469-483, Jun. 15 1995.

LAMOUROUX, F.; BOURRAT, X.; NASLAIN, R.; THEBAULT, J. Silicon carbide infiltration of porous C-C composites for improving oxidation resistance. **Carbon**, v. 33, n. 4, p. 525-535, 1995. ISSN 0008-6223. DOI:10.1016/0008-6223(94)00177-2.

LANGE, F. F.; TU, W. C.; EVANS, A. G. Processing of damage-tolerant, oxidation-resistant ceramic matrix composites by a precursor infiltration and pyrolysis method. **Materials science & engineering. A, Structural materials: properties, microstructure and processing**, v. 195, n. 1-2, p. 145-150, 1995.

LEE, S. S.; ZAWADA, L. P.; STAEHLER, J.; FOLSOM, C. A. Mechanical behavior and high-temperature performance of a woven Nicalon™/Si–N–C ceramic–matrix composite. **Journal of the American Ceramic Society**, v. 81, n. 7, p. 1797–1811, 1998.

LEVI, C. G.; YANG, J. Y.; DALGLEISH, B. J.; ZOK, F. W.; EVANS, A. G. Processing and performance of an all-oxide ceramic composite. **Journal of the American Ceramic Society**, v. 81, n. 8, p. 2077–2086, 1998.

LI., Y. Q.; QIU, T. Oxidation behaviour of boron carbide powder. **Materials Science and Engineering A**, v. 444, n. 1-2, p. 184-191, August 2007. DOI:10.1016/j.msea.2006.08.068.

LIU, D. Oxidation of polycrystalline α-silicon carbide ceramic. **Ceramics International**, v. 23, n. 5, p. 425-436, 1997. ISSN 0272-8842. DOI:10.1016/S0272-8842(96)00051-X.

LUNDBERG, R.; ECKERBOM, L. Design and Processing of Al-Oxide Composites. **Ceramic Transactions**, v. 58, n. 1, p. 95-104, 1995.

MACHRY, T. **Development of a new Oxide Ceramic Matrix Composite**. Proceeding of HT-CMC7 - 7th International Conference on High Temperature Ceramic Matrix Composites. Bayreuth: [s.n.]. 2010. p. 513-517.

MARTIN, J. **Materials for engineering**. 3ª. ed. [S.l.]: CRC Press (Woodhead Publishing in Materials), 2006.

MATTONI, M. A.; YANG, J. Y.; LEVI, C. G.; ZOK, F. W. Effects of matrix porosity on the mechanical properties of a porous-matrix, all-oxide ceramic composite. **Journal of the American Ceramic Society**, v. 84, n. 11, p. 2594–2602, 2001.

MATTONI, M. A.; YANG, J. Y.; LEVI, C. G.; ZOK, F. W.; ZAWADA, L. P. Effects of combustor rig exposure on a porous-matrix oxide composite. **International Journal of Applied Ceramic Technology**, v. 2, n. 2, p. 133 - 140, 2005.

MEHRMAN, J. M.; RUGGLES-WRENN, M. B.; BAEK, S. S. Influence of hold times on the elevated-temperature fatigue behavior of an oxide–oxide ceramic composite in air and in steam environment. **Composites Science and Technology**, v. 67, n. 7-8, p. 1425–1438, 2007.

MENTZ, J.; MÜLLER, M.; KUNTZ, M.; GRATHWOHL, G.; BUCHKREMER, H. P.; STÖVER, D. New porous silicon carbide composite reinforced by intact high-strength carbon fibres. **Journal of the European Ceramic Society**, v. 26, n. 9, p. 1715-1724, 2006.

MORGAN, P. E. D.; MARSHALL, D. B.; HOUSLEY, R. M. High-temperature stability of monazite-alumina composites. **Materials Science and Engineering A**, v. 195, n. 1, p. 215–222, 1995.

MOUCHON, E.; COLOMBAN, P. Oxide ceramic matrix-oxide fibers woven fabric composites exhibiting dissipative fracture behavior. **Composites**, 26, 1995. 175-182.

NIKLASSON, G. A.; KARMHAG, R. Oxidation kinetics of metallic nanoparticles. **Surface Science**, v. 532-535, n. 0, p. 324–327, June 2003. DOI:10.1016/S0039-6028(03)00178-X.

NIMITYONGSKUL, S.; JONES, M.; CHOI, H.; LAKES, S.; KOU, S.; LI, X. Grain refining mechanisms in Mg–Al alloys with Al4C3 microparticles. **Materials Science and Engineering A**, v. 527, p. 2104–2111, 2010. DOI:10.1016/j.msea.2009.12.030.

PARK, K.; LEE, D.; RAI, A.; MUKHERJEE, D.; ZACHARIAH, M. R. Size-Resolved Kinetic Measurements of Aluminum Nanoparticle Oxidation with Single Particle Mass Spectrometry. **The Journal of Physical Chemistry B**, v. 109, n. 15, p. 7725-7731, April 2005. DOI:10.1021/jp048041v.

PARLIER, M.; RITTI, M. H. State of the art and perspectives for oxide/oxide composites. **Aerospace Science and Technology**, v. 7, n. 3, p. 211–221, 2003.

PARTHASARATHY, T. A.; ZAWADA, L. P.; JOHN, R.; CINIBULK, M. K.; ZELINA, J. Evaluation of Oxide–Oxide Composites in a Novel Combustor Wall Application. **International Journal of Applied Ceramic Technology**, v. 2, n. 2, p. 122-132, 2005.

PERSSON, J.; KÄLL, P.-O.; NYGREN, M. Parabolic-non-parabolic oxidation kinetics of Si3N4. **Journal of the European Ceramic Society**, v. 12, n. 3, p. 177-184, February 1993. ISSN 0955-2219. DOI: 10.1016/0955-2219(93)90119-C.

PIVKINA, A.; STRELETSKII, A.; KOLBANEV, I.; UL'YANOVA, P.; FROLOV, Y.; BUTYAGIN, P. et al. Mechanochemically activated nano-aluminium: Oxidation behaviour. **JOURNAL OF MATERIALS SCIENCE**, v. 39, n. 16-17, p. 5451-5453, January 2004. DOI: 10.1023/B:JMSC.0000039264.33941.82.

QUANLI, J.; HAIJUN, Z.; SUPING, L.; XIAOLIN, J. Effect of particle size on oxidation of silicon carbide powders. **Ceramics International**, v. 33, n. 2, p. 309-313, March 2007. ISSN 0272-8842. DOI:10.1016/j.ceramint.2005.09.014.

RAHAMAN, M. N. **Ceramic Processing and Sintering**. 2ª. ed. [S.l.]: CRC Press, 2003. ISBN 978-0824709884.

RAI, A.; PARK, K.; ZHOU, L.; ZACHARIAH, M. R. Understanding the mechanism of aluminium nanoparticle oxidation. **Combustion Theory and Modelling**, v. 10, n. 5, p. 843-859, October 2006. DOI: 10.1080/13647830600800686.

RAMBO, C. R.; SIEBER, H. Novel Synthetic Route to Biomorphic Al2O3 Ceramics. **Advanced Materials**, v. 17, n. 8, p. 1088 - 1091, 2005.

RASHIDI, A. M. Isothermal oxidation kinetics of nanocrystalline and coarse grained. **Surface and Coatings Technology**, v. 205, n. 17-18, p. 4117–4123, May 2011. DOI:10.1016/j.surfcoat.2011.02.006.

REBEYRAT, S.; GROSSEAU-POUSSARD, J. L.; DINHUT, J. F.; RENAULT, P. O. Oxidation of phosphated iron powders. **Thin Solid Films**, v. 379, n. 1, p. 139-146, December 2000. DOI:10.1016/S0040-6090(00)01416-4.

RUGGLES-WRENN, M. B.; BRAUN, J. C. Influence of hold times on the elevated-temperature fatigue behavior of an oxide–oxide ceramic composite in air and in steam environment. **Composites Science and Technology**, v. 67, n. 7-8, p. 1425-1438, 2007.

RUGGLES-WRENN, M. B.; MALL, S.; EBER, C. A.; HARLAN, L. B. Effects of steam environment on high-temperature mechanical behavior of Nextel™720/alumina (N720/A) continuous fiber ceramic composite. **Composites Part A: Applied Science and Manufacturing**, v. 37, n. 11, 2006. ISSN 1359-835X. DOI: 10.1016/j.compositesa.2005.12.008.

RUGGLES-WRENN, M. B.; SIEGERT, G. T.; BAEK, S. S. Creep behavior of Nextel™720/alumina ceramic composite with ±45° fiber orientation at 1200 °C. **Composites Science and Technology**, v. 68, n. 6, p. 1588-1595, 2008.

SAVEKER, J. J.; BONNELL, T. D. **High speed cutting tool**. 6033789, March 2000.

SCHEPPOKAT, S.; HANNINK, R.; JANSSEN, R.; DEPORTU, G.; CLAUSSEN, N. Sliding wear of Cr–Al2O3–ZrO2 and Mo–Al2O3–ZrO2. **Journal of the European Ceramic Society**, v. 25, n. 6, p. 3553–3561, 2005.

SCHEPPOKAT, S.; JANSSEN, R.; CLAUSSEN, N. In situ synthesis of mullite—a route to zero shrinkage. **The Bulletin of the American Ceramic Society**, v. 77, n. 11, p. 67–69, 1998.

SCHEPPOKAT, S.; JANSSEN, R.; CLAUSSEN, N. Phase development and shrinkage of reaction bonded mullite composites with SiC of different particle sizes. **Journal of the American Ceramic Society**, v. 82, n. 2, p. 319–324, 1999.

SCHMIDT, S.; BEYER, S.; KNABE, H.; IMMICH, H.; MEISTRING, R.; GESSLER, A. Advanced ceramic matrix composite materials for current and future propulsion technology applications. **Acta Astronautica**, v. 55, n. 3-9, p. 409-420, 2004.

SCHOENITZ, M.; PATEL, B.; AGBOH, O.; DREIZIN, E. L. Oxidation of aluminum powders at high heating rates. **Thermochimica Acta**, v. 507-508, n. 0, p. 115-122, September 2010. DOI: 10.1016/j.tca.2010.05.010.

SHE, J.; MECHNICH, P.; SCHNEIDER, H.; SCHMUECKER, M.; KANKA, B. Effect of cyclic infiltrations on microstructure and

mechanical behavior of porous mullite/mullite composites. **Materials Science and Engineering A**, v. 325, n. 1-2, p. 19–24, 2002.

SIMON, R. A. Progress in Processing and Performance of Porous-Matrix. **International Journal of Applied Ceramic Technology**, v. 2, n. 2, p. 141–149, 2005.

SUVACI, E.; SIMKOVICH, G.; MESSING, G. L. The Reaction-Bonded Aluminum Oxide Process: I, The Effect of Attrition Milling on the Solid-State Oxidation of Aluminum Powder. **Journal of the American Ceramic Society**, v. 83, n. 2, p. 299-305, December 2004. DOI:10.1111/j.1151-2916.2000.tb01189.x.

SZWEDA, A.; MILLARD, M. L.; HARRISON, M. G. **Fiber reinforced ceramic–matrix composite member and method for making**. 5.601.674, 1997.

TRAVITZKY, N. A.; CLAUSSEN, N. Microstructure and properties of metal infiltrated RBSN composites. **Journal of the European Ceramic Society**, v. 9, n. 1, p. 61–65, 1992. DOI:10.1016/0955-2219(92)90078-R - [online version 2003].

TU, W. C.; LANGE, F. F.; EVANS, A. G. Concept for a damage-tolerant ceramic composite with strong interfaces. **Journal of the American Ceramic Society**, v. 79, n. 2, p. 417–424, 1996.

VENUGOPALAN, H.; TANKALA, K.; DEBROY, T. Kinetics of directed oxidation of Al-Mg alloys in the initial and final stages of synthesis of Al2O3/Al composites. **Materials Science and Engineering: A**, v. 210, n. 1-2, p. 64-75, June 1996. ISSN 0921-5093. DOI:10.1016/0921-5093(95)10072-5.

VIALA, J. C.; BOSSELET, F.; LAURENT, V.; LEPETITCORPS, Y. Mechanism and kinetics of the chemical interaction between liquid aluminium and silicon-carbide single crystals. **Journal of Materials Science**, v. 28, n. 19, p. 5301-5312, January 1993. ISSN 0022-2461. DOI:10.1007/BF00570081.

WAMSER, T. **Novel Processing of Porous Oxide Ceramic Matrix Composites**. Proceeding of HT-CMC7 - 7th International Conference on High Temperature Ceramic Matrix Composites. Bayreuth: [s.n.]. 2010. p. 517-522.

WANG, Z.; LIU, X.; ZHANG, J.; BIAN, X. Study of the reaction mechanism in the Al-C binary system through DSC and XRD. **Journal of Materials Science**, v. 39, n. 6, p. 2179 – 2181, 2004. DOI: 10.1023/B:JMSC.0000017782.61749.36.

WESTWOOD, M. E.; WEBSTER, J. D.; DAY, R. J.; HAYES, F. H.; R., T. Oxidation protection for carbon fibre composites. **Journal of Materials Science**, v. 31, n. 6, p. 1389-1397, 1996.

WU, S.; CLAUSSEN, N. Fabrication of low-shrinkage mullite-zirconia composites. **Proceedings of the British Ceramic Society**, v. 45, n. 1, p. 91–95, 1990.

WU, S.; HOLZ, D.; CLAUSSEN, N. Mechanisms and kinetics of reaction bonded aluminium oxide ceramics. **Journal of the American Ceramic Society**, v. 76, n. 4, p. 970–980, 1993.

XINMEI, H.; KUO-CHIH, C. Investigation of isothermal oxidation of AlN ceramics using different kinetic model. **Corrosion Science**, v. 51, n. 3, p. 556-561, March 2009. ISSN 0010-938X. DOI:10.1016/j.corsci.2008.12.007.

YANG, J. Y.; WEAVER, J. H.; ZOK, F. W.; MACK, J. J. Processing of Oxide Composites with Three-Dimensional Fiber Architectures. **Journal of the American Ceramic Society**, v. 92, n. 5, p. 1087-1092, May 2009. ISSN 1551-2916. DOI:10.1111/j.1551-2916.2009.03036.x.

YOUNG, D. J. **High Temperature Oxidation and Corrosion of Metals**. 1ª. ed. [S.l.]: Elsevier Science, 2008. ISBN 978-0080445878.

ZAWADA, L. P.; HAY, R. S.; LEE, S. S.; STAEHLER, J. Characterization and High-Temperature Mechanical Behavior of an Oxide/Oxide Composite. **Journal of the American Ceramic Society**, v. 86, n. 6, p. 981 - 990, 2003.

ZAWADA, L. P.; STAEHLER, J.; STEEL, S. Consequence of intermittent exposure to moisture and salt fog on the high-temperature fatigue durability of several ceramic–matrix composites. **Journal of the American Ceramic Society**, v. 86, n. 8, p. 1282–91, 2003.

ZHU, S. J.; PENG, L. M.; ZHOU, Q.; MA, Z. Y.; KUCHAŘOVÁ, K.; ČADEK, J. Creep behaviour of aluminium strengthened by fine aluminium carbide particles and reinforced by silicon carbide particulates DS Al-SiC/Al4C3composites. **Materials Science and Engineering A**, v. 282, n. 1-2, p. 273–284, April 2000.

ZOK, F. W. Developments in oxide fiber composites. **Journal of the American Ceramic Society**, v. 89, n. 11, p. 3309-3324, November 2006.

ZOK, F. W.; LEVI, G. C. Mechanical Properties of Porous-Matrix Ceramic Composites. **Advanced Engineering Materials**, v. 1-2, n. 3, p. 15-23, 2001.